

Spin Observables in Coincidence Electron Scattering from Nuclei I: Reduced Response Functions*

J.E. Amaro^{1,2} and T.W. Donnelly¹

¹ *Center for Theoretical Physics, Laboratory for Nuclear Science and Dept. of Physics,
Massachusetts Institute of Technology, Cambridge, MA 02139, U.S.A.*

² *Departamento de Física Moderna, Universidad de Granada, Granada 18071, Spain*

Abstract

A theoretical description of nucleon knockout reactions initiated by polarized electron scattering from polarized nuclei is presented. Explicit expressions for the complete set of reduced response functions (independent of the polarization angle) that can be experimentally obtained assuming plane waves for the electron are given in a general multipole expansion. The formalism is applied to the particular case of closed-shell-minus-one nuclei using two models for the ejected nucleon, including the final-state interaction phenomenologically with a complex optical potential and in the factorized plane-wave impulse approximation. Relativistic effects in the kinematics and in the electromagnetic current are incorporated throughout — specifically a new expansion of the electromagnetic current in powers only of the struck nucleon momentum is employed. Results are presented for the nucleus ^{39}K .

* This work is supported in part by funds provided by the U.S. Department of Energy (D.O.E.) under cooperative agreement #DE-FC01-94ER40818, in part by D.G.E.S. (Spain) under grant No. PB95-1204 and the Junta de Andalucía (Spain) and in part by NATO Collaborative Research Grant #940183.

1 Introduction

The completely unpolarized quasi-free ($e, e'p$) reaction has been systematically used to probe single-particle properties in complex nuclei, such as momentum distributions and spectroscopic factors [1], and the reliability of the spectroscopic information deduced from these data is based on the weak dependence of the extracted momentum distributions upon the electron scattering kinematical conditions of the experiment [2]. This is presumed to be especially true in the quasielastic region, namely at sufficiently high momentum transfer q and energy transfer $\omega \sim \sqrt{q^2 + M^2} - M$ (with M the nucleon mass) where the process is dominated by the interaction between the electron and a single nucleon in the target, final-state interactions (FSI) are assumed to play as small a role as they can and the plane-wave impulse approximation (PWIA) should be expected to become at least roughly valid. Thus, to the extent that this simple picture applies, the knockout cross section can be factorized into the product of the electron-nucleus cross section and the spectral function, although in analyzing experiments one must usually take into account at least some aspects of the FSI.

The last is certainly the situation when polarized electrons are used (but without hadronic polarizations — see later), since the beam analyzing power involves a new observable — the fifth response function — that vanishes in PWIA and accordingly depends fundamentally upon the presence of FSI [3, 4]. Something similar happens when polarized nuclei are used as targets. In that case a total of nine classes of structure functions can be obtained from $(\vec{e}, e'N)$ reactions, specific ones of these being zero in PWIA [5]. This means that some of the polarization observables are expected to be sensitive to specific aspects of the reaction mechanism that are less pronounced in the unpolarized cross section. It is then of interest to study which are the relevant observables in these kinds of reactions and to explore their importance and sensitivity to different aspects of the modeling in the kinematical ranges of interest.

In this paper we focus our attention on exclusive quasielastic scattering of polarized electrons from polarized nuclei. First, based on the general formalism for (polarized) coincidence reactions presented in Ref. [4] we specialize to the reaction $\vec{A}(\vec{e}, e'N)B$ and, as an extension of our recent work on the inclusive reaction [6], we introduce in Sec. 2 a set of reduced response functions which characterize the polarized cross section and which do not depend on the polarization angles, but only on the momentum and energy transfer (q, ω) and the missing momentum p of the nucleon, having fixed the missing energy to knockout of a nucleon from a specific shell. To do this, we perform a multipole expansion of the nuclear states and electromagnetic current. This involves a sum over third components of the angular momentum that is performed analytically. The resulting exclusive cross section and hadronic structure functions also depend on the polarization and emission angles, which we can write explicitly as a linear combination of spherical harmonics. In particular, a multipole expansion in terms of spherical harmonics of the polarization angles is obtained. The coefficients in this expansion are directly related to what we call angular reduced response functions. These functions constitute the basic ingredients which enter in the total cross section. We illustrate in Appendix A how to obtain the final multipole expansion for the particular case of the longitudinal response.

Although we shall see that the number of angular reduced response functions is very

large, too much so to hope for experimental extraction of all of them in the general case, it is of theoretical interest to study their sensitivity to specific details of the reaction mechanism with the goal of deciding which are the most relevant to measure. This is the subject of the present paper.

We explore these ideas within the context of the shell model. In Sec. 3 we specialize the general expressions to the particular case of nucleon knockout from closed-shell-minus-one nuclei, leaving the daughter nucleus in a discrete state which is described by two holes in the core. We apply the formalism to the ^{39}K nucleus which is described as a $d_{3/2}$ hole in the ^{40}Ca closed shell core. Our theoretical framework addresses the final-state interaction of the ejected nucleon with the residual nucleus by solving the Schrödinger equation with a phenomenological (complex) optical potential. The main result of this section is that in the extreme shell model the reduced nuclear responses are proportional to the polarized response functions for a single polarized particle in a shell. This is more or less obvious for one-particle nuclei, but not for the case of one-hole nuclei, because the involved shell and target nucleus can have different angular momenta, and the final daughter nucleus remains in a two-hole state with definite total angular momentum and then both holes are partially polarized. We prove the above result analytically for hole-nuclei by performing the sum over the total angular momenta of the final hadronic state composed of the daughter nucleus plus the ejected particle (see Appendix B).

One of the aims of our systematic investigation of spin observables initiated in this paper is to determine whether momentum distributions of polarized nuclei (in particular nuclei near closed shells) may look different from those in the unpolarized case. In fact, single-nucleon knockout from polarized nuclei can provide a new probe of the spin-dependent nuclear spectral function which represents the probability of finding a nucleon in the target with given energy, momentum and spin projection. Then, spin observables can be used to explore the spin distribution of the single-particle orbitals, from which one can extract valuable information about the complete spatial distribution of the orbits. The general framework for such studies in PWIA was provided in Refs. [5],[7], and it was applied in Ref. [6] to the study of the inclusive polarized responses of one-hole nuclei. Accordingly in Sec. 4 we introduce the formalism needed for the particular case of one-hole nuclei.

The factorized PWIA gives us a very clear picture of the initial state physics, but the final-state propagation of the outgoing nucleon has to be taken into account. In the present work we are able to go beyond PWIA and to determine to what degree the FSI effects can obscure the extraction of those single-particle properties. An exploratory study to set the scale of possible measurable quantities including the FSI was performed in Ref. [8].

It is important to note that the quasi-free conditions that favour the validity of the PWIA require a high value of the momentum transfer q which prohibits the usual non-relativistic expansions of the electromagnetic current in powers of q/M . Furthermore, for these kinematics the ejected nucleon becomes relativistic. Thus, in this work we use a new approximation to the on-shell relativistic one-body current that was tested in Ref. [9]; this involves an expansion only in powers of $\eta = p/M$, but not in $\kappa = q/2M$ or $\lambda = \omega/2M$. In addition we incorporate relativistic kinematics throughout in the calculations.

2 General formalism for exclusive electron scattering

2.1 Cross section

We begin this section by considering the scattering of polarized electrons from polarized targets. The general formalism for coincidence electron scattering in which all of the particles involved can be polarized has been presented in Ref. [4]. In the present treatment we have re-worked this formalism keeping in mind the specific process in which only the initial particles are polarized and written down the general equations in a way that is oriented towards studies of nucleon knockout reactions. For example, for the shell model applications considered here, it is convenient to use jj coupling instead of LS coupling as was used in Ref. [4]. Also, following the scheme introduced in Ref. [10], we make an expansion of the nuclear structure functions in a basis of spherical harmonics of the polarization angles, in that way introducing a set of reduced response functions that completely determine the process.

Insofar as the electron scattering process is concerned, as discussed in Ref. [4] we limit our attention to the one-photon-exchange or plane-wave Born approximation (PWBA). The four momenta of the incident and scattered electrons are labelled $K^\mu = (\epsilon_e, \mathbf{k}_e)$ and $K'^\mu = (\epsilon'_e, \mathbf{k}'_e)$, respectively. The four-momentum transfer is given by $Q^\mu = (\omega, \mathbf{q})$. We work in the laboratory system, where the initial nucleus is at rest in the state denoted by $|A\rangle$. After the interaction a proton or neutron with momentum direction $\hat{\mathbf{p}}'$ and energy E' is detected and the (undetected) daughter nucleus is left in a discrete state $|B\rangle$. We can assume that when the nucleon is detected in coincidence with the scattered electron, it is essentially at infinity, and therefore on-shell, so that the magnitude of the asymptotic value of the momentum p' is related to the energy by $E' = \sqrt{p'^2 + M^2}$, as usual for free particles, although at short distances when the effects of the FSI are important, the momentum of the ejected nucleon is not well-defined. Therefore, we define the momentum \mathbf{p}' of the ejectile as *the well-defined asymptotic value* and so can label the nucleon wave function as $|\mathbf{p}'\rangle \equiv |E', \hat{\mathbf{p}}'\rangle$.

On the other hand, later in using the formalism in the shell model where recoil is not handled properly we make no attempt to extract the center of mass motion from the nuclear wave function. Note that this is not a real limitation of the general formalism that follows, although a proper treatment of the problem is far from trivial. Indeed, an artificial extraction *by hand* of the center of mass motion in the shell model is known to generate spurious effects that only can be controlled in very specific cases, in particular not in the conventional continuum shell model. Our expectations here in applying the shell model are that the recoil effects in the quasi-free regime are not especially important for nuclei as heavy as ^{39}K .

Also, for the moment only the electron is treated relativistically. Later we will approximately include the relativistic effects in the ejectile nucleon by using relativistic kinematics and an appropriate electromagnetic current operator. Therefore, the S -matrix element for the above process can be written as

$$S_{fi} = -2\pi i \delta(E' + E_B - E_A - \omega) \frac{4\pi\alpha}{Q^2} \langle K'h' | j_\mu(0) | Kh \rangle \langle \mathbf{p}' m_s, B | J^\mu(\mathbf{q}) | A \rangle, \quad (1)$$

where h and h' are the helicities of the (ultra-relativistic) initial and final electrons, E_A and

E_B are the energies of the initial and daughter nuclei, $Q^2 = \omega^2 - q^2 \leq 0$ is the spacelike four-momentum transfer, α is the fine structure constant, $j_\mu(0)$ is the electromagnetic current operator for the electron, m_s is the spin projection of the ejectile, and $J^\mu(\mathbf{q})$ is the Fourier transform of the nuclear electromagnetic current operator. The differential cross section in the laboratory system is proportional to $|S_{fi}|^2$ and to the electron-nucleon phase space $\frac{V d^3 k'_e}{(2\pi)^3} dE' d\hat{\mathbf{p}}'$, where $d\hat{\mathbf{p}}' = d\phi' d\cos\theta'$ is the solid angle differential corresponding to the emission angles (θ', ϕ') . Performing the sum over final undetected electron helicity and integrating over the nucleon energy E' using the energy conservation condition $E' = E_A + \omega - E_B$, the resulting cross section is proportional to the contraction $\eta_{\mu\nu} W^{\mu\nu}$ of the leptonic and hadronic tensors $\eta_{\mu\nu}$ and $W^{\mu\nu}$ given in Ref. [10] and below, respectively. In practice, the ejectile energy E' is detected, so the integration over the energy corresponds to experimentally summing up all of the events that contribute to the selected peak in the missing energy spectrum.

Finally, the contraction $\eta_{\mu\nu} W^{\mu\nu}$ is performed as usual in the extreme relativistic limit for the electron and in the coordinate system with the z -axis along \mathbf{q} and the x -axis in the scattering plane. Using current conservation, the result can be written [10]

$$\begin{aligned} \frac{d\sigma}{d\epsilon'_e d\Omega'_e d\hat{\mathbf{p}}'} &= \sigma_M \left[v_L \mathcal{R}^L + v_T \mathcal{R}^T + v_{TL} \mathcal{R}^{TL} + v_{TT} \mathcal{R}^{TT} + h(v_{T'} \mathcal{R}^{T'} + v_{TL'} \mathcal{R}^{TL'}) \right] \quad (2) \\ &= \Sigma + h\Delta, \quad (3) \end{aligned}$$

where σ_M is the Mott cross section, The electron kinematic factors v_K are defined in Ref. [10]. The six exclusive nuclear response functions \mathcal{R}^K are the components given in Eqs. (9–14) below of the hadronic tensor for the exclusive process defined by

$$W^{\mu\nu} = \sum_{m_s M_B} \langle \mathbf{p}' m_s B | \hat{J}^\mu(\mathbf{q}) | A \rangle^* \langle \mathbf{p}' m_s B | \hat{J}^\nu(\mathbf{q}) | A \rangle, \quad (4)$$

where we sum over the undetected polarizations of the final particles. For a treatment of the general case where all of the particles are polarized, see Ref. [4]. Here we have followed a somewhat different derivation that is more appropriate for the particular application to the shell model.

2.2 Polarized response functions

2.2.1 Hadronic final states

Now some more detailed specifications of the nuclear states themselves are in order. The initial nuclear state is assumed to be 100% polarized relative to an arbitrary axis of quantization whose orientation is specified by the angles $\Omega^* = (\theta^*, \phi^*)$ relative to the coordinate system defined above. We also denote by $\boldsymbol{\Omega}^*$ the unit vector pointing in the Ω^* direction. Therefore, θ^* is the angle between \mathbf{q} and $\boldsymbol{\Omega}^*$; note that the conventions here have ϕ^* with respect to the electron plane, whereas Ref. [4] starts with reference to the hadron plane. We express the nuclear wave function in terms of state vectors defined with respect to the

z -axis:

$$|A\rangle = |J_i J_i(\Omega^*)\rangle = R(\phi^*, \theta^*, 0) |J_i J_i\rangle = \sum_{M_i} \mathcal{D}_{M_i J_i}^{(J_i)}(\Omega^*) |J_i M_i\rangle. \quad (5)$$

Note also that the three Euler angles $(\phi^*, \theta^*, 0)$ of the rotation matrix are different from those specified in Ref. [4]. However, since any rotation around the Ω^* axis does not modify the polarization vector, the resulting observables are exactly the same in the two approaches.

The final hadronic state corresponds asymptotically to a nucleon with energy E' , momentum direction $\hat{\mathbf{p}}'$ with angles (θ', ϕ') referred to the same coordinate system, and with (unobserved) spin projection m_s , together with an (undetected) residual nucleus in the discrete state $|B\rangle$ (that in the general case is recoiling with momentum \mathbf{P}_B). In analogy with the plane-wave expansion in spherical harmonics, we assume that a similar expansion can be performed for the hadronic states

$$|\mathbf{p}' m_s B\rangle = \sum_{lMjmJ_f M_f} i^l Y_{lM}^*(\hat{\mathbf{p}}') \langle \frac{1}{2} m_s l M | j m \rangle \langle j m J_B M_B | J_f M_f \rangle |(E' l j) J_B; J_f M_f\rangle. \quad (6)$$

Here $|(E' l j) J_B; J_f M_f\rangle$ is a continuum nuclear state having asymptotic behaviour

$$|(E' l j) J_B; J_f M_f\rangle \longrightarrow \left[a_{E' l j}^\dagger |J_B\rangle \right]_{J_f M_f}, \quad (7)$$

where $a_{E' l j}^\dagger$ creates a single nucleon with energy E' and angular momenta $(l j)$. Note that the condition in Eq. (7) only has to be verified asymptotically. Therefore we do not make any assumption about the particular nuclear model to be used until later, keeping the following steps in this section completely general. However, it may be helpful to anticipate the modeling used later by noting that any particular theory of the reaction mechanism has to be able to provide a suitable form for the continuum states $|(E' l j) J_B; J_f M_f\rangle$. In particular, in the simple case of the extreme shell model, Eq. (7) is assumed to be true not only asymptotically, but also at short distances. In the simplest case of the PWIA the radial wave function is proportional to a spherical Bessel function and then Eq. (6) reduces to a plane wave times the daughter state $|B\rangle$. As for the normalization of the states, it is

$$\langle (E' l' j') J'_B; J'_f M'_f | (E l j) J_B; J_f M_f \rangle = \delta(E - E') \delta_{ll'} \delta_{jj'} \delta_{J_B J'_B} \delta_{J_f J'_f} \delta_{M_f M'_f}. \quad (8)$$

This relation, together with the asymptotic condition in Eq. (7) uniquely determines the nuclear states.

2.2.2 Multipole analysis

In order to perform a multipole expansion of the responses, it is convenient to write them in terms of the spherical tensor components of the current [4]:

$$\mathcal{R}^L = W^{00} = \sum \rho^* \rho \quad (9)$$

$$\mathcal{R}^T = W^{xx} + W^{yy} = \sum [|J_{-1}|^2 + |J_{+1}|^2] \quad (10)$$

$$\mathcal{R}^{TT} = W^{yy} - W^{xx} = \sum [J_{-1}^* J_{+1} + J_{+1}^* J_{-1}] \quad (11)$$

$$\mathcal{R}^{TL} = \sqrt{2}(W^{0x} + W^{x0}) = -\sum 2\text{Re}[\rho^*(J_{+1} - J_{-1})] \quad (12)$$

$$\mathcal{R}^{TL'} = i\sqrt{2}(W^{0y} - W^{y0}) = -\sum 2\text{Re}[\rho^*(J_{+1} + J_{-1})] \quad (13)$$

$$\mathcal{R}^{T'} = i(W^{xy} - W^{yx}) = \sum [|J_{+1}|^2 - |J_{-1}|^2]. \quad (14)$$

Now we perform the usual multipole expansion for the charge and transverse current operators:

$$\hat{\rho}(\mathbf{q}) = \sqrt{4\pi} \sum_J i^J [J] \hat{M}_{J0}(q) \quad (15)$$

$$\hat{J}_m(\mathbf{q}) = -\sqrt{2\pi} \sum_J i^J [J] \left[\hat{T}_{Jm}^{el}(q) + m \hat{T}_{Jm}^{mag}(q) \right], \quad (16)$$

where m is the index of the spherical components and \hat{M}_{Jm} , \hat{T}_{Jm}^{el} and \hat{T}_{Jm}^{mag} are the usual Coulomb (CJ), electric (EJ) and magnetic (MJ) multipoles. Throughout we use the notation $[J] \equiv \sqrt{2J+1}$ for any angular momentum variable J .

Using the above expansion, the nuclear tensor can be written as a sum of factors of the type

$$B_{J'J}^{m'm} = \sum_{m_s M_B} \langle \mathbf{p}' m_s, J_B M_B | \hat{T}_{J'm'}^* | A \rangle^* \langle \mathbf{p}' m_s, J_B M_B | \hat{T}_{Jm} | A \rangle, \quad (17)$$

where \hat{T} and \hat{T}' are any of the C , E or M operators. For instance, in Appendix A we show the expression for the L response given in terms of the $B_{J'J}^{00}$ coefficients (see Eq. (132)). The parameters m or m' take on the value 0 when the electromagnetic operator involved in the corresponding response is the charge one, while they take on the values 1 or -1 when transverse current components occur. Inserting the expressions Eqs. (5,6) of the initial and final nuclear states, respectively, into Eq. (17), we need to evaluate the following multiple sum

$$\begin{aligned} B_{J'J}^{m'm} = & \sum_{m_s M_B} \sum_{l' M'} \sum_{j' m'_p} \sum_{J'_f M'_f} \sum_{l M} \sum_{j m_p} \sum_{J_f M_f} \sum_{M_i M'_i} i^{l'-l} Y_{lM}(\hat{\mathbf{p}}') Y_{l'M'}^*(\hat{\mathbf{p}}') \mathcal{D}_{M'_i J'_i}^{(J_i)*}(\Omega^*) \mathcal{D}_{M_i J_i}^{(J_i)}(\Omega^*) \\ & \times \langle \frac{1}{2} m_s l' M' | j' m'_p \rangle \langle j' m'_p J_B M_B | J'_f M'_f \rangle \langle \frac{1}{2} m_s l M | j m_p \rangle \langle j m_p J_B M_B | J_f M_f \rangle \\ & \times \langle (l' j') J_B, J'_f M'_f | \hat{T}_{J'm'}^* | J_i M'_i \rangle^* \langle (l j) J_B, J_f M_f | \hat{T}_{Jm} | J_i M_i \rangle. \end{aligned} \quad (18)$$

The procedure to simplify the above expression is then the following.

1. Write the product of the two spherical harmonics $Y_{lM} Y_{l'M'}^*$ as a linear combination of spherical harmonics $Y_{\mathcal{J}'\mathcal{M}'}(\hat{\mathbf{p}}')$. Therefore the index \mathcal{J}' below refers to the multipole expansion in emission angles.
2. Rewrite the dependence on the polarization direction in the product of two rotation matrices $\mathcal{D}_{M'_i J'_i}^{(J_i)*}(\Omega^*) \mathcal{D}_{M_i J_i}^{(J_i)}(\Omega^*)$ by developing this in spherical harmonics of the polarization angles $Y_{\mathcal{J}\mathcal{M}}(\Omega^*)$, and where the coefficients in the expansion also contain

as a factor the Fano tensor for 100% polarization given by $f_{\mathcal{J}}^i = \langle J_i J_i J_i - J_i | \mathcal{J} 0 \rangle$ (see, for example, Ref. [4]). Therefore, the indices $\mathcal{J}\mathcal{M}$ in the equations and reduced response functions defined below refer to this multipole expansion of the polarization dependence.

3. Use the Wigner-Eckart theorem in the matrix elements.

After these steps, all of the dependence upon third components is via 3- j coefficients, and the corresponding sums can be performed analytically using Racah algebra, but here we only quote the final result. Also, following Ref. [4], in order to simplify the notation it is convenient to define multiple indices σ, σ' by $\sigma \equiv \{l, j, J_f, J\}$ and $\sigma' \equiv \{l', j', J_f', J'\}$, and a coefficient

$$\begin{aligned} \Phi_{\sigma'\sigma}(\mathcal{J}, \mathcal{J}', L; J_i \rightarrow J_B) &\equiv [J][J'][j][j'][J_f][J_f'][\mathcal{J}'][L](-1)^{J'+J_B+J_f+1/2+\mathcal{J}+\mathcal{J}'} \\ &\times \begin{pmatrix} j' & j & \mathcal{J}' \\ \frac{1}{2} & -\frac{1}{2} & 0 \end{pmatrix} \left\{ \begin{matrix} j' & j & \mathcal{J}' \\ J_f & J_f' & J_B \end{matrix} \right\} \left\{ \begin{matrix} J & J' & L \\ J_i & J_i & \mathcal{J} \\ J_f & J_f' & \mathcal{J}' \end{matrix} \right\}. \end{aligned} \quad (19)$$

As the values of J_i and J_B are fixed, we shall usually not write them in the argument of $\Phi_{\sigma'\sigma}$. We quote here an important symmetry property of this coefficient under exchange of the two indices $\sigma'\sigma$ that can be easily verified:

$$\Phi_{\sigma'\sigma}(\mathcal{J}\mathcal{J}'L) = (-1)^{\mathcal{J}+\mathcal{J}'+L} \Phi_{\sigma\sigma'}(\mathcal{J}\mathcal{J}'L). \quad (20)$$

With these definitions, the general expression for $B_{J'J}^{m'm}$ becomes the following:

$$\begin{aligned} [J][J']B_{J'J}^{m'm} &= \sum_{ljJ_f} \sum_{l'j'J_f'} \sum_{\mathcal{J}\mathcal{J}'} \sum_{LM} i^{l'-l} P_{l+l'+\mathcal{J}'}^+ (-1)^m f_{\mathcal{J}}^i [Y_{\mathcal{J}}(\Omega^*) Y_{\mathcal{J}'}(\hat{\mathbf{p}}')]_{LM} \\ &\times \Phi_{\sigma'\sigma}(\mathcal{J}\mathcal{J}'L) \begin{pmatrix} J' & J & L \\ m' & -m & M \end{pmatrix} \langle f' | \hat{T}_{J'}' | J_i \rangle^* \langle f | \hat{T}_J | J_i \rangle, \end{aligned} \quad (21)$$

where we define parity projectors $P_J^{\pm} = (1 \pm (-1)^J)/2$ and use shorthand for the generic final states, $|f\rangle = |(E'lj)J_B; J_f\rangle$ and $|f'\rangle = |(E'l'j')J_B; J_f'\rangle$.

Now, in order to write compact expressions for the different response functions it is convenient to define the following Coulomb, electric and magnetic multipole matrix elements,

$$C_{\sigma} \equiv \langle f | \hat{M}_J | J_i \rangle \quad (22)$$

$$E_{\sigma} \equiv \langle f | \hat{T}_J^{el} | J_i \rangle \quad (23)$$

$$M_{\sigma} \equiv \langle f | i\hat{T}_J^{mag} | J_i \rangle, \quad (24)$$

that in general are complex functions only of (q, ω) , since the asymptotic value of the energy is given by $E' = E_A + \omega - E_B$, and both E_A and E_B are fixed. The response functions are defined through linear combinations of the real and imaginary parts of the following

quadratic products of the multipole matrix elements:

$$R_{\sigma'\sigma}^L + iI_{\sigma'\sigma}^L = C_{\sigma'}^* C_{\sigma} \quad (25)$$

$$R_{\sigma'\sigma}^{T1} + iI_{\sigma'\sigma}^{T1} = E_{\sigma'}^* E_{\sigma} + M_{\sigma'}^* M_{\sigma} \quad (26)$$

$$R_{\sigma'\sigma}^{T2} + iI_{\sigma'\sigma}^{T2} = E_{\sigma'}^* M_{\sigma} - M_{\sigma'}^* E_{\sigma} \quad (27)$$

$$R_{\sigma'\sigma}^{TL1} + iI_{\sigma'\sigma}^{TL1} = C_{\sigma'}^* E_{\sigma} \quad (28)$$

$$R_{\sigma'\sigma}^{TL2} + iI_{\sigma'\sigma}^{TL2} = C_{\sigma'}^* M_{\sigma} \quad (29)$$

$$R_{\sigma'\sigma}^{TT1} + iI_{\sigma'\sigma}^{TT1} = E_{\sigma'}^* E_{\sigma} - M_{\sigma'}^* M_{\sigma} \quad (30)$$

$$R_{\sigma'\sigma}^{TT2} + iI_{\sigma'\sigma}^{TT2} = E_{\sigma'}^* M_{\sigma} + M_{\sigma'}^* E_{\sigma}, \quad (31)$$

where the functions $R_{\sigma'\sigma}^K$ and $I_{\sigma'\sigma}^K$ are real functions only of (q, ω) . Also it is convenient to write the angular dependence in Eq. (21) as a sum of real plus imaginary parts. Thus we define the real functions $A_{\mathcal{J}\mathcal{J}'LM}(\Omega^*, \hat{\mathbf{p}}')$ and $B_{\mathcal{J}\mathcal{J}'LM}(\Omega^*, \hat{\mathbf{p}}')$ as

$$A_{\mathcal{J}\mathcal{J}'LM}(\Omega^*, \hat{\mathbf{p}}') + iB_{\mathcal{J}\mathcal{J}'LM}(\Omega^*, \hat{\mathbf{p}}') = [Y_{\mathcal{J}}(\Omega^*) \otimes Y_{\mathcal{J}'}(\hat{\mathbf{p}}')]_{LM}. \quad (32)$$

Finally we also define two parity functions

$$\xi_{J',J}^+ \equiv (-1)^{(J'-J)/2} P_{J'+J}^+, \quad \xi_{J',J}^- \equiv (-1)^{(J'-J+1)/2} P_{J'+J}^-. \quad (33)$$

After these preliminary definitions and following a procedure similar to that in Ref. [4] (summarized in Appendix A for the particular case of the L -response), we are then in a position to write the exclusive responses in the following relatively compact way:

$$\mathcal{R}^L = 4\pi \sum_{\mathcal{J}\mathcal{J}'L} f_{\mathcal{J}}^i \left\{ P_{\mathcal{J}}^+ A_{\mathcal{J}\mathcal{J}'L0} W_{\mathcal{J}\mathcal{J}'L}^{L(+)} - P_{\mathcal{J}}^- B_{\mathcal{J}\mathcal{J}'L0} W_{\mathcal{J}\mathcal{J}'L}^{L(-)} \right\} \quad (34)$$

$$\mathcal{R}^T = 4\pi \sum_{\mathcal{J}\mathcal{J}'L} f_{\mathcal{J}}^i P_{\mathcal{J}'+L}^+ \left\{ P_{\mathcal{J}}^+ A_{\mathcal{J}\mathcal{J}'L0} W_{\mathcal{J}\mathcal{J}'L}^{T(+)} - P_{\mathcal{J}}^- B_{\mathcal{J}\mathcal{J}'L0} W_{\mathcal{J}\mathcal{J}'L}^{T(-)} \right\} \quad (35)$$

$$\mathcal{R}^{T'} = 4\pi \sum_{\mathcal{J}\mathcal{J}'L} f_{\mathcal{J}}^i P_{\mathcal{J}'+L}^- \left\{ P_{\mathcal{J}}^- A_{\mathcal{J}\mathcal{J}'L0} W_{\mathcal{J}\mathcal{J}'L}^{T'(-)} - P_{\mathcal{J}}^+ B_{\mathcal{J}\mathcal{J}'L0} W_{\mathcal{J}\mathcal{J}'L}^{T'(+) } \right\} \quad (36)$$

$$\mathcal{R}^{TL} = 4\pi \sum_{\mathcal{J}\mathcal{J}'L} f_{\mathcal{J}}^i \left\{ P_{\mathcal{J}}^+ A_{\mathcal{J}\mathcal{J}'L1} W_{\mathcal{J}\mathcal{J}'L}^{TL(+)} - P_{\mathcal{J}}^- B_{\mathcal{J}\mathcal{J}'L1} W_{\mathcal{J}\mathcal{J}'L}^{TL(-)} \right\} \quad (37)$$

$$\mathcal{R}^{TL'} = 4\pi \sum_{\mathcal{J}\mathcal{J}'L} f_{\mathcal{J}}^i \left\{ P_{\mathcal{J}}^- A_{\mathcal{J}\mathcal{J}'L1} W_{\mathcal{J}\mathcal{J}'L}^{TL'(-)} - P_{\mathcal{J}}^+ B_{\mathcal{J}\mathcal{J}'L1} W_{\mathcal{J}\mathcal{J}'L}^{TL'(+) } \right\} \quad (38)$$

$$\mathcal{R}^{TT} = 4\pi \sum_{\mathcal{J}\mathcal{J}'L} f_{\mathcal{J}}^i \left\{ P_{\mathcal{J}}^+ A_{\mathcal{J}\mathcal{J}'L2} W_{\mathcal{J}\mathcal{J}'L}^{TT(+)} - P_{\mathcal{J}}^- B_{\mathcal{J}\mathcal{J}'L2} W_{\mathcal{J}\mathcal{J}'L}^{TT(-)} \right\}. \quad (39)$$

The *reduced response functions* $W_{\mathcal{J}\mathcal{J}'L}^{K(\pm)}(q, \omega)$ contain all of the information about the nuclear structure and reaction mechanism and they are the following real quadratic forms involving the basic (complex) multipoles C_{σ} , E_{σ} and M_{σ} :

$$W_{\mathcal{J}\mathcal{J}'L}^{L(+)} = \sum_{\sigma'\sigma} P_{l+l'+\mathcal{J}'}^+ \Phi_{\sigma'\sigma} \begin{pmatrix} J & J' & L \\ 0 & 0 & 0 \end{pmatrix} \xi_{J'-l', J-l}^+ R_{\sigma'\sigma}^L \quad (40)$$

$$W_{\mathcal{J}\mathcal{J}'L}^{L(-)} = \sum_{\sigma'\sigma} P_{l+l'+\mathcal{J}'}^+ \Phi_{\sigma'\sigma} \begin{pmatrix} J & J' & L \\ 0 & 0 & 0 \end{pmatrix} \xi_{J'-l',J-l}^+ I_{\sigma'\sigma}^L \quad (41)$$

$$W_{\mathcal{J}\mathcal{J}'L}^{T(+)} = - \sum_{\sigma'\sigma} P_{l+l'+\mathcal{J}'}^+ \Phi_{\sigma'\sigma} \begin{pmatrix} J & J' & L \\ 1 & -1 & 0 \end{pmatrix} (\xi_{J'-l',J-l}^+ R_{\sigma'\sigma}^{T1} + \xi_{J'-l',J-l}^- R_{\sigma'\sigma}^{T2}) \quad (42)$$

$$W_{\mathcal{J}\mathcal{J}'L}^{T(-)} = - \sum_{\sigma'\sigma} P_{l+l'+\mathcal{J}'}^+ \Phi_{\sigma'\sigma} \begin{pmatrix} J & J' & L \\ 1 & -1 & 0 \end{pmatrix} (\xi_{J'-l',J-l}^+ I_{\sigma'\sigma}^{T1} + \xi_{J'-l',J-l}^- I_{\sigma'\sigma}^{T2}) \quad (43)$$

$$W_{\mathcal{J}\mathcal{J}'L}^{T'(-)} = W_{\mathcal{J}\mathcal{J}'L}^{T(+)} \quad (44)$$

$$W_{\mathcal{J}\mathcal{J}'L}^{T'(+) } = W_{\mathcal{J}\mathcal{J}'L}^{T(-)} \quad (45)$$

$$W_{\mathcal{J}\mathcal{J}'L}^{TL(+)} = -2\sqrt{2}(-1)^{\mathcal{J}'+L} \sum_{\sigma'\sigma} P_{l+l'+\mathcal{J}'}^+ \Phi_{\sigma'\sigma} \begin{pmatrix} J & J' & L \\ 0 & 1 & -1 \end{pmatrix} \times (\xi_{J'-l',J-l}^+ R_{\sigma'\sigma}^{TL1} - \xi_{J'-l',J-l}^- R_{\sigma'\sigma}^{TL2}) \quad (46)$$

$$W_{\mathcal{J}\mathcal{J}'L}^{TL(-)} = -2\sqrt{2}(-1)^{\mathcal{J}'+L} \sum_{\sigma'\sigma} P_{l+l'+\mathcal{J}'}^+ \Phi_{\sigma'\sigma} \begin{pmatrix} J & J' & L \\ 0 & 1 & -1 \end{pmatrix} \times (\xi_{J'-l',J-l}^+ I_{\sigma'\sigma}^{TL1} - \xi_{J'-l',J-l}^- I_{\sigma'\sigma}^{TL2}) \quad (47)$$

$$W_{\mathcal{J}\mathcal{J}'L}^{TL'(-)} = W_{\mathcal{J}\mathcal{J}'L}^{TL(+)} \quad (48)$$

$$W_{\mathcal{J}\mathcal{J}'L}^{TL'(+)} = W_{\mathcal{J}\mathcal{J}'L}^{TL(-)} \quad (49)$$

$$W_{\mathcal{J}\mathcal{J}'L}^{TT(+)} = - \sum_{\sigma'\sigma} P_{l+l'+\mathcal{J}'}^+ (-1)^{\mathcal{J}'+L} \Phi_{\sigma'\sigma} \begin{pmatrix} J & J' & L \\ 1 & 1 & -2 \end{pmatrix} \times (\xi_{J'-l',J-l}^+ R_{\sigma'\sigma}^{TT1} - \xi_{J'-l',J-l}^- R_{\sigma'\sigma}^{TT2}) \quad (50)$$

$$W_{\mathcal{J}\mathcal{J}'L}^{TT(-)} = - \sum_{\sigma'\sigma} P_{l+l'+\mathcal{J}'}^+ (-1)^{\mathcal{J}'+L} \Phi_{\sigma'\sigma} \begin{pmatrix} J & J' & L \\ 1 & 1 & -2 \end{pmatrix} \times (\xi_{J'-l',J-l}^+ I_{\sigma'\sigma}^{TT1} - \xi_{J'-l',J-l}^- I_{\sigma'\sigma}^{TT2}). \quad (51)$$

2.3 Angular reduced response functions

The (q, ω) -dependent reduced response functions discussed above completely determine the responses; however, it is not always very convenient to work with them because their number is infinite. In fact, the multipole expansion in Eq. (6) of the nuclear wave function involves an infinite number of partial waves l . There are interferences between different partial waves l and l' in the response functions, where l and l' are effectively coupled to total angular momentum \mathcal{J}' . As a consequence, the sum over \mathcal{J}' in Eqs. (34-39) is also infinite. The same happens for the photon angular momenta, labeled by the multipole values J, J' coupled to L , that are also summed up to infinity. In practice, of course, we actually sum a (usually) large but finite number of terms until convergence is reached.

For experimental separation purposes and also for theoretical analysis it is convenient to define an alternative finite set of what we call *angular reduced response functions* using the

fact that the values of \mathcal{J} run from $\mathcal{J} = 0, \dots, 2J_i$. Then an expansion in Legendre functions $P_{\mathcal{J}}^{\mathcal{M}}(\cos \theta^*)$ and trigonometric functions of the angles ϕ^* and ϕ' has a finite well-defined number of terms, from which a useful set of response functions (coefficients of the expansion) that depend on q , ω and the emission angle θ' can be defined as some combinations of the functions $W_{\mathcal{J}\mathcal{J}'L}^{K(\pm)}(q, \omega)$ and Legendre functions of the angle θ' . To do this we note that all of the angular dependence of the response functions is through the coupling of two spherical harmonics that can be written as

$$[Y_{\mathcal{J}}(\Omega^*)Y_{\mathcal{J}'}(\hat{\mathbf{p}}')]_{LM} = \sum_{\mathcal{M}\mathcal{M}'} \langle \mathcal{J}\mathcal{M}\mathcal{J}'\mathcal{M}' | LM \rangle Y_{\mathcal{J}\mathcal{M}}(\theta^*, 0) Y_{\mathcal{J}'\mathcal{M}'}(\theta', 0) e^{iM\phi' - i\mathcal{M}\Delta\phi}, \quad (52)$$

where $\Delta\phi \equiv \phi' - \phi^*$ is the azimuthal emission angle measured with respect to the polarization projection on the scattering plane. Note that the spherical harmonic for azimuthal angle equal to zero, $Y_{\mathcal{J}\mathcal{M}}(\theta^*, 0)$, is proportional to a Legendre function $P_{\mathcal{J}}^{|\mathcal{M}|}(\cos \theta^*)$. If we take the real and imaginary parts of the above functions, as defined in Eq. (32), we have

$$\begin{aligned} A_{\mathcal{J}\mathcal{J}'LM}(\Omega^*, \hat{\mathbf{p}}') &= \cos M\phi' \sum_{\mathcal{M}=0}^{\mathcal{J}} h_{\mathcal{J}\mathcal{J}'LM}^{\mathcal{M}}(\theta') P_{\mathcal{J}}^{\mathcal{M}}(\cos \theta^*) \cos(\mathcal{M}\Delta\phi) \\ &\quad + \sin M\phi' \sum_{\mathcal{M}=0}^{\mathcal{J}} \tilde{h}_{\mathcal{J}\mathcal{J}'LM}^{\mathcal{M}}(\theta') P_{\mathcal{J}}^{\mathcal{M}}(\cos \theta^*) \sin(\mathcal{M}\Delta\phi) \end{aligned} \quad (53)$$

$$\begin{aligned} B_{\mathcal{J}\mathcal{J}'LM}(\Omega^*, \hat{\mathbf{p}}') &= \sin M\phi' \sum_{\mathcal{M}=0}^{\mathcal{J}} h_{\mathcal{J}\mathcal{J}'LM}^{\mathcal{M}}(\theta') P_{\mathcal{J}}^{\mathcal{M}}(\cos \theta^*) \cos(\mathcal{M}\Delta\phi) \\ &\quad - \cos M\phi' \sum_{\mathcal{M}=0}^{\mathcal{J}} \tilde{h}_{\mathcal{J}\mathcal{J}'LM}^{\mathcal{M}}(\theta') P_{\mathcal{J}}^{\mathcal{M}}(\cos \theta^*) \sin(\mathcal{M}\Delta\phi). \end{aligned} \quad (54)$$

These equations can also be taken as the definitions of the angular functions $h_{\mathcal{J}\mathcal{J}'LM}^{\mathcal{M}}(\theta')$ and $\tilde{h}_{\mathcal{J}\mathcal{J}'LM}^{\mathcal{M}}(\theta')$. Inserting Eqs. (53,54) into Eqs. (34-39) it is straightforward to write the response functions in the following way:

$$\mathcal{R}^L = W^L \quad (55)$$

$$\mathcal{R}^T = W^T \quad (56)$$

$$\mathcal{R}^{TL} = \cos \phi' W^{TL} + \sin \phi' \widetilde{W}^{TL} \quad (57)$$

$$\mathcal{R}^{TT} = \cos 2\phi' W^{TT} + \sin 2\phi' \widetilde{W}^{TT} \quad (58)$$

$$\mathcal{R}^{T'} = \widetilde{W}^{T'} \quad (59)$$

$$\mathcal{R}^{TL'} = \sin \phi' W^{TL'} + \cos \phi' \widetilde{W}^{TL'}. \quad (60)$$

The nine response functions W^K and \widetilde{W}^K without any sub-index depend on q , ω , θ' , θ^* , and $\Delta\phi$. Their explicit dependences on the angles $(\theta^*, \Delta\phi)$ are the following:

$$W^L = 4\pi \sum_{\mathcal{J}=0}^{2J_i} \sum_{\mathcal{M}=0}^{\mathcal{J}} f_{\mathcal{J}}^i P_{\mathcal{J}}^{\mathcal{M}}(\cos \theta^*) \left[P_{\mathcal{J}}^+ c_{\mathcal{M}} W_{\mathcal{J}\mathcal{M}}^{L(+)} + P_{\mathcal{J}}^- s_{\mathcal{M}} \widetilde{W}_{\mathcal{J}\mathcal{M}}^{L(-)} \right] \quad (61)$$

$$W^T = 4\pi \sum_{\mathcal{J}=0}^{2J_i} \sum_{\mathcal{M}=0}^{\mathcal{J}} f_{\mathcal{J}}^i P_{\mathcal{J}}^{\mathcal{M}}(\cos \theta^*) \left[P_{\mathcal{J}}^+ c_{\mathcal{M}} W_{\mathcal{J}\mathcal{M}}^{T(+)} + P_{\mathcal{J}}^- s_{\mathcal{M}} \widetilde{W}_{\mathcal{J}\mathcal{M}}^{T(-)} \right] \quad (62)$$

$$W^{TL} = 4\pi \sum_{\mathcal{J}\mathcal{M}} f_{\mathcal{J}}^i P_{\mathcal{J}}^{\mathcal{M}}(\cos \theta^*) \left[P_{\mathcal{J}}^+ c_{\mathcal{M}} W_{\mathcal{J}\mathcal{M}}^{TL(+)} + P_{\mathcal{J}}^- s_{\mathcal{M}} \widetilde{W}_{\mathcal{J}\mathcal{M}}^{TL(-)} \right] \quad (63)$$

$$\widetilde{W}^{TL} = 4\pi \sum_{\mathcal{J}\mathcal{M}} f_{\mathcal{J}}^i P_{\mathcal{J}}^{\mathcal{M}}(\cos \theta^*) \left[P_{\mathcal{J}}^+ s_{\mathcal{M}} \widetilde{W}_{\mathcal{J}\mathcal{M}}^{TL(+)} - P_{\mathcal{J}}^- c_{\mathcal{M}} W_{\mathcal{J}\mathcal{M}}^{TL(-)} \right] \quad (64)$$

$$W^{TT} = 4\pi \sum_{\mathcal{J}\mathcal{M}} f_{\mathcal{J}}^i P_{\mathcal{J}}^{\mathcal{M}}(\cos \theta^*) \left[P_{\mathcal{J}}^+ c_{\mathcal{M}} W_{\mathcal{J}\mathcal{M}}^{TT(+)} + P_{\mathcal{J}}^- s_{\mathcal{M}} \widetilde{W}_{\mathcal{J}\mathcal{M}}^{TT(-)} \right] \quad (65)$$

$$\widetilde{W}^{TT} = 4\pi \sum_{\mathcal{J}\mathcal{M}} f_{\mathcal{J}}^i P_{\mathcal{J}}^{\mathcal{M}}(\cos \theta^*) \left[P_{\mathcal{J}}^+ s_{\mathcal{M}} \widetilde{W}_{\mathcal{J}\mathcal{M}}^{TT(+)} - P_{\mathcal{J}}^- c_{\mathcal{M}} W_{\mathcal{J}\mathcal{M}}^{TT(-)} \right] \quad (66)$$

$$\widetilde{W}^{T'} = 4\pi \sum_{\mathcal{J}\mathcal{M}} f_{\mathcal{J}}^i P_{\mathcal{J}}^{\mathcal{M}}(\cos \theta^*) \left[P_{\mathcal{J}}^- c_{\mathcal{M}} W_{\mathcal{J}\mathcal{M}}^{T'(-)} + P_{\mathcal{J}}^+ s_{\mathcal{M}} \widetilde{W}_{\mathcal{J}\mathcal{M}}^{T'(+) } \right] \quad (67)$$

$$W^{TL'} = 4\pi \sum_{\mathcal{J}\mathcal{M}} f_{\mathcal{J}}^i P_{\mathcal{J}}^{\mathcal{M}}(\cos \theta^*) \left[P_{\mathcal{J}}^- s_{\mathcal{M}} \widetilde{W}_{\mathcal{J}\mathcal{M}}^{TL'(-)} - P_{\mathcal{J}}^+ c_{\mathcal{M}} W_{\mathcal{J}\mathcal{M}}^{TL'(+) } \right] \quad (68)$$

$$\widetilde{W}^{TL'} = 4\pi \sum_{\mathcal{J}\mathcal{M}} f_{\mathcal{J}}^i P_{\mathcal{J}}^{\mathcal{M}}(\cos \theta^*) \left[P_{\mathcal{J}}^- c_{\mathcal{M}} W_{\mathcal{J}\mathcal{M}}^{TL'(-)} + P_{\mathcal{J}}^+ s_{\mathcal{M}} \widetilde{W}_{\mathcal{J}\mathcal{M}}^{TL'(+) } \right], \quad (69)$$

where we define $s_{\mathcal{M}} \equiv \sin(\mathcal{M}\Delta\phi)$ and $c_{\mathcal{M}} \equiv \cos(\mathcal{M}\Delta\phi)$, the factors that contain all of the dependence on $\Delta\phi$, and where for brevity we have only written the ranges of the sums over \mathcal{J}, \mathcal{M} in the L and T pieces. In all of the others a sum for $\mathcal{J} = 0, \dots, 2J_i$ and for non-negative values of \mathcal{M} must be understood. The W 's and \widetilde{W} 's inside the sums are the *angular reduced response functions*. Note that for the limit values $\theta^* = 0^\circ, 180^\circ$ the Legendre function $P_{\mathcal{J}}^{\mathcal{M}}(\cos \theta^*)$ is zero for $\mathcal{M} \neq 0$. Therefore the functions W^K, \widetilde{W}^K do not depend on $\Delta\phi$ for these values of θ^* . Note also that the angular reduced response functions $W_{\mathcal{J}\mathcal{M}}^{K(\pm)}(q, \omega, \theta')$ are linear combinations of the reduced responses $W_{\mathcal{J}\mathcal{J}'L}^{K(\pm)}$ with the functions $h_{\mathcal{J}\mathcal{J}'LM}^{\mathcal{M}}$ as coefficients, while the angular reduced responses with a tilde $\widetilde{W}_{\mathcal{J}\mathcal{J}'L}^{K(\pm)}$ have as coefficients the functions $\widetilde{h}_{\mathcal{J}\mathcal{J}'LM}^{\mathcal{M}}$. Furthermore, in Eqs. (61–69) the responses without tildes are multiplied by $\cos(\mathcal{M}\Delta\phi)$, while the responses with tildes are multiplied by $\sin(\mathcal{M}\Delta\phi)$. They can be written as

$$W_{\mathcal{J}\mathcal{M}}^{K(\pm)}(q, \omega, \theta') = \sum_{\mathcal{J}'L} a_{\mathcal{J}'L} h_{\mathcal{J}\mathcal{J}'LM}^{\mathcal{M}}(\theta') W_{\mathcal{J}\mathcal{J}'LM}^{K(\pm)}(q, \omega) \quad (70)$$

$$\widetilde{W}_{\mathcal{J}\mathcal{M}}^{K(\pm)}(q, \omega, \theta') = \sum_{\mathcal{J}'L} a_{\mathcal{J}'L} \widetilde{h}_{\mathcal{J}\mathcal{J}'LM}^{\mathcal{M}}(\theta') W_{\mathcal{J}\mathcal{J}'LM}^{K(\pm)}(q, \omega), \quad (71)$$

where the index M depends on the particular response as

$$M = \begin{cases} 0 & \text{for } K = L, T, T' \\ 1 & \text{for } K = TL, TL' \\ 2 & \text{for } K = TT, \end{cases} \quad (72)$$

that is, the value of M depends on the particular response in the same way as in Eqs. (32,34–39). Finally, we have introduced a factor $a_{\mathcal{J}'L} = P_{\mathcal{J}'+L}^+$ for $K = T$, $a_{\mathcal{J}'L} = P_{\mathcal{J}'+L}^-$ for $K = T'$, while $a_{\mathcal{J}'L} = 1$ for the other responses.

From these general expressions, one can easily specialize to some important cases, such as:

1. *Nucleon knockout from spin-zero nuclei.* In this case in the above equations we have $J_i = 0$, and thus only the terms $\mathcal{J} = 0$, $\mathcal{J}' = L$, $J_f = J$ and $J'_f = J'$ contribute. For brevity we do not give the explicit expressions for this case, as in this work we are considering only odd nuclei with half-integer spin.
2. *Inclusive responses.* Integrating over the emission angles $\hat{\mathbf{p}}'$ and summing over the final nuclear states $|B\rangle$ (including over proton and neutron emission) we obtain the inclusive responses. Due to the presence of the spherical harmonic $Y_{\mathcal{J}'\mathcal{M}'}(\hat{\mathbf{p}}')$, the integral over $\hat{\mathbf{p}}'$ in all of the above equations restricts the values to $\mathcal{J}' = 0$, $\mathcal{J} = L$, $j = j'$, $J_f = J'_f$, $\mathcal{M} = M$ and $l = l'$, yielding an alternative derivation of the equations given in Ref. [6] and also providing a test of the multipole expansion.
3. *Unpolarized responses for any spin J_i nucleus.* The unpolarized responses can be computed as the polarized responses averaged over all polarization directions, that is

$$\mathcal{R}_{unpol}^K = \frac{1}{4\pi} \int \mathcal{R}^K(\Omega^*) d\Omega^*, \quad (73)$$

and therefore only the terms with $\mathcal{J} = 0$ in the above equations survive. These terms are obviously independent of Ω^* as is required for an unpolarized observable, so the integral trivially yields a factor 4π that cancels with the denominator in Eq. (73). As a consequence, the unpolarized responses are given by the terms with $\mathcal{J} = \mathcal{M} = 0$ in Eqs. (61–69).

3 Formalism for one-hole shell model nuclei

As a particular application of the formalism introduced in the last section to a simple model of a polarized target, in this work we consider the case of a one-hole shell model nucleus. Specifically we consider the same model introduced in Ref. [6] for the analysis of inclusive polarized responses and refer the reader to the discussions presented there for more details on the model.

The initial nuclear state is a hole in a closed-shell core $|C\rangle$:

$$|A\rangle = |i^{-1}(\Omega^*)\rangle = \sum_{m_i} \mathcal{D}_{m_i j_i}^{(j_i)}(\Omega^*) b_{i, m_i}^\dagger |C\rangle, \quad (74)$$

where $|i\rangle = |n_i, \frac{1}{2}, l_i, j_i\rangle$ is a single-particle state occupied in the core and b_{i, m_i}^\dagger is the creation operator for a hole. Here we follow the convention of using lower case letters j_i for half-integer angular momenta. As in the present work we only consider the one-body piece of

the electromagnetic nuclear current, the interaction with the virtual photon gives rise only to particle-hole (p-h) excitations. Thus the final nuclear states are described by

$$|f\rangle = |(E'lj)(h^{-1}, i^{-1})J_B; j_f\rangle. \quad (75)$$

Here $|h\rangle = |n_h, l_h, j_h\rangle$ is another (bound) single-particle state in the core, while $|E'lj\rangle$ is a single particle in the continuum. The residual nucleus is represented in this simple model as a two-hole nucleus $|B\rangle = |(h^{-1}, i^{-1})J_B\rangle$ with total angular momentum J_B , coupled with the outgoing particle $|E'lj\rangle$ to a total angular momentum j_f .

In the present work the wave functions of the single-particle hole states are obtained using a mean-field potential of Woods-Saxon type. More details on this aspect of the calculation, including the values of the potential parameters, can be found in Refs. [9] and [11]. On the other hand, the wave function for the ejected nucleon is obtained as the solution of the Schrödinger equation for positive energy $\epsilon' = E' - M$ (E' contains the rest mass), using a complex optical potential in order to include absorption processes in the FSI that are not described by a real mean-field potential. Below we give more details about this particular aspect of the modeling.

The basic quantities required are the reduced response functions in Eqs. (40–51). The sums in those equations run over $\sigma = (l, j, J, j_f)$ and $\sigma' = (l', j', J', j'_f)$, but as in the inclusive case [6], we are able to perform the sum over j_f, j'_f analytically, simplifying the final expressions and permitting us to draw several conclusions about the responses. We summarize the procedure to be followed in Appendix B. Worth mentioning here is the fact that in Ref. [6] where we considered only the inclusive case we were able to perform analytically an additional sum over the daughter angular momentum J_B , considerably simplifying the procedures: here we cannot perform this additional summation since the value of J_B is fixed.

It is noteworthy that in this model of coincidence scattering, after performing the sums that are permitted, the resulting nuclear responses can be expressed in terms of the polarized response functions for a single particle in the shell h . These single-particle responses are due to the scattering of the electron with a single nucleon in the shell h , and in this case Eq. (19) is also valid, with the exception that $J_i = j_h$ and $J_B = 0$, as explained in Appendix B. We denote the single-particle responses of the shell h by $w_{\mathcal{JM}}^{K(\pm)}[h \rightarrow 0]$. First we consider the case $h \neq i$. Then, as shown in Appendix B, the corresponding response for the entire nucleus, that we denote by $W_{\mathcal{JM}}^{K(\pm)}[i^{-1} \rightarrow (h^{-1}i^{-1})J_B]$, is proportional to the response of a single nucleon in the shell h via the simple relationship

$$W_{\mathcal{JM}}^{K(\pm)}[i^{-1} \rightarrow (h^{-1}i^{-1})J_B] = (-1)^{j_h+j_i+J_B+\mathcal{J}}[J_B]^2 \left\{ \begin{matrix} j_i & j_i & \mathcal{J} \\ j_h & j_h & J_B \end{matrix} \right\} w_{\mathcal{JM}}^{K(\pm)}[h \rightarrow 0]. \quad (76)$$

Actually in Appendix B we prove the result at the more elementary level, namely between the reduced responses $W_{\mathcal{J}'L}^{K(\pm)}[i^{-1} \rightarrow (h^{-1}i^{-1})J_B]$ and $w_{\mathcal{J}'L}^{K(\pm)}[h \rightarrow 0]$.

This relationship has important consequences. Indeed, although in this model the polarization of the nucleus is carried by the outer shell i , it is interesting to note that nucleon knockout can provide information about the polarized responses of the inner, complete (unpolarized) shell h , as long as the 6- j coefficient is nonzero. In particular, if i is a neutron (or

a proton) we can measure polarization observables with $(e, e'p)$ (or $(e, e'n)$) reactions. The reason for that behaviour is that the final particles are partially polarized because they are coupled to a definite angular momentum J_B .

For further insight into this last comment, let us consider the sum over all possible values of J_B in Eq. (76). Then we obtain the sum rule for the angular reduced responses

$$\sum_{J_B} W_{\mathcal{JM}}^{K(\pm)} [i^{-1} \rightarrow (h^{-1}i^{-1})J_B] = \delta_{\mathcal{J}0} \delta_{\mathcal{M}0} [j_i][j_h] w_{00}^{K(\pm)} [h \rightarrow 0], \quad (77)$$

and a similar result for the total responses. For instance, using Eq. (61) for the longitudinal case we have

$$\sum_{J_B} \mathcal{R}^L [i^{-1} \rightarrow (h^{-1}i^{-1})J_B] = 4\pi [j_h] w_{00}^{L(+)} [h \rightarrow 0], \quad (78)$$

where we have used $f_0^i = 1/[j_i]$. We can compare this equation with the longitudinal response for electron scattering from an unpolarized particle in shell h . From Eq. (73) and the comments that follow it, we see that the unpolarized response is given by the term with $\mathcal{J} = 0$ in Eq. (61), with $J_i = j_h$

$$\mathcal{R}_{unpol}^L [h \rightarrow 0] = 4\pi \frac{1}{[j_h]} w_{00}^{L(+)} [h \rightarrow 0]. \quad (79)$$

Then, inserting this equation in Eq. (78), we obtain a relation that is valid for all of the responses, $K = L, T, \dots$, and not only for the longitudinal case:

$$\sum_{J_B} \mathcal{R}^K [i^{-1} \rightarrow (h^{-1}i^{-1})J_B] = [j_h]^2 \mathcal{R}_{unpol}^K [h \rightarrow 0]. \quad (80)$$

This shows that the sum over J_B of all of the exclusive polarized K -responses for different final states of the type $(h^{-1}i^{-1})J_B$ is equal to the unpolarized K -response of the shell h (that is, arising from unpolarized nucleon knockout from a nucleon in the shell h) times the number of particles in the complete shell h . As a consequence, the sum over J_B of all of the polarized responses (i.e. with $\mathcal{J} \neq 0$) is equal to zero. Of course this theorem is only valid in the extreme shell model, which means that observable deviations of this result can provide valuable information about configuration mixing and the nuclear structure of the final states. In summary, we see that the reason why unpolarized shells yield polarization observables is due to the fact that the angular momentum J_B of the daughter nucleus is fixed. If we sum over J_B all of the polarization observables go away for a closed shell.

Now we consider the case $h = i$, where we extract a nucleon from the same shell in which the hole is located. This is the case with more practical applications, because the shell model is expected to provide a better description of the nuclear states for small excitation energy and, in particular, for the ground state of the daughter nucleus with $J_B = 0$. The derivation of the results that follows is similar to the $h \neq i$ case, with the exception that a factor of two arises due to the fact that the two holes in the same shell are undistinguishable, and, in addition, that the nuclear spin J_B is restricted to be an even number. Then, if we set $h = i$

in Eq. (76) and multiply by two, we obtain

$$W_{\mathcal{JM}}^{K(\pm)} [i^{-1} \rightarrow (i^{-1}i^{-1})J_B] = 2(-1)^{\mathcal{J}+1}[J_B]^2 \left\{ \begin{matrix} j_i & j_i & \mathcal{J} \\ j_i & j_i & J_B \end{matrix} \right\} w_{\mathcal{JM}}^{K(\pm)} [i \rightarrow 0]. \quad (81)$$

In particular, for the daughter nucleus in the ground state with $J_B = 0$ the 6- j symbol is equal to $(-1)^{\mathcal{J}+1}/[j_i]^2$ and we have

$$W_{\mathcal{JM}}^{K(\pm)} [i^{-1} \rightarrow (i^{-1}i^{-1})0] = \frac{2}{[j_i]^2} w_{\mathcal{JM}}^{K(\pm)} [i \rightarrow 0]. \quad (82)$$

For example, for the simplest case of a hole in a $j_i = \frac{1}{2}$ shell, we have $[j_i]^2 = 2$ and therefore we obtain

$$W_{\mathcal{JM}}^{K(\pm)} \left[\frac{1}{2}^{-1} \rightarrow \left(\frac{1}{2}^{-1} \frac{1}{2}^{-1} \right) 0 \right] = w_{\mathcal{JM}}^{K(\pm)} \left[\frac{1}{2} \rightarrow 0 \right]. \quad (83)$$

Then we recover the result that one hole in a $\frac{1}{2}$ shell is equivalent to a particle in that shell, as expected.

Also, if we sum over J_B as before, we obtain an interesting sum rule. Taking into account that the sum now runs over $J_B = \text{even}$ and using the property

$$\sum_{J_B=\text{even}} [J_B]^2 \left\{ \begin{matrix} j_i & j_i & \mathcal{J} \\ j_i & j_i & J_B \end{matrix} \right\} = \frac{1}{2}(1 - \delta_{\mathcal{J}0}[j_i]^2) \quad (84)$$

then, from Eq. (81), we obtain for the sum of the angular reduced responses

$$\sum_{J_B} W_{\mathcal{JM}}^{K(\pm)} [i^{-1} \rightarrow (i^{-1}i^{-1})J_B] = (\delta_{\mathcal{J}0}[j_i]^2 - (-1)^{\mathcal{J}}) w_{\mathcal{JM}}^{K(\pm)} [i \rightarrow 0], \quad (85)$$

i.e., the unpolarized response of the $2j_i + 1$ particles in the complete shell minus the polarized response of a single particle multiplied by $(-1)^{\mathcal{J}}$. The same relation holds between the sum $\sum_{J_B} W_{\mathcal{JJ}'L}^{K(\pm)} [i^{-1} \rightarrow (i^{-1}i^{-1})J_B]$ and the responses $w_{\mathcal{JJ}'L}^{K(\pm)} [i \rightarrow 0]$. The origin of the phase $(-1)^{\mathcal{J}}$ is easily explained by looking at the total responses. For instance, from Eq. (34) we obtain for the longitudinal one

$$\begin{aligned} \sum_{J_B} \mathcal{R}^L [i^{-1} \rightarrow (i^{-1}i^{-1})J_B] &= [j_i]^2 \mathcal{R}_{unpol}^L [i \rightarrow 0] \\ &- 4\pi \sum_{\mathcal{JJ}'L} f_{\mathcal{J}}^i (-1)^{\mathcal{J}} \left\{ P_{\mathcal{J}}^+ A_{\mathcal{JJ}'L0} w_{\mathcal{JJ}'L}^{L(+)} [i \rightarrow 0] - P_{\mathcal{J}}^- B_{\mathcal{JJ}'L0} w_{\mathcal{JJ}'L}^{L(-)} [i \rightarrow 0] \right\}. \end{aligned} \quad (86)$$

We notice that we can include the factor $(-1)^{\mathcal{J}}$ in the angular functions $A_{\mathcal{JJ}'L0}$ and $B_{\mathcal{JJ}'L0}$ using the parity property of the spherical harmonics $Y_{\mathcal{JM}}(-\mathbf{\Omega}^*) = (-1)^{\mathcal{J}} Y_{\mathcal{JM}}(\mathbf{\Omega}^*)$. Then we can write the above result for any response, and not only for the longitudinal case, as

$$\sum_{J_B} \mathcal{R}^K [i^{-1} \rightarrow (i^{-1}i^{-1})J_B] = [j_i]^2 \mathcal{R}_{unpol}^K [i \rightarrow 0] - \mathcal{R}^K [i \rightarrow 0] \big|_{\mathbf{\Omega}^* \rightarrow -\mathbf{\Omega}^*}. \quad (87)$$

Now it becomes evident that the factor $(-1)^{\mathcal{J}+1}$ for the difference between particle and hole cases which was also mentioned in Ref. [6] comes from the fact that a hole nucleus which is polarized in the direction $\mathbf{\Omega}^*$ is physically equivalent to the absence of a particle which is polarized in the opposite direction $-\mathbf{\Omega}^*$. The factor $(-1)^{\mathcal{J}}$ comes from a spherical harmonic $Y_{\mathcal{J}\mathcal{M}}(\mathbf{\Omega}^*)$ which is always in front of the responses of rank \mathcal{J} in the multipole expansion.

A similar result to Eq. (87) was obtained also in the inclusive case (see Ref. [6]), where it was shown that any polarized (inclusive) response of a hole nucleus can be written as the unpolarized response of the complete shell minus the polarized response of the hole (multiplied again by the factor $(-1)^{\mathcal{J}}$). We can re-obtain here that result by integration of Eq. (87), thereby showing another connection between the two formalisms.

To finish this section we show a result for the sum of the unpolarized (exclusive) responses of a hole nucleus:

$$\sum_{J_B} \mathcal{R}_{unpol}^K [i^{-1} \rightarrow (i^{-1}i^{-1})J_B] = ([j_i]^2 - 1) \mathcal{R}_{unpol}^K [i \rightarrow 0], \quad (88)$$

i.e., the sum of the unpolarized responses for each one of the particles in the shell.

Equations (76) and (81) are the basic results of this section. They show that the reduced polarized responses corresponding to different values of the final angular momenta of the daughter nucleus $|(h^{-1}i^{-1})J_B\rangle$ are scaled by a well-defined coupling coefficient that only depends on the values of the angular momenta involved. This fact could be experimentally checked and any deviation from that relationship would imply interesting conclusions about the nuclear structure of the daughter states.

4 PWIA

4.1 Factorization of the responses

The main reason for considering the PWIA for the ejectile is that in such a limit, when the final-state interaction is turned off, the exclusive cross section factorizes and we can perform part of the calculations analytically. The resulting cross section contains the basic electron-nucleon (in general off-shell) responses and the scalar and vector momentum distributions, giving a picture of the physics that is more transparent than the general formalism where the multipole analysis obscures the physical interpretation of the process.

In order to extract valuable information about the nuclear momentum distribution, it would be desirable to find a set of polarization observables that is more or less independent of the FSI. The general formalism for PWIA in polarized nuclei was developed in Refs. [5, 7], and it was recently specialized in Ref. [6] to the particular case of polarized, one-hole nuclei, although in that work the exclusive responses were integrated over the emission angle in order to study the inclusive case. Here we briefly summarize the essential results from that work so that the nomenclature can be introduced, referring to Ref. [6] for more detailed discussions.

In PWIA we write the factorized exclusive responses as

$$\mathcal{R}^K = M p' w_S^K M^S(\mathbf{p}) \quad (89)$$

$$\mathcal{R}^{K'} = Mp' \mathbf{w}_V^{K'} \cdot \mathbf{M}^V(\mathbf{p}), \quad (90)$$

where $\mathbf{p} \equiv \mathbf{p}' - \mathbf{q}$ is the missing momentum with angles (θ, ϕ) , and w_S^K and $\mathbf{w}_V^{K'}$ are respectively the scalar and vector single-nucleon responses, which are related with the components Eqs. (9–14), of the single-nucleon tensor spin matrix

$$w^{\mu\nu}(\mathbf{p}', \mathbf{p}) = J^\mu(\mathbf{p}', \mathbf{p})^\dagger J^\nu(\mathbf{p}', \mathbf{p}), \quad (91)$$

where $J^\mu(\mathbf{p}', \mathbf{p})$ is the electromagnetic current spin matrix for the nucleon, evaluated with plane waves $\langle \mathbf{r} | \mathbf{p} s \rangle = (2\pi)^{-3/2} e^{i\mathbf{p} \cdot \mathbf{r}} \chi_s$. Taking the appropriate components of the single-nucleon tensor $w^{\mu\nu}(\mathbf{p}', \mathbf{p})$, the resulting unprimed responses are diagonal in spin (spin-scalar), so we can write for the L , T , TL and TT responses $w^K = w_S^K$, while the T' and TL' (primed) responses are spin-vectors and can be written as $w^{K'} = \mathbf{w}_V^{K'} \cdot \boldsymbol{\sigma}$. Explicit expressions for the current matrices and single-nucleon responses are given in Ref. [6].

The momentum distribution for residual nucleus $|B\rangle$ is defined in general as the spin matrix

$$n(\mathbf{p})_{s's} = \sum_{M_B} \langle B | a_{\mathbf{p},s} | A \rangle^* \langle B | a_{\mathbf{p},s'} | A \rangle, \quad (92)$$

where the spin J_B is fixed and we sum over undetected orientations of the daughter nucleus. Therefore the definition of the scalar M^S and vector \mathbf{M}^V momentum distributions is

$$n(\mathbf{p}) = \frac{1}{2} (M^S(\mathbf{p}) + \mathbf{M}^V(\mathbf{p}) \cdot \boldsymbol{\sigma}). \quad (93)$$

Obviously, the polarized momentum distribution depends upon the initial state $|A\rangle$, the final state $|B\rangle$ and the polarization angles Ω^* , apart from the missing momentum \mathbf{p} . When we need to clarify this dependence below, we sometimes write in the momentum distribution the explicit process to which we are referring as an argument, for example, $n[A(\Omega^*) \rightarrow B]$.

4.2 Momentum distributions of hole nuclei

Here we obtain the polarized momentum distribution in the particular case of a hole nucleus. For the general expression of the polarized spectral function of deformed nuclei, see Ref. [7]. In this work we are also interested in examining in more detail the relations between the single-particle momentum distribution and that of the whole nucleus in the extreme shell model, and thus we will follow a somewhat different approach (although one that is completely equivalent). For this reason we begin examining the polarized momentum distribution of a single particle (or hole) in a shell.

4.2.1 Single-particle momentum distribution

Let us consider a single particle in the bound state $|jj(\Omega^*)\rangle = \sum_m \mathcal{D}_{mj}^{(j)} |jm\rangle$ of a mean field; here one should understand there to be the argument Ω^* in all the rotation matrices, polarized states and momentum distributions. In this simple case, the momentum distribution can be written as the matrix element

$$n_{s's}[j(\Omega^*)] = \langle \mathbf{p} s' | N[j(\Omega^*)] | \mathbf{p} s \rangle \quad (94)$$

of the spin density operator $N[j(\Omega^*)]$ which projects onto the state $|jj^*\rangle$

$$N[j(\Omega^*)] = |jj^*\rangle\langle jj^*| = \sum_{mm'} \mathcal{D}_{m'j}^{(j)} \mathcal{D}_{mj}^{(j)*} |jm'\rangle\langle jm|. \quad (95)$$

Expanding the product of the two rotation matrices, we are able to write a multipole expansion for the operator $N[j(\Omega^*)]$ in a basis of spherical harmonics of the polarization angle:

$$N[j(\Omega^*)] = \sum_{\mathcal{J}} f_{\mathcal{J}}^j N^{\mathcal{J}}[j(\Omega^*)], \quad (96)$$

where $N^{\mathcal{J}}[j(\Omega^*)]$ is the operator of rank \mathcal{J} in the expansion, given by

$$N^{\mathcal{J}}[j(\Omega^*)] = \sqrt{4\pi} \sum_{mm'\mathcal{M}} (-1)^{j+m+\mathcal{J}} \begin{pmatrix} j & j & \mathcal{J} \\ -m & m' & \mathcal{M} \end{pmatrix} Y_{\mathcal{J}\mathcal{M}}(\Omega^*) |jm'\rangle\langle jm|. \quad (97)$$

A similar expansion can be written for the case of a single hole, namely, the focus in the present work. In the shell model a hole is described by a single-particle state with wave function $|\widetilde{jj^*}\rangle = \sum_m \mathcal{D}_{mj}^{(j)*} |\widetilde{j\widetilde{m}}\rangle$, i.e., the time inversion of the single-particle state, with $|\widetilde{j\widetilde{m}}\rangle = (-1)^{j+m} |j, -m\rangle$. In this case one can prove that the corresponding spin-density matrix operator multipole expansion can be written as

$$N[\widetilde{j(\Omega^*)}] = \sum_{\mathcal{J}} f_{\mathcal{J}}^j (-1)^{\mathcal{J}} N^{\mathcal{J}}[j(\Omega^*)], \quad (98)$$

where we have used the fact that the spin-density multipoles of particles and holes differ only by the phase factor $(-1)^{\mathcal{J}}$. This is a consequence of the fact that the state $|j, -j\rangle$ rotated by an angle Ω^* is the same as the state $|jj\rangle$ rotated by an angle $-\Omega^*$ and of the parity $(-1)^{\mathcal{J}}$ of the spherical harmonics which are the basis of the multipole expansion.

4.2.2 Hole nucleus

In analogy with the single-particle case, we can write the momentum distribution as the matrix element of a one-body density matrix. In fact, consider the transition

$$|A\rangle = |i^{-1}(\Omega^*)\rangle \rightarrow |B\rangle = |(h^{-1}i^{-1})J_B\rangle. \quad (99)$$

Inserting the appropriate matrix elements of the destruction operator into the momentum distribution, Eq. (92), we obtain

$$n_{s's}(\mathbf{p}) = \langle \mathbf{p}s' | N [i^{-1}(\Omega^*) \rightarrow (h^{-1}i^{-1})J_B] | \mathbf{p}s \rangle, \quad (100)$$

where $N [i^{-1}(\Omega^*) \rightarrow (h^{-1}i^{-1})J_B]$ is the spin density matrix operator

$$\begin{aligned} N [i^{-1}(\Omega^*) \rightarrow (h^{-1}i^{-1})J_B] = \\ \sum_{M_B} \sum_{m_h m'_i} \sum_{m'_h m''_i} \langle j_h m_h j_i m'_i | J_B M_B \rangle \langle j_h m'_h j_i m''_i | J_B M_B \rangle \mathcal{D}_{m'_i j_i}^{(j_i)*} \mathcal{D}_{m''_i j_i}^{(j_i)} |\widetilde{h m'_h}\rangle \langle \widetilde{h m_h}|. \end{aligned} \quad (101)$$

Expanding again the product of the two rotation matrices we obtain a sum of the product of three $3-j$ coefficients, that can be written as a $6-j$ coefficient times a $3-j$ coefficient. As consequence, we straightforwardly obtain the multipole expansion

$$N [i^{-1}(\Omega^*) \rightarrow (h^{-1}i^{-1})J_B] = \sum_{\mathcal{J}} f_{\mathcal{J}}^i N^{\mathcal{J}} [i^{-1}(\Omega^*) \rightarrow (h^{-1}i^{-1})J_B], \quad (102)$$

with the simple relationship between the nuclear multipoles and the single-hole h results:

$$N^{\mathcal{J}} [i^{-1}(\Omega^*) \rightarrow (h^{-1}i^{-1})J_B] = [J_B]^2 (-1)^{j_i+j_h+J_B+\mathcal{J}} \left\{ \begin{matrix} j_h & j_h & \mathcal{J} \\ j_i & j_i & J_B \end{matrix} \right\} N^{\mathcal{J}}[h(\Omega^*)]. \quad (103)$$

This relation is the same as the one found between the reduced nuclear responses and the responses of the shell h (see Eq. (76)). In fact, the general equations of the last section are of course also applicable to the PWIA when we take the single-particle state $|E'lj\rangle$ to be a free wave function, i.e, proportional to a Bessel function. Therefore, Eq. (76) had to be valid also in PWIA. And that fact is again recovered here in another completely different way, providing a test of both formalisms. But also the fact that the relation between momentum distributions can be extended to response functions even with FSI leads us to believe that some information about the single-particle momentum distribution can be extracted from these kinds of observables. It is remarkable that, although the FSI involving the ejected nucleon destroys the factorization of the cross section, it does not modify the relation in Eq. (103), implying that this property is general for the independent-particle model.

Until now we have only considered the case $h \neq i$. The other situation $h = i$ that arises when the particle is ejected from the polarized shell is analogous, with the exception that now the residual nucleus has a wave function with a factor $2^{-1/2}$

$$|B\rangle = \frac{1}{\sqrt{2}} [b_i^\dagger b_i^\dagger]_{J_B M_B} |C\rangle. \quad (104)$$

Therefore the expression for the momentum distribution as the matrix element of a spin density matrix operator is

$$n_{s's} [i^{-1}(\Omega^*) \rightarrow (i^{-1}i^{-1})B] = \langle \mathbf{p}s' | N [i^{-1}(\Omega^*) \rightarrow (i^{-1}i^{-1})B] | \mathbf{p}s \rangle \quad (105)$$

with

$$N^{\mathcal{J}} [i^{-1}(\Omega^*) \rightarrow (i^{-1}i^{-1})J_B] = 2[J_B]^2 (-1)^{1+\mathcal{J}} \left\{ \begin{matrix} j_i & j_i & \mathcal{J} \\ j_i & j_i & J_B \end{matrix} \right\} N^{\mathcal{J}}[i(\Omega^*)], \quad (106)$$

and we again recover the relation in Eq. (81) between reduced response functions in the shell model.

These relations between the multipole components of the density matrix lead us to obtain sum rules when summing over the values of J_B , as we did for the responses in the shell model. In fact, performing the sum over J_B in the case $h \neq i$ we obtain a the result analogous to Eq. (80)

$$\sum_{J_B} N [i^{-1}(\Omega^*) \rightarrow (h^{-1}i^{-1})J_B] = [j_h]^2 N[h]_{unpol}, \quad (107)$$

where $N[h]_{unpol}$ is the unpolarized density matrix of the single-particle wave function. This result was also obtained in Ref. [6] in relation with the inclusive PWIA, where the final state B is not observed and the sum over J_B must be performed. Strictly speaking, what in Ref. [6] is called *polarized momentum distribution*

of a shell actually is the matrix element of the sum over J_B given by Eq. (107). Then we can say that the momentum distribution of a complete shell ($h \neq i$) is the sum over all of the unpolarized momentum distributions of all of the particles in the shell.

In the case $h = i$ we have the restriction $J_B = \text{even}$. The sum over J_B gives an equation similar to Eq. (85), and the total density matrix is

$$\sum_{J_B=\text{even}} N [i^{-1}(\Omega^*) \rightarrow (h^{-1}i^{-1})J_B] = [j_i]^2 N[i]_{unpol} - N[i(-\Omega^*)], \quad (108)$$

which corresponds to Eq. (87) at the response level. This result was also obtained in Ref. [6] for the polarized momentum distribution of a shell with a hole: it is equal to the unpolarized momentum distribution of the complete shell minus the polarized momentum distribution of the hole, although in this work we are able to explain geometrically the origin of the factors $(-1)^J$ that appeared in that reference and also to understand the fact that the momentum distribution of a hole is equal to the momentum distribution of a particle pointing in the opposite direction.

4.3 Scalar and vector momentum distributions

Until now we have seen that when the polarized momentum distribution (or in general the spin density matrix operator) of hole nuclei is expanded in multipoles of the polarization angles, each one of the individual multipoles is proportional to the corresponding multipole of the single-particle momentum distribution of the struck nucleon. Therefore the same proportionality relation also holds for the scalar and vector pieces in Eq. (93) of that spin operator. Thus we only need to describe the scalar and vector momentum distributions of a single particle in the state $|j(\Omega^*)\rangle$. A detailed derivation of these expressions was performed in Ref. [6]. Therefore here we only write the results in a way more suited to use in the exclusive responses. The multipole expansion for the scalar and vector momentum distributions reads

$$M^S[j(\Omega^*)] = \sum_{\mathcal{J}} f_{\mathcal{J}}^j P_{\mathcal{J}}^+ M_{\mathcal{J}}^S[j(\Omega^*)] \quad (109)$$

$$\mathbf{M}^V[j(\Omega^*)] = \sum_{\mathcal{J}} f_{\mathcal{J}}^j P_{\mathcal{J}}^- \mathbf{M}_{\mathcal{J}}^V[j(\Omega^*)], \quad (110)$$

where in addition we have used the result that only even (odd) multipoles enter in the expansion of the scalar (vector) momentum distribution for a single particle. Although not explicitly written, the functions $M_{\mathcal{J}}^S$ and $\mathbf{M}_{\mathcal{J}}^V$ depend on (Ω^*, \mathbf{p}) . The only scalar that can be constructed with $Y_{\mathcal{J}\mathcal{M}}(\Omega^*)$ and \mathbf{p} is $[Y_{\mathcal{J}}(\Omega^*)Y_{\mathcal{J}}(\hat{\mathbf{p}})]_{00}$, therefore the scalar momentum distribution for a single particle has the form

$$M_{\mathcal{J}}^S(\Omega^*, \mathbf{p}) = m_{\mathcal{J}}^S(p) [Y_{\mathcal{J}}(\Omega^*)Y_{\mathcal{J}}(\hat{\mathbf{p}})]_{00}. \quad (111)$$

Also, the vector momentum distribution can be written as a linear combination

$$\mathbf{M}_{\mathcal{J}}^V(\Omega^*, \mathbf{p}) = \sum_{\mathcal{J}'=\mathcal{J}\pm 1} m_{\mathcal{J}\mathcal{J}'}^V(p) \mathbf{X}_{\mathcal{J}\mathcal{J}'}(\Omega^*, \mathbf{p}) \quad (112)$$

of the vectors $\mathbf{X}_{\mathcal{J}\mathcal{J}'}(\Omega^*, \mathbf{p})$ with spherical components

$$X_{\mathcal{J}\mathcal{J}'}(\Omega^*, \mathbf{p})_{\alpha} \equiv [Y_{\mathcal{J}}(\Omega^*) Y_{\mathcal{J}'}(\hat{\mathbf{p}})]_{1\alpha}. \quad (113)$$

Finally, the functions $m_{\mathcal{J}}^S(p)$ and $m_{\mathcal{J}\mathcal{J}'}^V(p)$ for a particle are given by

$$m_{\mathcal{J}}^S[j(\Omega^*)] = 2A_{\mathcal{J}}[j]^2 |\tilde{R}(p)|^2 \quad (114)$$

$$m_{\mathcal{J}\mathcal{J}'}^V[j(\Omega^*)] = -\frac{2}{\sqrt{3}} A_{\mathcal{J}\mathcal{J}'}[j]^2 |\tilde{R}(p)|^2, \quad (115)$$

where $\tilde{R}(p) = \sqrt{2/\pi} \int_0^\infty dr r^2 j_l(pr) R(r)$ is the radial wave function in momentum space, normalized to $\int_0^\infty dp p^2 |\tilde{R}(p)|^2 = 1$, and the factors $A_{\mathcal{J}}$ and $A_{\mathcal{J}\mathcal{J}'}$ are coupling coefficients which can be found in Ref. [6]. Finally, the same relations in Eqs. (111,112) are valid for the scalar and vector momentum distributions for the process $i^{-1}(\Omega^*) \rightarrow (h^{-1}i^{-1})J_B$ and we have the following result:

$$m_{\mathcal{J}}^S [i^{-1}(\Omega^*) \rightarrow (h^{-1}i^{-1})J_B] = (1 + \delta_{hi}) [J_B]^2 (-1)^{j_i+j_h+J_B+\mathcal{J}} \left\{ \begin{matrix} j_h & j_h & \mathcal{J} \\ j_i & j_i & J_B \end{matrix} \right\} m_{\mathcal{J}}^S[h(\Omega^*)] \quad (116)$$

and a similar result for $m_{\mathcal{J}\mathcal{J}'}^V [i^{-1}(\Omega^*) \rightarrow (h^{-1}i^{-1})J_B]$ in terms of the single particle vector multipole $m_{\mathcal{J}\mathcal{J}'}^V[h(\Omega^*)]$.

4.4 Single-nucleon current and exclusive nuclear responses in PWIA

For the single-nucleon current we follow the formalism of Refs. [9, 6], where the on-shell relativistic electromagnetic single-nucleon current was expanded up to order $\eta = p/M$, but keeping all orders and not expanding in the dimensionless variables $\kappa = q/2M$ and $\lambda = \omega/2M$. The expressions for the charge and transverse current components in the coordinate system used in this work are given in Ref. [6], where also can be found the expressions for the single-nucleon responses w^K . The important point here, and used for the results of next section, is that the L , T , TL and TT single-nucleon responses are spin-independent, while the T' and TL' ones involve linear combinations of the Pauli spin matrices.

We now have all of the ingredients needed to obtain the reduced responses of a one-hole nucleus in PWIA. The following equations have been derived for a one-hole nucleus, although actually they are a little more general — in fact, they are valid for any nuclear model as long as the multipoles of the scalar and vector momentum distributions can be written as in Eqs. (111,112).

For comparison with the general model it is convenient to write the responses in a form similar to Eqs. (61–69). Therefore, for the unprimed responses that are proportional to the

scalar momentum distribution M^S , we develop the (real) scalar coupling of two spherical harmonics as in Eq. (53):

$$[Y_{\mathcal{J}}(\Omega^*)Y_{\mathcal{J}}(\hat{\mathbf{p}})]_{00} = \sum_{\mathcal{M}=0}^{\mathcal{J}} P_{\mathcal{J}}^{\mathcal{M}}(\cos \theta^*) \cos[\mathcal{M}\Delta\phi] h_{\mathcal{J}\mathcal{J}00}^{\mathcal{M}}(\theta), \quad (117)$$

and so we have

$$M_{\mathcal{J}}^S(\Omega^*, \hat{\mathbf{p}}) = \sum_{\mathcal{M}=0}^{\mathcal{J}} P_{\mathcal{J}}^{\mathcal{M}}(\cos \theta^*) \cos[\mathcal{M}\Delta\phi] h_{\mathcal{J}\mathcal{J}00}^{\mathcal{M}}(\theta) m_{\mathcal{J}}^S(p), \quad (118)$$

where $m_{\mathcal{J}}^S$ refers to the considered transition (see Eq. (116)). For the vector momentum distribution we need to develop the three components of the vector $\mathbf{X}_{\mathcal{J}\mathcal{J}'}$ in terms of the functions $h_{\mathcal{J}\mathcal{J}'11}^{\mathcal{M}}$, $\tilde{h}_{\mathcal{J}\mathcal{J}'11}^{\mathcal{M}}$ and $h_{\mathcal{J}\mathcal{J}'10}^{\mathcal{M}}$ in a similar way.

As for the nuclear responses, using Eq. (118) we see that the scalar momentum distribution depends on the azimuthal angles only via $\cos \mathcal{M}\Delta\phi$, where $\Delta\phi = \phi' - \phi^*$, but not on $\phi = \phi'$ or ϕ^* independently. The only dependence of the nuclear responses on ϕ is therefore through the single-nucleon responses w^{TL} and w^{TT} , see Ref. [6]. Then it is straightforward to read off the following expressions for the angular reduced responses:

$$W_{\mathcal{J}\mathcal{M}}^{L(+)} = \frac{Mp'}{4\pi}(\rho_c^2 + \rho_{so}^2\delta^2)h_{\mathcal{J}\mathcal{J}00}^{\mathcal{M}}(\theta)m_{\mathcal{J}}^S(p) \quad (119)$$

$$W_{\mathcal{J}\mathcal{M}}^{T(+)} = \frac{Mp'}{4\pi}(2J_m^2 + J_c^2\delta^2)h_{\mathcal{J}\mathcal{J}00}^{\mathcal{M}}(\theta)m_{\mathcal{J}}^S(p) \quad (120)$$

$$W_{\mathcal{J}\mathcal{M}}^{TL(+)} = \frac{Mp'}{4\pi}2\sqrt{2}(\rho_c J_c + \rho_{so} J_m)\delta h_{\mathcal{J}\mathcal{J}00}^{\mathcal{M}}(\theta)m_{\mathcal{J}}^S(p) \quad (121)$$

$$W_{\mathcal{J}\mathcal{M}}^{TT(+)} = -\frac{Mp'}{4\pi}J_c^2\delta^2 h_{\mathcal{J}\mathcal{J}00}^{\mathcal{M}}(\theta)m_{\mathcal{J}}^S(p). \quad (122)$$

The odd-rank unprimed responses and the $\widetilde{W}_{\mathcal{J}\mathcal{M}}^{TL(+)}$ and $\widetilde{W}_{\mathcal{J}\mathcal{M}}^{TT(+)}$ responses are zero in PWIA. Here $\delta = \eta \sin \theta$ labels the order of the relativistic correction and (θ, ϕ) is the direction of the missing momentum \mathbf{p} . The factors ρ_c (charge), ρ_{so} (spin-orbit), J_m (magnetization) and J_c (convection) come from the electromagnetic charge and current operators; they are only (q, ω) -dependent, and are defined by (see Ref. [6])

$$\rho_c = \frac{\kappa}{\sqrt{\tau}}G_E \quad (123)$$

$$\rho_{so} = \frac{2G_M - G_E}{\sqrt{1+\tau}}\frac{\kappa}{2} \quad (124)$$

$$J_m = \sqrt{\tau}G_M \quad (125)$$

$$J_c = \frac{\sqrt{\tau}}{\kappa}G_E, \quad (126)$$

where G_E , G_M are the electric and magnetic form factors of the nucleon for which we use the Galster parametrization [12].

Finally, for the primed responses, after performing the scalar product between \mathbf{M}^V and $\mathbf{w}_V^{K'}$ we obtain

$$W_{\mathcal{J}\mathcal{M}}^{T'(-)} = -\frac{Mp'}{2\pi} \sum_{\mathcal{J}'=\mathcal{J}\pm 1} \left[J_m^2 h_{\mathcal{J}\mathcal{J}'10}^{\mathcal{M}}(\theta) + \sqrt{2} J_c J_m \delta h_{\mathcal{J}\mathcal{J}'11}^{\mathcal{M}}(\theta) \right] m_{\mathcal{J}\mathcal{J}'}^V(p) \quad (127)$$

$$W_{\mathcal{J}\mathcal{M}}^{TL'(-)} = -\frac{Mp'}{\sqrt{2}\pi} \sum_{\mathcal{J}'=\mathcal{J}\pm 1} \left[\sqrt{2} \rho_c J_m h_{\mathcal{J}\mathcal{J}'11}^{\mathcal{M}}(\theta) + \rho_{so} J_m \delta h_{\mathcal{J}\mathcal{J}'10}^{\mathcal{M}}(\theta) \right] m_{\mathcal{J}\mathcal{J}'}^V(p) \quad (128)$$

$$\widetilde{W}_{\mathcal{J}\mathcal{M}}^{TL'(-)} = -\frac{Mp'}{\pi} \sum_{\mathcal{J}'=\mathcal{J}\pm 1} (\rho_c J_m - \rho_{so} J_c \delta^2) \widetilde{h}_{\mathcal{J}\mathcal{J}'11}^{\mathcal{M}}(\theta) m_{\mathcal{J}\mathcal{J}'}^V(p). \quad (129)$$

All of the other responses not written here are exactly zero in PWIA.

5 Results and discussion

In this section we present numerical results for the reaction $^{39}\text{K}(\vec{e}, e'p)^{38}\text{Ar}$ in the shell model for both PWIA and with FSI, namely the distorted-wave impulse approximation (DWIA). An overview is provided in Sec. 5.1, followed by Sec. 5.2 where detailed results are shown and discussed. Section 5.3 contains a brief discussion of the relativistic corrections incorporated in our model. Throughout all of these sections we have had to select only the most important results for presentation, since the entire set vastly exceeds what can be shown in published form. A more complete set of figures may be found on the WWW [21]. The reader is directed to the conclusions in the next section for discussion of what can be learned from such studies.

The bound states of the target and daughter nuclei are represented by one-hole and two-holes in the core of ^{40}Ca , as discussed in Sec. 2 and in Ref. [6]. It is clear that more sophisticated treatments of nuclei such as ^{39}K and ^{38}Ar than the extreme shell model we are using in this work can also be studied, however, since our aims here and in the next paper [19] are to analyze how FSI effects are reflected in the various polarization observables and to determine if it is possible to obtain information about the different pieces of the polarized momentum distribution or about the FSI with these kinds of measurements, this basic model should provide an adequate starting point. Indeed, given the complexity that already exists for our basic model and the fact that no such extensive study for a complex nucleus is available, the initial studies presented in Refs. [7, 15, 8] being all that we are aware of for coincidence polarization observables, at this time explorations with more sophisticated nuclear configurations are probably unwarranted. Of course, when experimental studies of this type become imminent these extensions can be undertaken.

In our modeling the single-particle bound wave functions and (negative) energies are obtained using a mean-field potential of Woods-Saxon type, using the values of the potential parameters that may be found in Refs. [11, 16]. For the ejectile wave function we solve the Schrödinger equation for positive energies using a (local) complex optical potential fitted to proton elastic scattering data. For the particular case of the nucleus ^{39}K we use the potential of Schwandt *et al.* [17], that was fitted to cross section and analyzing power

angular distributions for a number of target nuclei and polarized protons of 80–180 MeV. Although the daughter nucleus ^{38}Ar was not included in this analysis, it falls in the range $24 < A < 208$ of applicability of the Schwandt potential. As a first test of our model, we have computed the cross section and analyzing powers for proton scattering from a variety of nuclei with different optical potentials and have compared the results with the literature. In particular, we have reproduced the calculations shown in Figs. 2 and 3 of Ref. [17] for the analyzing power of protons elastically scattered from ^{24}Mg , ^{28}Si , ^{40}Ca , ^{90}Zr and ^{208}Pb at different energies, using the Schwandt potential.

The normalization of the partial wave (l, j) with energy ϵ and wave number $k = \sqrt{2M\epsilon}$ is determined by the following asymptotic condition for the radial wave function

$$R_{lj}(r) \sim \sqrt{\frac{2M}{\pi\hbar^2 k}} e^{i(\sigma_l + \delta_{lj})} \sin\left(kr - \eta \log 2kr - l\frac{\pi}{2} + \sigma_l + \delta_{lj}\right), \quad (130)$$

where δ_{lj} is the complex nuclear phase-shift and σ_l is the Coulomb phase-shift. In the limit when the imaginary part of the potential goes to zero, the radial wave functions are normalized with a Dirac δ -function containing the energies, so that condition in Eq. (8) is satisfied. The imaginary part of the potential modifies the normalization of the continuum states, since the flux of outgoing particles is reduced due to the absorptive property of the optical potential. In addition, in this model the continuum nuclear wave functions are no longer orthogonal to the bound ones. However, at high momentum transfer $q \sim 500$ MeV/c and near quasi-free conditions where $p' \sim q$, the orthogonality between the bound and high-momentum ejected particles is approximately satisfied. Several prescriptions to restore orthogonality and to take into account non-locality effects have been proposed, such as the inclusion of Perey-like factors [18] in the wave functions. In our calculations we include a Perey factor of the kind

$$f(r) = \left[1 - \frac{M\beta^2}{2\hbar^2} \text{Re}V_C(r)\right]^{-1/2}, \quad (131)$$

where V_C is the central part of the optical potential and we take the non-locality parameter $\beta = 0.85$ fm.

In order to take into account relativistic effects that are important for high momentum transfer we use relativistic kinematics in all of the calculations [6]. For nucleon knockout from shell h we compute the momentum of the ejected particle with kinetic energy $\epsilon' = \epsilon_h + \omega$ using the relativistic energy-momentum relation $p'^2 = (M + \epsilon')^2 - M^2$. In the shell model we solve the Schrödinger equation with eigenvalue $\epsilon'(1 + \epsilon'/2M)$.

In DWIA the sums over partial waves or multipoles J are infinite, while in practice we must sum all multipoles until convergence is reached. In this work we test the degree of convergence by comparing with the exact result in factorized PWIA. In fact, in the limit in which the optical potential goes to zero, the DWIA and PWIA approaches should be identical and therefore in that limit we adjust the number of multipoles so that differences with exact PWIA responses are indistinguishable. The number of multipoles needed to reach convergence is in general greater than in the inclusive case [6]. For example, for ^{39}K at $q = 500$ and 700 MeV/c in the region of the quasielastic peak it is enough to include multipoles up to $J = 15$ and 23 , respectively, for the inclusive responses, while for the

exclusive process we need to sum up to $J = 22$ and 32 , respectively. The reason is that in the inclusive case the integration over the angles $\hat{\mathbf{p}}'$ of the ejectile is performed analytically. In all of the calculations that follow we include multipoles up to $J = 32$.

5.1 Overview of the responses

We apply the formalism of previous sections to the nucleus ^{39}K . In our model we describe the ground state as a proton hole in the shell $1d_{3/2}$. Therefore we have $J_i = 3/2$. Since $\mathcal{J} = 0, \dots, 2J_i$, the angular reduced response functions $W_{\mathcal{J}\mathcal{M}}^{K(\pm)}$ and $\widetilde{W}_{\mathcal{J}\mathcal{M}}^{K(\pm)}$ that enter in Eqs. (61,69) range from $(\mathcal{J}, \mathcal{M}) = (0, 0)$ to $(\mathcal{J}, \mathcal{M}) = (3, 3)$. Taking into account that all of the responses with a tilde are zero for $\mathcal{M} = 0$ (because they are defined as the coefficient of $\sin \mathcal{M} \Delta \phi$), we are confronted with a total of 72 angular reduced response functions (only 32 of them are nonzero in PWIA).

In this work we focus our study of polarization observables upon a systematic analysis of the complete set of angular reduced response functions, which contain all of the information about the process. An analysis of more direct observables, such as cross sections and asymmetries for different values of the polarization angle is in progress [19].

We discuss only the case in which the daughter nucleus ^{38}Ar is in the ground state $J_B = 0^+$, which we describe as a $d_{3/2}$ two-hole nucleus. Under knockout from the $d_{3/2}$ shell the daughter nucleus also can be in a $J_B = 2^+$ state, but as proven in Sec. 3, the reduced response functions $W_{\mathcal{J}\mathcal{M}}^{K(\pm)}$ for the two possible values of J_B differ only in a constant recoupling coefficient (see Eq. (81)) and therefore they are proportional in this simple model, so no new information is obtained from their analysis. Of course, in a more sophisticated treatment of the nuclear structure, configuration mixing will produce deviations from this proportionality theorem, which may prove to be useful in obtaining new information about the nuclear structure involved.

In theory the angular reduced response functions $W_{\mathcal{J}\mathcal{M}}^{K(\pm)}$ and $\widetilde{W}_{\mathcal{J}\mathcal{M}}^{K(\pm)}$ could be extracted by performing a number of measurements with different electron helicity h , target polarization Ω^* , azimuthal emission angle ϕ , and, additionally, a Rosenbluth analysis in order to separate the longitudinal from the transverse responses. The number of ways to carry out the extraction is not unique. For example, a discussion of the minimal asymmetry measurements needed to extract the reduced response functions in deuteron electrodisintegration is given in Ref. [20], although in the ^{39}K case the presence of the octupole terms $\mathcal{J} = 3$, which do not appear in the deuteron case, modifies the extraction rules given in that reference. Rather than discussing the separation procedure or even to attempt to discuss the entire set of reduced responses in great detail, our goal in the following analysis in the present work is to take into account that some of these reduced responses are very small relative to the unpolarized ones, and hence to focus on those with the largest magnitude. We postpone any detailed discussion of cross sections and asymmetries for future presentation [19].

The angular reduced response functions are defined in Eqs. (61–69). Those without a tilde $W_{\mathcal{J}\mathcal{M}}^K$ are multiplied in the cross section by $\cos \mathcal{M} \Delta \phi$, while the responses with a tilde $\widetilde{W}_{\mathcal{J}\mathcal{M}}^K$ are multiplied by $\sin \mathcal{M} \Delta \phi$. Therefore the latter are zero for $\mathcal{M} = 0$ or $\Delta \phi = 0$, and hence the tilde responses do not contribute to the cross section when the target is

Ia $q = 300 \text{ MeV/c}$ $\omega = 40 \text{ MeV}$ $p' = 244.3 \text{ MeV/c}$ $\epsilon' = 31.3 \text{ MeV}$	Ib $q = 300 \text{ MeV/c}$ $\omega = 56 \text{ MeV}$ $p' = 301.6 \text{ MeV/c}$ $\epsilon' = 47.3 \text{ MeV}$	Ic $q = 300 \text{ MeV/c}$ $\omega = 80 \text{ MeV}$ $p' = 372.6 \text{ MeV/c}$ $\epsilon' = 71.3 \text{ MeV}$
IIa $q = 500 \text{ MeV/c}$ $\omega = 110 \text{ MeV}$ $p' = 447.6 \text{ MeV/c}$ $\epsilon' = 101.3 \text{ MeV}$	IIb $q = 500 \text{ MeV/c}$ $\omega = 133.5 \text{ MeV}$ $p' = 499.7 \text{ MeV/c}$ $\epsilon' = 124.8 \text{ MeV}$	IIc $q = 500 \text{ MeV/c}$ $\omega = 160 \text{ MeV}$ $p' = 553.9 \text{ MeV/c}$ $\epsilon' = 151.3 \text{ MeV}$
IIIa $q = 700 \text{ MeV/c}$ $\omega = 180 \text{ MeV}$ $p' = 592.3 \text{ MeV/c}$ $\epsilon' = 171.3 \text{ MeV}$	IIIb $q = 700 \text{ MeV/c}$ $\omega = 241 \text{ MeV}$ $p' = 699.9 \text{ MeV/c}$ $\epsilon' = 232.3 \text{ MeV}$	IIIc $q = 700 \text{ MeV/c}$ $\omega = 300 \text{ MeV}$ $p' = 794.6 \text{ MeV/c}$ $\epsilon' = 291.2 \text{ MeV}$

Table 1: *Values of the momentum and energy transfer (q, ω) , and of the momentum p' and kinetic energy ϵ' for which the reduced response functions have been computed.*

longitudinally polarized, i.e. in the direction of \mathbf{q} (L -polarized) or $-\mathbf{q}$, because in those cases $\cos\theta^* = \pm 1$ and the Legendre function $P_{\mathcal{J}}^{\mathcal{M}}(\pm 1) = 0$ for $\mathcal{M} \neq 0$. Also they do not contribute when the azimuthal angles of the polarization direction ϕ^* and the emission direction ϕ are the same ($\Delta\phi = 0$). As noted above, the total number of angular reduced response functions for nucleon knockout from the $d_{3/2}$ shell of ^{39}K is 72, which is too large for a complete presentation and therefore in the following we only show figures for the most relevant. The complete set of figures is presently available from the authors [21].

The polarized responses $W_{\mathcal{J}\mathcal{M}}^{K(\pm)}$ and $\widehat{W}_{\mathcal{J}\mathcal{M}}^{K(\pm)}$ depend on the three variables (q, ω, p) , since the missing energy is determined. In order to study their dependence on all of the variables, we have computed the entire set of responses as functions of the missing momentum p for nine values of (q, ω) . In each one of the following figures we show a particular response function and each figure is composed of nine panels corresponding to the values of (q, ω) given in Table 1. In each one of the rows in the table the value of q is fixed to one of the three values $q = 300 \text{ MeV/c}$ (regions Ia, Ib, Ic), $q = 500 \text{ MeV/c}$ (regions IIa, IIb, IIc) or $q = 700 \text{ MeV/c}$ (regions IIIa, IIIb, IIIc). We show three values of ω for each q . The second column corresponds approximately to the quasielastic peak (QEP) defined by $p' \simeq q$. The first column corresponds to slightly below the peak, $p' < q$, while the third column is in the region above the QEP, $p' > q$. The values of the momentum p' and kinetic energy ϵ' of the ejectile for each of the panels are also shown in Table 1.

First notice that the Schwandt optical potential we use was originally parametrized for elastic scattering of protons with energies between 80 and 180 MeV, and therefore it has been extrapolated in some of the kinematic regions. Also the daughter nucleus ^{38}Ar was not used

in the analysis of Schwandt *et al.*, but it is in the mass range of the nuclei originally used. One of the aims of this work is to analyze the sensitivity of the different responses to the FSI model, and, in particular, in each one of the panels in Figs. 1–15 we show four curves, each one corresponding to a particular model for the final proton state. Specifically, the solid lines have been computed with the complete optical potential, while for the dashed lines we have set the spin-orbit potential (SOP) equal to zero (both real and imaginary parts). Thus comparison between solid and dashed lines shows the effect of the SOP in the responses. These two curves do not include a Perey factor in the wave function, and therefore we also show with dot-dashed lines the same responses computed with the total potential and with Perey parameter $\beta = 0.85$ in the wave function. Finally, the dotted curves correspond to the PWIA, that is, they do not include FSI.

In order to get a feeling about the relative order of magnitude of the 72 responses it is convenient to choose some quantity which characterizes the importance of each response. The total variation of a response defined as the maximum minus the minimum values $\Delta W_{\mathcal{JM}}^{K(\pm)} \equiv W_{\mathcal{JM}}^{K(\pm)}(\text{max}) - W_{\mathcal{JM}}^{K(\pm)}(\text{min})$, that is always positive, is a quantity that is very useful for that purpose. Specifically, we take the variation of the unpolarized longitudinal $\Delta W_{00}^{L(+)}$ as reference and therefore give the others as a percentage of this response, so the variation of the unpolarized longitudinal response is 100% by definition. We have computed the total variation of all of the responses using the complete optical potential for the nine kinematic conditions and the results are shown in Tables 2–4 for $q = 300, 500$ and 700 MeV/c, respectively. Note that under the columns for the L , T and T' responses both kinds of responses (with and without tilde) are displayed because in these cases there is no confusion: the L and T responses without (with) tilde are always of even (odd) rank, while the opposite happens for the T' responses.

With reference to the PWIA responses, only the 32 responses given in Eqs. (119–129) survive in that limit. Therefore, a total of 40 of the 72 responses are exclusively due to the FSI, and then it is expected that they will be especially sensitive to the details of the interaction, as we shall show below for some of the more important cases.

5.2 Detailed discussion of selected responses

5.2.1 L-responses

Unpolarized response. The unpolarized response $W_{00}^{L(+)}$ displayed in Fig. 1 serves to set the scale of the remaining responses. The three panels in the middle row of Table 1 at $q = 500$ MeV/c are representative and well within the range of validity of the Schwandt potential. The one in the middle at $\omega = 133.5$ MeV (region IIb) approximately corresponds to the QEP. The FSI (solid lines) produce a reduction of the plane-wave results (dotted lines) of about 35%. When we set the SOP to zero, the response increases by a few percent (dashed lines); also we see that the effect is bigger for higher energy. The introduction of a Perey factor slightly reduces the total response (dot-dashed lines), but the effect is very small. A significant effect of the FSI with respect to the PWIA is seen in the extreme cases, $q = 300$ MeV/c, $\omega = 40$ MeV (region Ia) and $q = 700$ MeV/c, $\omega = 300$ MeV (region IIIc), although these results should be viewed with caution, being far outside the range of validity

of the potential. Indeed, in the former case the real attractive part of the potential is too large, while in the latter the imaginary absorptive part is too large. In region IIIa ($q = 700$ MeV/c, $\omega = 180$ MeV) the spin-orbit interaction produces an increment of the response (the opposite to what happens in the other cases). The effect of the Perey factor decreases with the energy because it only depends on the real part of the potential, which also decreases with the energy (this conclusion is also applicable to the remaining responses).

Vector response. The vector longitudinal response $\widetilde{W}_{11}^{L(-)}$, shown in Fig. 2, is zero in PWIA. Thus it is due only to the FSI and expected to be more sensitive to details of the potential. In addition, it is not as large as the unpolarized one, but we find that it is large enough to make its extraction feasible — in fact, in region IIb at the maximum $p \simeq 150$ MeV/c, its magnitude is about 24% of $W_{00}^{L(+)}$ (see Table 3). In regions Ib,c and IIIb,c, it is even bigger. For instance, we see in Tables 2 and 4 that the variation $\Delta W_{11}^{L(-)}$ in regions Ib and IIIb is about 56% and 44%, respectively, of the unpolarized longitudinal.

Without the spin-orbit interaction this response is much larger and in some cases its behaviour as a function of p is even different. Specifically, in the QEP region (second column of Fig. 2) the SOP produces a small shift to the right, which is more important for low q . The same happens in the region to the right of the QEP. However, more important effects are seen below the QEP, where the response is significantly reduced by the spin-orbit interaction and its shape is smoothed and broadened. The effect is more pronounced at high energy; for instance, at $\omega = 180$ MeV (region IIIa) the SOP produces a reduction of the peak of more than 60%.

This response contributes the most to the cross section when the polarization is normal to q , namely at $\theta^* = 90^\circ$ because it is multiplied by a Legendre function $P_1^1(\cos \theta^*) = \sin \theta^*$, and for $\Delta\phi = \pm 90^\circ$. Therefore we expect the spin-orbit interaction to be important under these conditions. For example, for coplanar kinematics ($\phi = 0$) and normal (N) polarized ^{39}K ($\theta^* = \phi^* = 90^\circ$), where $\Delta\phi = \phi - \phi^* = -90^\circ$.

Quadrupole responses. In this case the PWIA responses $W_{2\mathcal{M}}^{L(+)}$ are nonzero and in general they are large, as seen in Tables 2–4. The biggest one corresponds to $\mathcal{M} = 0$, shown in Fig. 3, which contributes significantly for L -polarization: for instance, its size is about one-half of the unpolarized response in region IIb (see Table 3). For low p this response is in general negative and here the PWIA provides insight into why this happens. From Eq. (119), we see that this response is proportional to the angular function $h_{2200}^0(\theta)$ and to the radial function $m_2^S(p)$. From its definition, eqs. (53,54) it is easy to see that the function $h_{2200}^0(\theta)$ is proportional to $P_2^0(\cos \theta) = \frac{1}{2}(3\cos^2 \theta - 1)$, while the radial function $m_2^S(p)$, defined by Eq. (114), is proportional to the factor A_2 , given in ref. [6], which is proportional to a negative $3-j$ coefficient. Therefore, this response includes a factor $1 - 3\cos^2 \theta$. Below the QEP we have $p' < q$ and therefore, for p small, \mathbf{p} is almost anti-parallel to \mathbf{q} because $\mathbf{p} + \mathbf{q} = \mathbf{p}'$, and so the angle θ is near 180° and therefore $1 - 3\cos^2 \theta \simeq -2$ is negative and the total response is negative. As p increases, the angle θ quickly reaches a value near 90° degrees, and so the factor $1 - 3\cos^2 \theta \simeq 1$ changes its sign. This change in sign is almost immediate for QE conditions because $p' \sim q$, while above the QEP $p' > q$ and for p small

now $\theta \sim 0^\circ$ and again the response is negative and changes its sign as p increases. An interesting feature of this response is that the effect of the FSI is about the same as that in the unpolarized case in the QEP and above it, but below the QEP the FSI produce an increase of the response that is significant at low q . In fact, for fixed q (i.e., for each row in Fig. 3), we see that there is an inversion of the PWIA and DWIA responses at some point below the QEP between regions a and b (first and second columns of Fig. 3). At $q = 500$ MeV/c and QE conditions (region IIb) the effect of the SOP is somewhat bigger than in the unpolarized case.

5.2.2 T responses

Unpolarized response. The unpolarized response $W_{00}^{T(+)}$ shown in Fig. 4 presents features that are similar to those seen in the longitudinal one, with the exception that it is rather insensitive to the spin-orbit part of the interaction. As we can see in the figure, the solid and dashed lines are very similar. An interesting characteristic can be seen if we compare the behaviour of the variations $\Delta W_{00}^{T(+)}$ both in DWIA (Tables 2–4) and PWIA. In DWIA the total variation — relative to the longitudinal — increases with energy for $q = 500$ MeV/c from $\sim 100\%$ (region IIa) to $\sim 104\%$ (region IIc), see table 3, while in PWIA we have verified that the reverse occurs: there is a decrease from $\sim 101\%$ to $\sim 91\%$. Therefore one expects an increase of the T/L ratio with ω due to FSI, whereas in pure PWIA the T/L ratio decreases with energy. This means that the FSI is stronger in the L-response than in the T-response. As we can see comparing Figs. 1 and 4, this is due to the fact that the SOP produces an additional reduction of the L-response, while the T-response appears to be insensitive to the SOP.

Vector response The same behaviour of the small SOP effects in the unpolarized transverse response is also observed in the polarized T responses. For instance, the very large effect observed in the $\widetilde{W}_{11}^{L(-)}$ response does not happen for $\widetilde{W}_{11}^{T(-)}$ (not shown). We conclude that the L responses are sensitive to the SOP, while the T responses are almost independent of it. This may be due to the different spin-dependence of the corresponding electromagnetic operator. In the L response the electromagnetic operator in leading order involves the spin-independent charge operator, which cannot flip the spin. Therefore the transition matrix element of the L response is sensitive to the change of the spin part of the wave function induced by the SOP. On the other hand, the transverse current is proportional to the Pauli spin matrices in leading order, and therefore it is less dependent on the relative change of the $l + \frac{1}{2}$ and $l - \frac{1}{2}$ components of the partial waves. With regard to size, the $\widetilde{W}_{11}^{T(-)}$ response is about 25% of the unpolarized longitudinal for $q = 500$ MeV/c and is much bigger for $q = 700$ MeV/c (see Tables 2–4). We have observed that the vector transverse response approximately scales with the vector longitudinal one when this is computed without the SOP and that the scaling factor is about the same as in the unpolarized case (and this is the reason for not showing figures for this response).

5.2.3 TL responses

Unpolarized response. The $W_{00}^{TL(+)}$ shown in Fig. 5 is an interference between L and T multipoles and thus some similar behaviour to the responses discussed above is expected, although the interference can produce a reduction or enhancement of some of the features. In fact, in PWIA the TL response is of first-order in $\delta = \eta \sin \theta$, as we can see from Eq. (121), and it is due to the interference between charge and convection, and spin-orbit and magnetization terms. In the QEP, the TL strength is around 50% of the longitudinal (Tables 2–4). For $q = 300$ MeV/c the TL response is bigger than the T response. This can be understood by looking at the expressions for the responses, Eqs. (78–83) of reference [6]: in leading order the T response is proportional to the single-nucleon response $w^T \sim 2J_m^2 = 2\tau G_M^2$, while the TL response is proportional to

$$w^{TL} = 2\sqrt{2}(\rho_c J_c + \rho_{so} J_m)\delta = 2\sqrt{2} \left(G_E^2 + \frac{2G_M - G_E}{\sqrt{1+\tau}} \frac{\kappa}{2} \sqrt{\tau} G_M \right) \delta.$$

For $q = 300$ MeV/c we have $\tau \sim \kappa^2$, while for the maximum of the momentum distribution at $p \sim 150$ MeV/c, $\theta \sim 90^\circ$, we have $\delta \sim \kappa$ and therefore

$$\frac{w^T}{w^{TL}} \sim \frac{2\kappa\mu_P^2}{\sqrt{2}} \sim 0.9.$$

Thus, for low q the TL response is bigger than the T response, although the latter is of zeroth-order in δ , while the TL one is of first-order in the expansion. Of course, the currents contain terms which are (q, ω) -dependent, whose magnitude has to be taken into account. For high q the factor τ is bigger and the T response dominates over the TL one.

With respect to the FSI effect, it is bigger than the one found in the T and L responses. The reduction in all cases is more than 50%. This suggests that the convection and spin-orbit electromagnetic matrix elements are more sensitive to the dynamics of the FSI. Also this response is more sensitive to the SOP than the longitudinal one. In fact, if the SOP is set to zero, the FSI effects are almost the same as in the L and T responses. Therefore it appears to be the *spin-orbit potential* that is responsible for the very significant reduction of this response when compared with the other two.

In order to understand this feature better, we have performed a calculation of the responses with the SOP set to zero and without spin-orbit and convection pieces in the current. As a result, we have checked numerically that the interference between charge and magnetization goes to zero when the SOP does so. This happens for all of the polarized TL responses. In addition, when the SOP is turned on, the zeroth-order contribution is nonzero and negative for $q > 500$ MeV/c at the QEP, providing the reason why the FSI are so large in this response.

Vector responses. There is no counterpart of the $W_{10}^{TL(-)}$ response in the T and L cases. We show this response in Fig. 6. As seen in Eqs. (63,64) the vector responses without a tilde contribute only to the \widetilde{W}^{TL} structure function, which is nonzero only for out-of-plane emission (see Eq. (57)). This vector response presents an oscillatory behaviour, its

magnitude being $\sim 26\%$ of the unpolarized longitudinal in region IIb. From the figure it is evident that this response is very sensitive to the interaction, the results with and without SOP being completely different in all of the kinematical regions here studied. In fact, the dependence of this response on the SOP is much more dramatic than for the case of the vector longitudinal (compare Figs. 2 and 6), and therefore such big effects, even changing the sign in many cases, could in principle be measured if a separation of this response could be performed.

Quadrupole responses. The responses $W_{2\mathcal{M}}^{TL(+)}$ are nonzero in PWIA and, under that approximation, the relation between $W_{2\mathcal{M}}^{TL(+)}$ and the corresponding $W_{2\mathcal{M}}^{L(+)}$ and $W_{2\mathcal{M}}^{T(+)}$ is the same as in the unpolarized case. The FSI effects in the $W_{20}^{TL(+)}$ response shown in Fig 7 are stronger than in the case of W_{20}^L and W_{20}^T , as can be seen comparing Figs. 3 and 7. This is again a consequence of the different sensitivities of these responses to the spin-orbit interaction (compare the dashed curves in Figs. 3 and 7). The reason for this behaviour is again that the SOP generates a contribution from zero-order terms (interference between charge and magnetization) in the current matrix elements, which would be zero if there were no SOP.

The FSI effects in the $W_{20}^{TL(+)}$ response also are very dependent on the choice of kinematics. For $q = 500$ MeV/c at the QEP (region IIb), the FSI reduce the response by about 60% and below the QEP in region IIa, they produce a change of sign. The SOP importance is very large at low q , but small above the QEP in region IIc. On the other hand, at the QEP the importance of FSI and SOP strongly increases with q : at $q = 300$ MeV/c the total effect is about 10%, while the response is drastically reduced for $q = 700$ MeV/c.

5.2.4 T' responses

Polarized electrons are required for the primed responses T' , TL' . There are a total of 24 reduced response functions of this kind which we now discuss. Note that there is no T' response in absence of nuclear polarization. In fact, for $\mathcal{J} = \text{even}$ the T' responses are only of the tilde type, and therefore all of them are zero for $\mathcal{M} = 0$.

Vector responses. The $W_{10}^{T'(-)}$ response shown in Fig. 8 is nonzero in PWIA and has no counterpart in the set of unprimed responses, since there is no vector T response of this kind. From Eq. (127) we see that in leading order in δ this response is expected to be of the same order of magnitude as the T responses and in fact in PWIA this response is comparable with the T unpolarized one, and the same happens in DWIA, as we can see by inspection of Tables 2–4. The FSI produce a reduction that in general is smaller than that found for $W_{00}^{T(+)}$; however we find several exceptions to this statement, the most important one being that in region IIIa the FSI only slightly affect this response. In this region the only noticeable FSI effect is found for parallel emission ($\theta' \sim 0$), although for higher missing momentum ($p' \sim 200$ MeV/c) the response is almost independent of the interaction. In addition for $q \geq 500$ MeV the SOP effect is negligible. Therefore this could be a good place to look for other model dependences such as on the specifics of the single-nucleon current or

nuclear structure. A second exception is in region Ia, where the FSI enhance and produce a shift of the response, although we are far away from the range of applicability of the potential.

With respect to the $W_{11}^{T'(-)}$ response (Fig. 9), one would expect that it should in general be bigger than $\widetilde{W}_{11}^{T(-)}$ which is zero in PWIA, but we find that in many cases the FSI produce a significant reduction of the PWIA results for this response, the effect being more than 60% in the QEP region, where the variation $\Delta W_{11}^{T'(-)}$ of this response is always smaller than the corresponding $\Delta W_{11}^{T(-)}$ (see Tables 2–4). On the other hand, in regions IIa,c, this variation is $\sim 50\%$ of the unpolarized longitudinal case, and it is above 100% in regions IIIa,c. The reason why this response is so small at the QEP can be seen by looking at its behaviour for fixed q , as a function of ω (Fig. 9). There is a tendency for this response to change from positive at lower ω to negative at some point slightly above the QEP. Comparing the DWIA and PWIA results we also see a general tendency for the former to be reduced in magnitude with respect to the latter, where this reduction is seen to be significant below the QEP and is larger for low q . On the other hand, above the QEP (regions Ic, IIc) the mean (negative) peak of this response is almost not affected by FSI, so these could be good places to investigate other aspects of the reaction. This trend does not apply for $q = 700$ MeV/c, $\omega = 300$ MeV (region IIIc), but here again we are far away from the validity of the potential parametrization. As in the case of the T response, this response is insensitive to the SOP.

Octupole responses. The $W_{30}^{T'(-)}$ response shown in Fig. 10 is comparable to the $W_{10}^{T'(-)}$ one in both PWIA and DWIA, and over the entire kinematical range considered. In some places there are drastic changes due to the FSI with respect to the PWIA. For example, in region IIa below the QEP this response is almost opposite to the $W_{10}^{T'(-)}$ in PWIA, that is reduced by FSI by less than 20%, while the $W_{30}^{T'(-)}$ is almost canceled by FSI. On the other hand, in region IIb, the FSI effect provides a reduction of around 20%. If we go further in energy (to region IIc), where the PWIA presents an oscillatory behaviour, the FSI yield a reduction by 50% at the maximum, and almost do not affect the first minimum. We observe a similar behaviour in region Ic where the reduction due to FSI is even bigger, around 75%. Again, the SOP effect is negligible in this response.

The $W_{31}^{T'(-)}$ response is shown in Fig. 11 and is also important. It reaches its greatest values above the QEP (see also Tables 2–4). For instance, its variation is about 25%, 50% and 120% of the unpolarized longitudinal in regions Ic, IIc, and IIIc, respectively. At the QEP, its magnitude is around 70% of $W_{11}^{T'(-)}$, and the FSI effects are almost identical in both of them, in general very strong for low q (producing even a change of sign) and moderate at $q = 700$ MeV/c (with a reduction of $\sim 65\%$). Below the QEP in region IIa this response is around 80% of the $W_{11}^{T'(-)}$ and about one half of $W_{10}^{T'(-)}$, the FSI effects being smaller than in the $W_{11}^{T'(-)}$ response. FSI effects are also seen to be very different at the QEP upon comparing the $\mathcal{M} = 0$ and $\mathcal{M} = 1$ odd T' responses. It is important to note that the identification of places where FSI effects are very different, as in the case of the $W_{11}^{T'(-)}$ and

$W_{31}^{T'(-)}$ in region IIa, could play an important role in this type of study where the goal is to isolate such effects. The remaining octupole responses $W_{32}^{T'(-)}$ and $W_{33}^{T'(-)}$ (not shown in the figures) tend to be smaller than the one discussed above, although the former could be noticeable in some cases, while the latter is negligible.

In all cases we find that the influence of the SOP in the T' responses is small, as in the T case, thus making it possible to use these transverse responses to study the central part of the interaction and to use the responses which are sensitive to the SOP, such as the L or TL cases, to study the spin-dependent part of the interaction.

5.2.5 TL' responses

Unpolarized response. The “fifth response function” $W_{00}^{TL'(+)}$ (shown in Fig. 12) is zero in PWIA. It can be separated by performing an asymmetry measurement by flipping the electron helicity in experiments with unpolarized nuclei, therefore providing an alternative way of studying the FSI. First we note that its size is large and comparable with the unpolarized TL response, with which it is related by Eqs. (46–49). In fact, the TL and TL' responses differ in that they select different combinations of the real or imaginary parts of the interference multipoles in Eqs. (28,29). Specifically, the $W_{00}^{TL(+)}$ and $W_{00}^{TL'(+)}$ contributions contain the real and imaginary parts, respectively, of the same combination of multipoles (see Eqs. (37,38)). Therefore their magnitudes are roughly determined by the averages $\langle \cos \Delta\delta \rangle$ and $\langle \sin \Delta\delta \rangle$ of $\cos[\text{Re}(\delta_{l'j'} - \delta_{lj})]$ and $\sin[\text{Re}(\delta_{l'j'} - \delta_{lj})]$, respectively, that is, of the differences between the real phase-shifts for different partial waves. The magnitudes of these averages are determined by factors involving the weighting amplitudes $|C_{\sigma'}E_{\sigma}|$ and $|C_{\sigma'}M_{\sigma}|$ in Eqs. (46–49). The intercomparison between TL and TL' responses can therefore provide information about the mean real phase-shift deviation. Of course, within the average the relation $\langle \cos \Delta\delta \rangle^2 + \langle \sin \Delta\delta \rangle^2 = 1$ is in general not true, although for QE conditions it is approximately satisfied. In fact, the values of the pair $(W_{00}^{TL(+)}, W_{00}^{TL'(+)})$ at the peak in regions Ib, IIb and IIIb are $\sim (70, 40)$, $(70, 45)$ and $(30, 70)$ [$\text{GeV}^{-1} \times 10^{-3}$] and therefore the combination $[W_{00}^{TL(+)}]^2 + [W_{00}^{TL'(+)}]^2 \simeq \text{constant}$. Outside the QEP this relation does not hold, but in any case the two responses are always comparable in magnitude. Moreover, the effect of the SOP is of similar importance, $\sim 20\%$ in both responses.

With regard to their behaviour as functions of the kinematic variables, the TL and TL' responses have different structures, the most significant variations being found below the QEP and at low energy. It is interesting to note that the behaviour of the $W_{00}^{TL'(+)}$ response is more similar to that of the $\widetilde{W}_{11}^{L(-)}$ and $\widetilde{W}_{11}^{T(-)}$ responses. Our results show that the effect of the SOP in the $W_{00}^{TL'(+)}$ and $\widetilde{W}_{11}^{L(-)}$ responses is similar, and it presents a tendency to modify the response in the same way. It is also noteworthy that when the SOP is set to zero, the three responses $W_{00}^{TL'(+)}$, $\widetilde{W}_{11}^{L(-)}$ and $\widetilde{W}_{11}^{T(-)}$ acquire the same shape and that $W_{10}^{TL(-)}$ also shows the same tendency (compare Figs. 2, 6 and 12). This is related to the fact that all of these responses are given by imaginary parts of the single transition responses for each partial wave.

Vector responses The TL' vector responses are large in magnitude and in all cases considered they are comparable to the $W_{00}^{L(+)}$ response. From Tables 2–4 we see that their importance increases with the momentum transfer, and for high q the $\widetilde{W}_{11}^{TL'}$ response is the dominant one, being around 160% and 220% of the unpolarized longitudinal case for $q = 500$ and 700 MeV/c, respectively. The $W_{10}^{TL'(-)}$ response is shown in Fig. 13, and it presents a behaviour which is opposite in sign to $W_{11}^{T'(-)}$, both with and without FSI, but the effect of the SOP is different at the QEP (regions Ib, IIb, IIIb). For instance, in region IIb the introduction of the SOP changes the sign and peak position, and in region IIIb the response is negligible without SOP, while its inclusion produces an increase of the absolute strength of the PWIA results by more than 100%. On the contrary, in region Ic the FSI effects are negligible. The $W_{11}^{TL'(-)}$ and $\widetilde{W}_{10}^{TL'(-)}$ responses are very large in magnitude and almost opposite in sign. It is interesting that the $\widetilde{W}_{11}^{TL'(-)}$ response, not shown in the figures, has a behaviour that is very similar to $W_{00}^{L(+)}$, although opposite in sign, and that the effect of the FSI and SOP is also similar in these two responses. This is related to the fact that all of these responses are composed of real parts of responses for single multipole transitions $R_{\sigma'\sigma}^L$, $R_{\sigma'\sigma}^{T1}$, $R_{\sigma'\sigma}^{T2}$, $R_{\sigma'\sigma}^{TL1}$, and $R_{\sigma'\sigma}^{TL2}$ in Eqs. (40,42,46,48), and that all of them are dominated by the zeroth-order static component of the electromagnetic current.

Quadrupole responses. The $W_{20}^{TL'(+)}$, shown in Fig. 14, has no T' counterpart. This response is bigger than the fifth response function below the QEP, but is smaller at and near the QEP. This response shows a large sensitivity to the SOP, which completely changes its behaviour in many cases, especially at the QEP. Specifically, the SOP produces the tendency to reduce this response to negative values for quasielastic conditions. In general all of the $W_{2\mathcal{M}}^{TL'(+)}$ and $\widetilde{W}_{2\mathcal{M}}^{TL'(+)}$ responses have almost the same magnitude in region IIb, and they are about twice that of the transverse $\widetilde{W}_{2\mathcal{M}}^{T'(+)}$ (see Tables 2–4), which could help in making an experimental separation of these quadrupole responses feasible. In general all of the quadrupole TL' responses are very sensitive to the SOP, in contrast to what happens for the quadrupole T' responses.

Octupole responses. There are four $W_{3\mathcal{M}}^{TL'(-)}$ and three $\widetilde{W}_{3\mathcal{M}}^{TL'(-)}$ octupole responses and in general all of them are big compared with the fifth response function, the biggest ones being for $\mathcal{M} = 0, 1$, as seen by inspection of Tables 2–4. In fact, $W_{30}^{TL'(-)}$, shown in Fig. 15, is the response with the biggest variation in regions IIa,c and IIIa,c, and $W_{30}^{T'(-)}$ is the second response of importance in this ranking. The $W_{30}^{TL'(-)}$, $W_{31}^{TL'(-)}$ and $\widetilde{W}_{32}^{TL'(-)}$ responses are strongly affected by FSI, both in size and sign at QE conditions, and the last two are significantly suppressed by the FSI. The SOP does not play a particularly important role in these responses, with some exceptions. In regions IIa, IIc and IIIa, the $W_{30}^{TL'(-)}$ response is larger in magnitude than the unpolarized longitudinal response even with the inclusion of FSI and it is rather insensitive to the SOP. Also $W_{31}^{TL'(-)}$ is large in these regions, where it is similar in shape and magnitude to $W_{30}^{T'(-)}$. In summary, the large magnitude of these

octupole responses indicates that they could possibly be separated through a sequence of asymmetry measurements.

5.3 Relativistic corrections

In this section we briefly discuss the importance of the different terms in the first-order expansion of the relativistic current in powers of $\delta = \eta \sin \theta$ [6]. In particular, the goal is to study the importance of the first-order terms which we call spin-orbit (in the longitudinal) and convection (in the transverse), but which differ from the terms usually used in non-relativistic calculations in that they maintain the full dependence on (q, ω) in the relativistic current (see the definitions in Eqs. (123–126)), and therefore they are more suited for use at high momentum transfer near the QEP. Also the spin-orbit charge (SOC) term is usually not included in non-relativistic calculations, but as seen in Eq. (121), it contributes to the single-nucleon TL response at the same level as the convection current and therefore its inclusion in the longitudinal component can be important for properly describing the TL responses at high momentum transfer, as was found in Ref. [6] in the inclusive polarized case. Moreover, the FSI can affect each one of these contributions in a different way, as may be reflected especially in the responses which are zero in PWIA.

In the following we show only two figures to illustrate the most interesting cases. As in the last section, we show a separate response function in the nine panels corresponding to the same choices of kinematics made above. Now the solid line in Figs. 16–17 represents the total response computed in DWIA with the complete optical potential. With dashed lines we show the responses computed in leading order in the expansion, and therefore the dashed lines only include charge plus magnetization (zeroth-order) terms. Finally, the dot-dashed lines include, in addition, the convection current, and thus they are representative of what can be found in a standard non-relativistic calculation (with the important difference that we include the relativistic (q, ω) behaviour which is significant at high q). In other words, the effect of the spin-orbit term in the longitudinal current is to transform the dot-dashed curves to the solid ones.

We now discuss the importance of the different parts of the electromagnetic current in the case of the TL responses. In PWIA these responses are entirely due to interferences between charge and convection, and spin-orbit and magnetization terms, and as a consequence the first-order terms of the current are crucial when describing these responses. Of course, when FSI are turned on, the cancellation of the zeroth-order terms is not exact and the interference between charge and magnetization is nonzero with FSI (dashed lines in the figures), although its magnitude is comparable with the total response or smaller in some cases. As stated above, we have checked that the zero-order contribution to these responses goes away when the SOP is set to zero, and this is the reason why the TL responses are so sensitive to the spin-orbit part of the interaction.

The $W_{00}^{TL(+)}$, shown in Fig. 16, is especially sensitive to the first-order terms. The zeroth-order terms (interference between charge and magnetization pieces) are shown with dashed lines and they are zero in the absence of a spin-orbit interaction in the optical potential. The importance of the zeroth-order terms increases with the momentum transfer in all kinematic regions. For $q = 300$ MeV/c this contribution is almost negligible, while

for $q = 700$ MeV/c it is of the same order of magnitude as the total responses and opposite in sign. The increasing importance of the zeroth-order term is closely related with what we found in last section — the effect of the SOP increases with q in this response and the inclusion of the SOP potential in the FSI prevents the spin cancellations from occurring in the zeroth-order term. Shown with dot-dashed lines is the response computed including only charge, magnetization and convection terms in the electromagnetic current. These are the expected results if a standard non-relativistic treatment is used to compute the responses (no spin-orbit correction to the longitudinal piece). The effect of the convection term is to completely change the behaviour of this response with respect with the zeroth-order, even changing the sign for $q \geq 500$ MeV/c. When we include also the SOC piece, we obtain the solid lines in the figure, thereby showing the importance that this correction has in the TL response. The SOC contribution also increases with q . The effect of this term is to increase the total (dot-dashed) response by $\sim 15\%$, $\sim 75\%$ and $\sim 200\%$ at the peak for $q = 300$, 500 and 700 MeV/c, respectively, and QE conditions (regions Ib, IIb, IIIb). The effect is even bigger below the QEP, in regions Ia,b,c. As seen in Eqs. (124,126), the spin-orbit charge is proportional to $\kappa/\sqrt{1+\tau}$, which increases with q , while the convection piece is proportional to $\sqrt{\tau}/\kappa$, which slightly decreases with q . Therefore the relative importance of the SOC versus the convection current increases with q , as seen in the plots. Accordingly we conclude that any non-relativistic model which does not include the spin-orbit term significantly underestimates this response at a typical value of $q = 500$ MeV/c and QE conditions.

The zeroth-order term is important in the $W_{1\mathcal{M}}^{TL(-)}$ responses. For QE conditions, the convection effect is crucial at $q = 300$ MeV/c, and decreases with q . In region IIIb spin-orbit and convection effects are only around 20% of the total response in $W_{10}^{TL(-)}$ and smaller in $W_{11}^{TL(-)}$. These effects are much more important below the QEP, although in this region these responses are small compared with the $W_{00}^{L(+)}$. On the other hand, the first-order terms are more important in the $\widetilde{W}_{11}^{TL(-)}$ case shown in Fig. 17, which is exactly zero in PWIA. The zeroth-order terms are small in $\widetilde{W}_{11}^{TL(-)}$ which presents the same trends as the unpolarized response, $W_{00}^{TL(+)}$, and both responses are of the same order for $q = 700$ MeV/c (see Table 4). For instance, in region IIIb at the QEP, these two responses are the most important ones of the TL -type. The spin-orbit effects are 20%, 60% and 75% of the response computed with only zeroth-order plus convection terms in QE conditions at the peak.

Similar trends as those found in the unpolarized TL case are observed for the rest of the TL -responses although each one of them presents particular features for different kinematics and different values of \mathcal{JM} . For obvious reasons it is not possible to show all of the figures here; the complete set is presently available from the authors at [21].

We now discuss the TT responses very briefly because they are also in general very small and hard to measure. The unpolarized response is mainly due to the zeroth-order magnetization term, the convection current contributing only a small fraction to this response. The PWIA response is completely due to the convection current and the response computed in PWIA is much larger than the effect of the convection upon the DWIA response, which implies that the pure convection current is significantly suppressed by the FSI. Also

the response without the SOP is more similar to a pure reduction of the convection PWIA results than with it. This suggests that the SOP significantly modifies the cancellation of the pure magnetization response. And in fact, when a calculation was made of the different contributions to the TT responses with the SOP set to zero we found that the magnetization contribution goes away for all of the TT responses, and not only for the unpolarized one. In the other responses of the TT -type, we find that the magnetization contribution is in general dominant; yet in many cases, the convection contribution is important and several times crucial to describe these responses properly. The effect of the convection current in general decreases with q .

More interesting is the effect of relativistic corrections upon the fifth response function. In general the first-order terms (spin-orbit and convection contributions) are found to be negligible in the QEP region and above it, although there is a noticeable effect below the QEP in regions Ia and IIa where the fifth response function has two maxima at $p \sim 80$ and 220 MeV/c, and one (positive) minimum in between at $p \sim 130$ MeV/c (see Fig. 12). The effect of the convection current is to decrease the response for low p and to increase it for high p . The spin-orbit charge increases this response for low p , while it slightly decreases it for high p . The effects are noticeable: for instance, in region IIa the two maxima would be approximately equal if only magnetization is present. If the convection also contributes, then the second peak is bigger than the first one by a factor 1.5. If the SOC is also present, then the difference between the first and second maxima is about 20%; that is the situation shown in Fig. 12, where the complete current is used. Of course, the FSI effects play an important role here and the situation is completely changed if the SOP is zero.

Finally, we have found non-negligible first-order contributions to some of the remaining TL' responses, the most important case being the $W_{10}^{TL'(-)}$ and $W_{20}^{TL'(-)}$ responses for a variety of different kinematics.

6 Conclusions

In this work we have investigated polarization observables in coincidence electron scattering from nuclei when both beam and target are polarized. Our primary objective has been to develop the formalism for the $\vec{A}(\vec{e}, e'N)B$ reaction, introducing a complete set of reduced response functions which are independent of the polarization angles and azimuthal nucleon emission angle, and which contain the maximum information about nuclear structure and reaction mechanisms of interest. We have applied the above formalism to the particular case of a one-hole nucleus in the shell model using both PWIA and DWIA, and we have examined theoretically the differences which arise when the nucleon is ejected from different complete or incomplete shells, and when the daughter nucleus is left in states with different angular momenta. With respect to the theoretical results for the extreme shell model it is worth pointing out the following:

1. The reduced response functions for nucleon knockout from the same shell but different spin for the daughter nucleus are proportional to the responses of a single polarized particle in a shell. The proportionality constant contains a recoupling coefficient of

the angular momenta involved. When a more sophisticated nuclear model with configuration mixing is used, interferences between different shells are expected [7] and deviations from this proportionality could provide information about the nuclear structure involved.

2. Nucleon knockout from a complete inner shell in a polarized nucleus can show polarization effects although the involved shell has spin zero. The reason is that the final nuclear state is left in a state with definite angular momentum, and therefore the remaining incomplete shell is partially polarized. When the sum over final daughter spin is performed, all of the polarization responses add to zero. Again, deviations from this result arise in a more realistic model and, for instance, for a deformed nucleus such as ^{21}Ne , it has been found in Ref. [7] using PWIA for the ejected proton that as more states of the residual nucleus are involved, the effect of the target polarization is weakened.
3. The two above results are also valid for PWIA with the addition that similar conclusions are obtained for the polarized momentum distribution of the nucleus: it is proportional to the polarized momentum distribution of a single hole in the shell from which the nucleon is ejected, with the same proportionality coefficient as found between the reduced response functions. Within the context of this approximation, the study of this reaction opens the possibility of measuring the complete tri-dimensional momentum distribution of the nucleus.

In this work we have focused on the study of the angular reduced response functions because they are the basic quantities that describe the reaction. Nevertheless, the large number of these functions (72 for the case of ^{39}K studied here) makes it very difficult to attempt a separation of all of them experimentally, although, of course, specific combinations of the reduced responses could be isolated by performing a combination of asymmetry measurements. To understand the relative importance of these combinations in (the usual) circumstances where they are not entirely isolated it is important to perform an analysis of all of the response functions and to study their sensitivities to details of the reaction mechanism prior to any measurement.

That is what we have done in this work for the particular case of the ^{39}K nucleus described as a hole in the $d_{3/2}$ shell of ^{40}Ca . For the ejected proton we have used the DWIA with an optical potential and compared the results obtained with the PWIA. We have included relativity in the kinematics and in the electromagnetic current.

We have studied the model dependence of the reduced response functions by intercomparison between models, specifically addressing the question of what is the role of the central and spin-orbit pieces of the optical potential and exploring the effects of the first-order pieces of the electromagnetic current (convection and spin-orbit charge) in the responses. Let us summarize the main conclusions that may be drawn from our work.

1. In general the FSI produce a reduction of the absolute strength of the unpolarized responses with respect to the PWIA. The percentage of this reduction depends on the kinematic conditions, being typically of $\sim 35\%$ for the L and T responses and

for $q = 500$ MeV/c at QE conditions, however being more than a 50% effect for the TL response. The reason of this big reduction is because the FSI generate a nonzero contribution from the charge-magnetization, zeroth-order interference term, which is exactly zero in PWIA, but is negative with FSI for $q \geq 500$ MeV/c. We have checked that this effect is produced mainly by the spin-orbit potential, since the zeroth-order terms go away when we set the SOP equal to zero. The TT response is a few percent of the others and negative in PWIA, but again the FSI produce a drastic change, even inverting the sign, mainly due to the zeroth-order magnetization term in the current, which is zero in PWIA, although not in DWIA when the SOP is turned on.

2. The fifth response function $W_{00}^{TL'(+)}$ which arises for unpolarized nuclei and polarized electrons is comparable in size with the $W_{00}^{TL(+)}$ response, being around 20–90% of the longitudinal unpolarized response under different kinematics, and it is quite sensitive to the SOP, the most important effects being seen below the QEP.
3. In general the FSI effects are large in those responses that are nonzero in PWIA, especially the quadrupole L , T and TL , and vector and octupole T' and TL' cases; there is dependence on the particular rank $\mathcal{J}\mathcal{M}$ of each response and in some cases the FSI even produce a change of sign. The variety of effects found is too large to be summarized in a few lines, but we can cite as most outstanding cases with dramatic dependence on FSI the responses $W_{21}^{L(+)}$, $W_{21}^{T(+)}$, $W_{20}^{TL(+)}$, $W_{21}^{TL(+)}$, $W_{11}^{T'(-)}$, $W_{3\mathcal{M}}^{T'(-)}$, $W_{10}^{TL'(-)}$ and $W_{3\mathcal{M}}^{TL'(-)}$. Also some cases have been found where the FSI are negligible, therefore providing an ideal place to study other reaction issues, such as those involving the nucleon current or details of nuclear structure. The octupole responses $W_{3\mathcal{M}}^{T'(-)}$ and $W_{3\mathcal{M}}^{TL'(-)}$ are found to be large for $\mathcal{M} = 0, 1$, especially for high q , and these responses are dominant over the others below and above the QEP, probably making their extraction experimentally feasible.
4. The polarized responses which are zero in PWIA are *a fortiori* sensitive to the FSI. Additionally, the $\widetilde{W}_{11}^{L(-)}$ response is rather dependent on the SOP, although the $\widetilde{W}_{11}^{T(-)}$ response is not. The effects of the SOP are dramatic in $W_{1\mathcal{M}}^{TL(-)}$ due to the fact that zeroth-order terms in the current only contribute to this response if the SOP is nonzero. Also the $W_{20}^{TL'(+)}$ is very sensitive to the SOP.
5. All of the T and T' responses are largely insensitive to the spin-orbit interaction; therefore they could be used to study the central part of the FSI. On the other hand, the L , TL and TL' responses are much more sensitive to the SOP, especially in the case of the TL responses.
6. The spin-orbit first-order term in the charge operator is crucial for properly describing the TL responses and some of the TL' ones, especially at high q where relativistic effects are expected to be more important. At $q = 700$ MeV/c the spin-orbit and convection contribution are of the same order for both polarized and unpolarized TL

responses. In other cases the first-order effects are smaller, but noticeable in some situations, for instance, in the fifth response function.

7. The non-locality correction with a Perey-like factor is in general smaller than the effects mentioned above and it can be safely ignored in a first exploratory study of this kind.

In conclusion, we have found a wide variety of effects of the FSI and relativistic corrections in the different reduced response functions of polarized nuclei. As the effects are different for different responses, systematic intercomparisons between selected separated responses could provide important information about different aspects of the reaction mechanism. The quantity of information which may be obtained with exclusive polarized electron scattering from polarized nuclei is more than one order of magnitude richer than in the unpolarized case and this should allow much more stringent constraints to be placed on any particular model of the dynamics.

Experimentally, however, the amount of work involved in measuring and extracting all of the angular reduced response functions is daunting, with little hope for a complete extraction of all of them in the near future, and therefore it is desirable to extend this analysis to the study of spin observables which can be directly measured, such as cross sections and asymmetries. Our aim here has been to provide a first detailed insight into the basic quantities describing the reaction, namely the reduced response functions, as a first step towards understanding the role of the different reaction ingredients in the problem. It is our intent to apply the present formalism to study various classes of asymmetries and investigate their utility for extracting fundamental properties of polarized nuclei such as polarized momentum distributions and spin distributions. Work along these lines is in progress.

Acknowledgement

The authors wish to thank Dr. Sabine Jeschonnek for her helpful comments on the manuscript.

Appendix A. Calculation of the longitudinal response

Here we present a proof of Eqs. (34,40,41) for the longitudinal response. We begin from the definition, Eq. (9), and inserting the multipole expansion in Eq. (15), we have

$$\mathcal{R}^L = \sum \rho^* \rho = 4\pi \sum_{JJ'} i^{J-J'} [J][J'] B_{J'J}^{00}, \quad (132)$$

where $B_{J'J}^{00}$ is given by Eq. (17), with $\hat{T}_{J'} = \hat{M}_{J'}$ and $\hat{T}_J = \hat{M}_J$. Using the general result in Eq. (21) we obtain

$$\mathcal{R}^L = 4\pi \sum_{\sigma\sigma'} \sum_{J J' L} i^{J-J'} i^{l'-l} P_{l+l'+J'}^+ f_{\mathcal{J}}^i [Y_{\mathcal{J}} Y_{\mathcal{J}'}]_{L0} \Phi_{\sigma'\sigma} \begin{pmatrix} J & J' & L \\ 0 & 0 & 0 \end{pmatrix} C_{\sigma'}^* C_{\sigma}, \quad (133)$$

where the Coulomb amplitudes in Eq. (22) have been introduced. Now we use the fact that the Coulomb operator \hat{M}_J has natural parity $(-1)^J$. If we denote by Π_i and Π_B the parities of the target and daughter nuclei, respectively, we conclude that the matrix element C_{σ} is nonzero only for transitions satisfying $\Pi_i \Pi_B (-1)^{l+J} = 1$, while for $C_{\sigma'}$ we have $\Pi_i \Pi_B (-1)^{l'+J'} = 1$. Therefore, for the product $C_{\sigma'}^* C_{\sigma}$ we have the selection rule $l + J + l' + J' = \text{even}$. Taking this into account and using the parity function in Eq. (33), we can write

$$i^{J-l-(J'-l')} C_{\sigma'}^* C_{\sigma} = \xi_{J'-l', J-l}^+ C_{\sigma'}^* C_{\sigma} \quad (134)$$

and we have for the longitudinal response

$$\mathcal{R}^L = 4\pi \sum_{\sigma\sigma'} \sum_{J J' L} P_{l+l'+J'}^+ f_{\mathcal{J}}^i [Y_{\mathcal{J}} Y_{\mathcal{J}'}]_{L0} \Phi_{\sigma'\sigma} \begin{pmatrix} J & J' & L \\ 0 & 0 & 0 \end{pmatrix} \xi_{J'-l', J-l}^+ C_{\sigma'}^* C_{\sigma}. \quad (135)$$

Now, using $\xi_{mn}^+ = \xi_{nm}^+$, we can write the sum over $\sigma'\sigma$ in a symmetrized way

$$\begin{aligned} \sum_{\sigma\sigma'} P_{l+l'+J'}^+ \Phi_{\sigma'\sigma} \begin{pmatrix} J & J' & L \\ 0 & 0 & 0 \end{pmatrix} \xi_{J'-l', J-l}^+ C_{\sigma'}^* C_{\sigma} = \\ \frac{1}{2} \sum_{\sigma\sigma'} P_{l+l'+J'}^+ \begin{pmatrix} J & J' & L \\ 0 & 0 & 0 \end{pmatrix} \xi_{J'-l', J-l}^+ [\Phi_{\sigma'\sigma} C_{\sigma'}^* C_{\sigma} + \Phi_{\sigma\sigma'} C_{\sigma}^* C_{\sigma'}], \end{aligned} \quad (136)$$

because, due to the parity functions, $l + l' + J' = \text{even}$, $l + l' + J + J' = \text{even}$, and due to the parity properties of the 3- j , we have that $J + J' + L = \text{even}$. Using now the symmetry property in Eq. (20), we have $\Phi_{\sigma\sigma'} = (-1)^{\mathcal{J}} \Phi_{\sigma'\sigma}$ because, due to the parity functions, we have that $J' + L = \text{even}$. Therefore we can write the symmetrized product as

$$\begin{aligned} \frac{1}{2} [\Phi_{\sigma'\sigma} C_{\sigma'}^* C_{\sigma} + \Phi_{\sigma\sigma'} C_{\sigma}^* C_{\sigma'}] &= \frac{1}{2} \Phi_{\sigma'\sigma} [C_{\sigma'}^* C_{\sigma} + (-1)^{\mathcal{J}} C_{\sigma}^* C_{\sigma'}] \\ &= \Phi_{\sigma'\sigma} [P_{\mathcal{J}}^+ R_{\sigma'\sigma}^L + i P_{\mathcal{J}}^- I_{\sigma'\sigma}^L], \end{aligned} \quad (137)$$

where we have used the definition in Eq. (25), and noticed that when $\mathcal{J} = \text{even}$, we are taking twice the real part of $C_{\sigma'}^* C_{\sigma}$, and when $\mathcal{J} = \text{odd}$, we have twice the imaginary part of $C_{\sigma'}^* C_{\sigma}$ times the imaginary unit.

On the other hand, we have the conjugation property

$$[Y_{\mathcal{J}} Y_{\mathcal{J}'}]_{L0}^* = (-1)^{J+J'+L} [Y_{\mathcal{J}} Y_{\mathcal{J}'}]_{L0} = (-1)^{\mathcal{J}} [Y_{\mathcal{J}} Y_{\mathcal{J}'}]_{L0} \quad (138)$$

because again $J' + L = \text{even}$, and therefore the coupling $[Y_{\mathcal{J}} Y_{\mathcal{J}'}]_{L0}$ is real for $\mathcal{J} = \text{even}$ and imaginary for $\mathcal{J} = \text{odd}$; and so we can write

$$[Y_{\mathcal{J}} Y_{\mathcal{J}'}]_{L0} = P_{\mathcal{J}}^+ A_{\mathcal{J}J'L0} + i P_{\mathcal{J}}^- B_{\mathcal{J}J'L0}. \quad (139)$$

Finally, inserting Eqs. (136,137,139) in Eq. (135) we obtain:

$$\begin{aligned} \mathcal{R}^L = & 4\pi \sum_{\sigma'\sigma} \sum_{\mathcal{J}\mathcal{J}'L} P_{l+l'+\mathcal{J}}^+ f_{\mathcal{J}}^i \Phi_{\sigma'\sigma} \begin{pmatrix} J & J' & L \\ 0 & 0 & 0 \end{pmatrix} \xi_{J'-l',J-l}^+ \\ & \times [P_{\mathcal{J}}^+ A_{\mathcal{J}\mathcal{J}'L0} R_{\sigma'\sigma}^L - P_{\mathcal{J}}^- B_{\mathcal{J}\mathcal{J}'L0} I_{\sigma'\sigma}^L], \end{aligned} \quad (140)$$

from which it is straightforward to read off Eqs. (34,40,41). Although the derivations of the remaining responses are somewhat more involved, the basic steps for obtaining them are natural extensions of the ones given here.

Appendix B. Reduced responses for a one-hole nucleus

In this appendix we show how to perform the sums over the angular momenta of the final states in the reduced responses for a one-hole nucleus whose ground state can be described as an extreme one-hole configuration $|i^{-1}\rangle$. Since the following steps are analogous for each one of the reduced responses $W_{\mathcal{J}\mathcal{J}'L}^{K(\pm)}$, we only consider the case of the $W_{\mathcal{J}\mathcal{J}'L}^{L(+)}$ response, given in general by Eq. (40)

$$W_{\mathcal{J}\mathcal{J}'L}^{L(+)} = \sum_{\sigma\sigma'} P_{l+l'+\mathcal{J}}^+ \Phi_{\sigma'\sigma} \begin{pmatrix} J & J' & L \\ 0 & 0 & 0 \end{pmatrix} \xi_{J'-l',J-l}^+ R_{\sigma'\sigma}^L \quad (141)$$

with $R_{\sigma'\sigma}^L = \text{Re } C_{\sigma'}^* C_{\sigma}$. First consider the case $h \neq i$, when the struck nucleon is in a shell other than the polarized one. In this case the final states are

$$|f\rangle = \left[a_j^\dagger [b_h^\dagger b_i^\dagger]_{J_B} \right]_{j_f} |C\rangle, \quad (142)$$

where $|j\rangle \equiv |E'lj\rangle$ is a single particle in the continuum with energy E' . Here it is useful to define, in addition to the index $\sigma = \{l, j, j_f, J\}$, indices $\gamma = \{l, j, J\}$, $\gamma' = \{l', j', J'\}$, that do not contain the final angular momenta j_f, j'_f which are going to be summed. With these indices, the many-body Coulomb matrix element can be written as

$$C_{\sigma} = \langle f || \hat{M}_J || i^{-1} \rangle = [J_B][j_f](-1)^{J-j-j_h} \begin{Bmatrix} j_i & j_f & J \\ j & j_h & J_B \end{Bmatrix} c_{\gamma}, \quad (143)$$

where we denote with a lower-case letter the Coulomb matrix element for the single-nucleon transition from the shell h to the continuum:

$$c_{\gamma} = \langle j || M_J || h \rangle. \quad (144)$$

We can then write the real part of the product $C_{\sigma'}^* C_{\sigma}$ in the following way

$$R_{\sigma'\sigma}^L = [J_B]^2 [j_f][j'_f](-1)^{J-j-j_h}(-1)^{J'-j'-j_h} \begin{Bmatrix} j_i & j'_f & J' \\ j' & j_h & J_B \end{Bmatrix} \begin{Bmatrix} j_i & j_f & J \\ j & j_h & J_B \end{Bmatrix} r_{\gamma'\gamma}^L, \quad (145)$$

where now $r_{\gamma'\gamma}^L$ is the real part of the interference between single-particle Coulomb multipoles

$$r_{\gamma'\gamma}^L = \text{Re } c_{\gamma'}^* c_{\gamma}. \quad (146)$$

Therefore we can write the response as

$$\begin{aligned} W_{\mathcal{J}\mathcal{J}'L}^{L(+)} &= \sum_{j_f j'_f} \sum_{\gamma'\gamma} P_{l+l'+\mathcal{J}'}^+ \Phi_{\sigma'\sigma} \left(\begin{array}{ccc} J & J' & L \\ 0 & 0 & 0 \end{array} \right) \xi_{J'-l', J-l}^+ [J_B]^2 [j_f] [j'_f] \\ &\times (-1)^{J+J'+j+j'+1} \left\{ \begin{array}{ccc} j_i & j'_f & J' \\ j' & j_h & J_B \end{array} \right\} \left\{ \begin{array}{ccc} j_i & j_f & J \\ j & j_h & J_B \end{array} \right\} r_{\gamma'\gamma}^L. \end{aligned} \quad (147)$$

Now we are interested in performing the sums over j_f, j'_f . Specifically we are going to compute the following coefficient:

$$A \equiv \sum_{j_f j'_f} \Phi_{\sigma'\sigma} [j_f] [j'_f] \left\{ \begin{array}{ccc} j_i & j'_f & J' \\ j' & j_h & J_B \end{array} \right\} \left\{ \begin{array}{ccc} j_i & j_f & J \\ j & j_h & J_B \end{array} \right\}. \quad (148)$$

Inserting the definition in Eq. (19) of $\Phi_{\sigma'\sigma}$,

$$\begin{aligned} A &= \sum_{j_f j'_f} [J] [J'] [j] [j'] [j_f] [j'_f] [\mathcal{J}'] [L] (-1)^{J'+J_B+j_f+1/2+\mathcal{J}+\mathcal{J}'} \\ &\times \left(\begin{array}{ccc} j' & j & \mathcal{J}' \\ \frac{1}{2} & -\frac{1}{2} & 0 \end{array} \right) \left\{ \begin{array}{ccc} j' & j & \mathcal{J}' \\ j_f & j'_f & J_B \end{array} \right\} \left\{ \begin{array}{ccc} J & J' & L \\ J_i & J_i & \mathcal{J} \\ j_f & j'_f & \mathcal{J}' \end{array} \right\} \\ &\times [j_f] [j'_f] \left\{ \begin{array}{ccc} j_i & j'_f & J' \\ j' & j_h & J_B \end{array} \right\} \left\{ \begin{array}{ccc} j_i & j_f & J \\ j & j_h & J_B \end{array} \right\} \end{aligned} \quad (149)$$

The sum over j_f, j'_f can be written as the product of a 6- j and a 9- j symbol using the relation

$$\begin{aligned} &\left\{ \begin{array}{ccc} a & b & c \\ a' & b' & c' \\ d & e & f \end{array} \right\} \left\{ \begin{array}{ccc} d & e & f \\ h & i & j \end{array} \right\} = \\ &= \sum_{\lambda\mu} (-1)^{S+\lambda} [\lambda]^2 [\mu]^2 \left\{ \begin{array}{ccc} c & c' & f \\ h & i & \lambda \end{array} \right\} \left\{ \begin{array}{ccc} a' & b' & c' \\ h & \lambda & \mu \end{array} \right\} \left\{ \begin{array}{ccc} b & b' & e \\ h & j & \mu \end{array} \right\} \left\{ \begin{array}{ccc} a & b & c \\ a' & \mu & \lambda \\ d & j & i \end{array} \right\}, \end{aligned} \quad (150)$$

with $S = b + c - a' - c' - d - e + 2h + j$. Note that Rotenberg's version [13] of this equation (Eq. (3.23)) has an error in the third 6- j of the righthand side: instead of h , in that reference appear an i . In order to obtain the correct expression, in this work we have proven the above relation using the graphical method of Ref. [14]; for brevity we do not reproduce the procedures used here.

Using the above relation and after some rearrangement and simplification of phases we obtain for the sum A the result

$$A = [J][J'][j][j'][\mathcal{J}'][L](-1)^{J'+J_B+\mathcal{J}+\mathcal{J}'} \begin{pmatrix} j' & j & \mathcal{J}' \\ \frac{1}{2} & -\frac{1}{2} & 0 \end{pmatrix} \\ \times (-1)^{J+J'+\mathcal{J}+\mathcal{J}'} (-1)^{j+j_h+j_i-1/2} \left\{ \begin{matrix} J & J' & L \\ j_h & j_h & \mathcal{J} \\ j & j' & \mathcal{J}' \end{matrix} \right\} \left\{ \begin{matrix} j_i & j_i & \mathcal{J} \\ j_h & j_h & J_B \end{matrix} \right\}. \quad (151)$$

The 9- j coefficient has the same structure as a polarized particle with spin j_h would have. In order to relate the result with the response of a polarized particle in the shell h and spin-zero daughter nucleus, $J_B = 0$, we first notice that the coefficient $\Phi_{\gamma'\gamma}$ corresponding to Eq. (19) for that process can be written

$$\Phi_{\gamma'\gamma}(\mathcal{J}\mathcal{J}'L, h \rightarrow 0) = [J][J'][j][j'][\mathcal{J}'][L][j][j'](-1)^{J'+j+1/2+\mathcal{J}+\mathcal{J}'} \\ \times \begin{pmatrix} j' & j & \mathcal{J}' \\ \frac{1}{2} & -\frac{1}{2} & 0 \end{pmatrix} \left\{ \begin{matrix} j' & j & \mathcal{J}' \\ j & j' & 0 \end{matrix} \right\} \left\{ \begin{matrix} J & J' & L \\ j_h & j_h & \mathcal{J} \\ j & j' & \mathcal{J}' \end{matrix} \right\}. \quad (152)$$

Inserting the simple result $(-1)^{j+j'+\mathcal{J}'}/[j][j']$ for the 6- j symbol with one argument equal to zero, the coefficient $\Phi_{\gamma'\gamma}$ becomes

$$\Phi_{\gamma'\gamma}(\mathcal{J}\mathcal{J}'L, h \rightarrow 0) = [J][J'][j][j'][\mathcal{J}'][L](-1)^{J'+j+1/2+\mathcal{J}+\mathcal{J}'} \\ \times \begin{pmatrix} j' & j & \mathcal{J}' \\ \frac{1}{2} & -\frac{1}{2} & 0 \end{pmatrix} (-1)^{\mathcal{J}'+j+j'} \left\{ \begin{matrix} J & J' & L \\ j_h & j_h & \mathcal{J} \\ j & j' & \mathcal{J}' \end{matrix} \right\}. \quad (153)$$

Then we obtain for the sum A the value

$$A = (-1)^{J+J'+\mathcal{J}+j+j'} (-1)^{j_h+j_i+J_B+1} \Phi_{\gamma'\gamma}(h \rightarrow 0) \left\{ \begin{matrix} j_i & j_i & \mathcal{J} \\ j_h & j_h & J_B \end{matrix} \right\}. \quad (154)$$

Finally, inserting this value into Eq. (147) we have for the longitudinal response

$$W_{\mathcal{J}\mathcal{J}'L}^{L(+)} = (-1)^{j_h+j_i+J_B+\mathcal{J}} [J_B]^2 \left\{ \begin{matrix} j_i & j_i & \mathcal{J} \\ j_h & j_h & J_B \end{matrix} \right\} \\ \times \sum_{\gamma'\gamma} P_{l+l'+\mathcal{J}'}^+ \Phi_{\gamma'\gamma}(h \rightarrow 0) \begin{pmatrix} J & J' & L \\ 0 & 0 & 0 \end{pmatrix} \xi_{J'-l', J-l}^+ r_{\gamma'\gamma}^L \quad (155)$$

from which we directly obtain Eq. (76).

For the other case, $h = i$, the final hadronic states are of the type

$$|f\rangle = \frac{1}{\sqrt{2}} \left[a_j^\dagger [b_i^\dagger b_i^\dagger]_{J_B} \right]_{j_f} |C\rangle, \quad (156)$$

and the transition matrix element is now

$$C_\sigma = \langle f || \hat{M}_J || i^{-1} \rangle = \sqrt{2} [J_B] [j_f] (-1)^{J-j-j_i} \left\{ \begin{matrix} j_i & j_f & J \\ j & j_i & J_B \end{matrix} \right\} c_\gamma. \quad (157)$$

The rest of the derivation is completely analogous, with the exception of the factor $\sqrt{2}$, that becomes a factor of two in the response. Therefore, making $h = i$ in the above equations and multiplying by two, it is straightforward to obtain Eq. (81).

References

- [1] S. Frullani and J. Mougey, in *Advances in Nuclear Physics*, edited by J.W. Negele and E. W. Vogt, volume 14, Plenum Press, New York (1984).
- [2] J. J. Kelly, in *Advances in Nuclear Physics*, edited by J.W. Negele and E. W. Vogt, volume 23, Plenum Press, New York (1996).
- [3] T. W. Donnelly in *Proceedings of the Workshop on perspectives in Nuclear Physics at Intermediate Energies*, edited by S. Boffi and C. C. degli Atti and M. Giannini, World Scientific, Trieste (1984).
- [4] A.S. Raskin and T.W. Donnelly, *Ann. Phys. (NY)* **191** (1989), 78.
- [5] J.A. Caballero, T.W. Donnelly and G.I. Poulis, *Nucl. Phys.* **A555** (1993), 709.
- [6] J.E. Amaro, J.A. Caballero, T.W. Donnelly and E. Moya de Guerra, *Nucl. Phys.* **A611** (1996), 163.
- [7] J.A. Caballero, T.W. Donnelly, G.I. Poulis, E. Garrido and E. Moya de Guerra, *Nucl. Phys.* **A577** (1994), 528.
- [8] S. Boffi, C. Giusti and F.D. Pacati, *Nucl. Phys.* **A476** (1988), 617.
- [9] J.E. Amaro, J.A. Caballero, T.W. Donnelly, A.M. Lallena, E. Moya de Guerra and J.M. Udías, *Nucl. Phys.* **A602** (1996), 263.
- [10] T.W. Donnelly and A.S. Raskin, *Ann. Phys. (NY)*, **169** (1986), 247.
- [11] J.E. Amaro, G. Co', E. Fasanelli and A.M. Lallena, *Phys. Lett.* **B277** (1992), 365; J.E. Amaro, G. Co', and A.M. Lallena, *Ann. Phys.* **221** (1993), 306; J.E. Amaro, G. Co', and A.M. Lallena, *Nucl. Phys.* **A578** (1994), 365; J.E. Amaro, A.M. Lallena, and G. Co', *Int. J. Mod. Phys.* **E3** (1994), 735.
- [12] S. Galster, *et al.*, *Nucl. Phys.* **B32** (1971), 221.
- [13] M. Rotenberg, R. Bivins, N. Metropolis and J. K. Wooten, Jr, *The 3-j and 6-j symbols* (The Technology Press, MIT, Cambridge, MA, 1959).

- [14] M. Danos and V. Gillet, *Angular Momentum Calculus in Quantum Physics* (World Scientific, 1990).
- [15] E. Garrido, J.A. Caballero, E. Moya de Guerra, P. Sarriguren, J.M. Udias, Nucl. Phys. **A584** (1995) 256; J.A. Caballero, E. Garrido, E. Moya de Guerra, P. Sarriguren, J.M. Udias, Ann. Phys. **239** (1995) 351;
- [16] J. E. Amaro, C. García-Recio and A. M. Lallena, Nucl. Phys. **A567** (1994), 701; S. Moraghe, J. E. Amaro, C. García-Recio and A. M. Lallena, Nucl. Phys. **A576** (1994), 553.
- [17] P. Schwandt *et al.*, Phys. Rev. **C26** (1982), 55.
- [18] S. Boffi, F. Cannata, F. Capuzzi, C. Giusti, and F. D. Pacati, Nuclear Physics **A379** (1982), 509; S. Boffi, C. Giusti and F. D. Pacati, Phys. Rep. 226 (1993), 1.
- [19] J. E. Amaro and T. W. Donnelly, in preparation.
- [20] H. Arenhövel, W. Leidemann and E. L. Tomusiak, Phys. Rev. C46 (1992), 455.
- [21] <http://marie.mit.edu/~donnelly/paper1.html>

$\omega[\text{MeV}]$	\mathcal{J}	\mathcal{M}	W^L	W^T	W^{TL}	\widetilde{W}^{TL}	W^{TT}	\widetilde{W}^{TT}	$W^{T'}$	$W^{TL'}$	$\widetilde{W}^{TL'}$
40	0	0	100.0	38.9	53.3	-	10.8	-	-	23.8	-
	1	0	-	-	30.5	-	7.4	-	42.0	16.6	-
	1	1	29.6	15.3	17.9	34.1	8.3	10.5	11.3	116.2	78.7
	2	0	129.1	36.0	29.7	-	9.4	-	-	61.6	-
	2	1	24.0	4.0	24.1	7.7	5.8	9.6	3.4	48.7	74.3
	2	2	13.7	7.6	8.6	10.1	3.0	4.2	8.1	4.9	11.7
	3	0	-	-	15.4	-	8.8	-	28.1	52.7	-
	3	1	15.4	2.1	17.1	13.4	2.7	1.2	10.0	38.1	39.2
	3	2	9.8	3.1	4.7	5.7	3.6	2.2	2.1	7.0	5.7
	3	3	2.4	0.3	2.3	1.7	1.0	1.1	1.2	5.8	5.4
56	0	0	100.0	39.8	53.6	-	5.2	-	-	58.2	-
	1	0	-	-	24.3	-	3.6	-	41.5	36.6	-
	1	1	55.6	22.2	12.2	31.7	9.1	8.1	10.4	79.3	70.7
	2	0	89.1	23.5	36.5	-	9.2	-	-	14.1	-
	2	1	19.7	6.9	6.8	3.3	4.7	5.7	7.2	24.7	27.8
	2	2	18.9	8.1	10.8	3.9	1.3	1.3	3.9	14.7	21.4
	3	0	-	-	17.0	-	7.5	-	20.5	69.5	-
	3	1	7.3	2.9	12.4	9.9	3.6	5.0	10.0	34.1	21.5
	3	2	7.1	1.8	5.0	3.3	1.4	1.8	4.0	8.9	5.0
	3	3	0.9	0.3	2.2	1.9	1.0	1.1	0.9	6.4	6.3
80	0	0	100.0	36.8	45.1	-	3.2	-	-	38.4	-
	1	0	-	-	12.4	-	3.2	-	38.6	86.0	-
	1	1	38.9	14.6	13.3	21.0	5.2	3.5	26.2	97.0	93.2
	2	0	99.6	31.9	28.3	-	2.3	-	-	20.2	-
	2	1	49.5	17.0	19.7	0.9	1.0	1.0	5.3	22.6	18.5
	2	2	17.1	6.1	9.6	0.9	1.1	0.5	2.0	11.6	11.6
	3	0	-	-	40.3	-	15.9	-	55.5	147.9	-
	3	1	4.4	0.8	23.5	14.6	5.3	7.0	23.6	87.1	41.5
	3	2	0.3	0.3	5.0	3.0	1.5	3.0	5.2	16.6	12.6
	3	3	0.9	0.3	1.5	1.5	0.5	0.8	1.2	3.5	4.6

Table 2: *Total variation (maximum minus minimum) of the reduced response functions as a percentage of the variation of the unpolarized longitudinal. The responses are computed in DWIA for $q = 300 \text{ MeV}/c$.*

$\omega[\text{MeV}]$	\mathcal{J}	\mathcal{M}	W^L	W^T	W^{TL}	\widetilde{W}^{TL}	W^{TT}	\widetilde{W}^{TT}	$W^{T'}$	$W^{TL'}$	$\widetilde{W}^{TL'}$
110.0	0	0	100.0	100.1	43.9	-	9.8	-	-	20.8	-
	1	0	-	-	16.5	-	16.1	-	74.1	89.3	-
	1	1	16.0	25.7	14.1	14.1	16.2	5.5	46.6	70.0	165.6
	2	0	36.9	44.1	19.0	-	4.8	-	-	51.8	-
	2	1	25.0	30.8	21.0	5.6	3.0	4.2	6.4	22.3	28.3
	2	2	22.8	21.2	9.7	2.0	2.9	5.2	7.0	5.5	7.3
	3	0	-	-	16.0	-	12.3	-	25.6	135.4	-
	3	1	5.5	5.5	13.2	7.6	3.1	4.4	37.7	35.8	17.2
	3	2	0.7	2.7	1.6	3.7	2.5	2.4	3.9	23.4	12.7
	3	3	1.5	0.3	1.3	1.5	0.8	1.1	3.7	7.9	9.6
133.5	0	0	100.0	103.1	48.7	-	9.1	-	-	37.5	-
	1	0	-	-	26.1	-	8.5	-	96.4	11.6	-
	1	1	23.9	32.0	4.9	17.9	9.3	8.0	18.2	97.2	158.2
	2	0	50.4	57.5	18.8	-	9.1	-	-	19.9	-
	2	1	8.6	8.6	13.3	3.9	3.4	5.5	7.4	19.6	17.7
	2	2	23.7	24.4	12.2	1.4	2.6	3.5	5.3	13.4	14.3
	3	0	-	-	14.1	-	5.5	-	61.8	42.9	-
	3	1	1.8	1.6	4.7	2.6	1.9	3.5	17.6	67.6	22.9
	3	2	2.2	2.1	2.6	3.2	1.3	0.9	10.4	6.1	3.7
	3	3	1.0	0.7	0.8	0.6	1.1	1.0	1.8	11.3	11.1
160.0	0	0	100.0	104.0	50.5	-	4.8	-	-	42.9	-
	1	0	-	-	22.5	-	3.2	-	100.3	95.4	-
	1	1	29.2	33.8	12.4	19.5	8.0	5.4	53.1	101.7	160.1
	2	0	53.7	65.9	23.6	-	11.4	-	-	15.4	-
	2	1	34.5	38.4	4.6	5.7	6.8	5.7	9.9	7.0	13.4
	2	2	21.5	22.2	12.3	2.7	2.3	3.6	2.2	15.2	14.2
	3	0	-	-	17.1	-	9.8	-	78.5	182.7	-
	3	1	2.3	2.0	10.4	7.2	3.5	5.3	49.8	81.1	33.3
	3	2	1.2	0.6	3.0	2.1	1.3	1.7	13.3	26.7	16.3
	3	3	0.5	0.9	1.2	1.3	0.8	0.9	3.3	8.9	10.2

Table 3: *Total variation (maximum minus minimum) of the reduced response functions as a percentage of the variation of the unpolarized longitudinal. The responses are computed in DWIA for $q = 500 \text{ MeV}/c$.*

$\omega[\text{MeV}]$	\mathcal{J}	\mathcal{M}	W^L	W^T	W^{TL}	\widetilde{W}^{TL}	W^{TT}	\widetilde{W}^{TT}	$W^{T'}$	$W^{TL'}$	$\widetilde{W}^{TL'}$
180	0	0	100.0	162.6	30.4	-	3.6	-	-	22.9	-
	1	0	-	-	1.4	-	7.3	-	94.0	181.7	-
	1	1	5.9	31.0	12.0	20.1	12.0	6.2	105.2	177.9	230.6
	2	0	80.9	112.5	10.7	-	10.1	-	-	38.0	-
	2	1	49.8	80.0	9.5	13.0	7.3	6.4	8.5	23.6	12.8
	2	2	14.5	21.2	8.0	3.8	3.7	3.6	3.3	2.3	1.2
	3	0	-	-	37.0	-	19.3	-	246.0	271.1	-
	3	1	1.2	6.7	23.3	18.3	8.5	11.0	76.4	187.3	76.1
	3	2	0.4	1.5	3.7	3.4	3.4	5.1	18.9	29.4	27.1
	3	3	0.2	0.1	0.6	0.7	0.7	0.8	4.9	4.1	7.5
241	0	0	100.0	177.0	45.7	-	6.2	-	-	80.4	-
	1	0	-	-	14.2	-	12.8	-	164.8	42.0	-
	1	1	43.7	80.1	10.4	32.5	5.8	3.3	29.7	117.4	212.9
	2	0	53.2	99.5	22.8	-	3.9	-	-	5.7	-
	2	1	5.0	15.6	7.8	0.5	4.4	6.2	20.6	11.9	6.5
	2	2	23.5	41.0	12.0	1.7	2.0	2.0	5.5	28.9	19.3
	3	0	-	-	3.4	-	10.0	-	89.9	43.2	-
	3	1	2.1	5.2	11.4	2.5	0.5	0.4	26.0	72.3	28.4
	3	2	0.9	2.0	0.5	1.5	1.8	1.9	15.8	7.8	4.5
	3	3	0.7	2.2	0.7	0.9	0.5	0.5	2.8	14.9	15.0
300	0	0	100.0	188.4	40.1	-	5.2	-	-	91.0	-
	1	0	-	-	13.5	-	1.9	-	174.5	170.8	-
	1	1	52.4	86.6	10.4	38.5	6.3	3.0	127.4	206.8	223.9
	2	0	80.7	177.1	9.4	-	15.9	-	-	59.4	-
	2	1	47.3	92.4	7.7	10.8	10.1	8.3	19.8	33.4	40.8
	2	2	16.4	31.2	11.1	4.1	5.3	5.9	11.2	26.3	16.2
	3	0	-	-	16.3	-	4.8	-	294.0	335.3	-
	3	1	6.0	9.7	8.9	4.6	1.3	3.0	118.5	195.1	93.4
	3	2	2.4	5.1	1.8	0.9	0.8	0.6	25.1	38.2	30.0
	3	3	0.6	1.7	0.7	1.1	0.5	0.5	6.1	8.1	10.8

Table 4: *Total variation (maximum minus minimum) of the reduced response functions as a percentage of the variation of the unpolarized longitudinal. The responses are computed in DWIA for $q = 700 \text{ MeV}/c$.*

Figure 1: Response function $W_{00}^{L(+)}$ shown as a function of the missing momentum p for the nine kinematical conditions specified in Table 1. Solid lines: computed with the complete optical potential; dashed lines: computed with the spin-orbit potential equal to zero; dot-dashed lines: computed with the total potential and with Perey parameter $\beta = 0.85$ in the wave function; dotted curves: PWIA.

Figure 2: The same as Fig. 1, but for the vector longitudinal response $\widetilde{W}_{11}^{L(-)}$

Figure 3: The same as Fig. 1, but for the quadrupole longitudinal response $W_{20}^{L(+)}$

Figure 4: The same as Fig. 1, but for the unpolarized transverse response $W_{00}^{T(+)}$

Figure 5: The same as Fig. 1, but for the unpolarized transverse-longitudinal response $W_{00}^{TL(+)}$

Figure 6: The same as Fig. 1, but for the vector TL response $W_{10}^{TL(-)}$

Figure 7: The same as Fig. 1, but for the quadrupole TL response $W_{20}^{TL(+)}$

Figure 8: The same as Fig. 1, but for the vector T' response $W_{10}^{T'(-)}$

Figure 9: The same as Fig. 1, but for the vector T' response $W_{11}^{T'(-)}$

Figure 10: The same as Fig. 1, but for the octupole T' response $W_{30}^{T'(-)}$

Figure 11: The same as Fig. 1, but for the octupole T' response $W_{31}^{T'(-)}$

Figure 12: The same as Fig. 1, but for the fifth response function $W_{00}^{TL'(+)}$

Figure 13: The same as Fig. 1, but for the vector TL' response $W_{10}^{TL'(-)}$

Figure 14: The same as Fig. 1, but for the quadrupole TL' response $W_{20}^{TL'(+)}$

Figure 15: The same as Fig. 1, but for the octupole TL' response $W_{30}^{TL'(-)}$

Figure 16: Response function $W_{00}^{TL(+)}$ computed in DWIA with the complete optical potential, shown as a function of the missing momentum p , for the nine kinematical conditions specified in Table 1. Solid lines: total response including all the pieces of the electromagnetic current; dashed lines: only including charge plus magnetization (zeroth-order) terms; dot-dashed lines: including, in addition, the convection current.

Figure 17: The same as Fig. 16, but for the vector TL response $\widetilde{W}_{11}^{TL(-)}$.

$$W_{00}^{L(+)} [\text{GeV}^{-1} \times 10^{-3}]$$

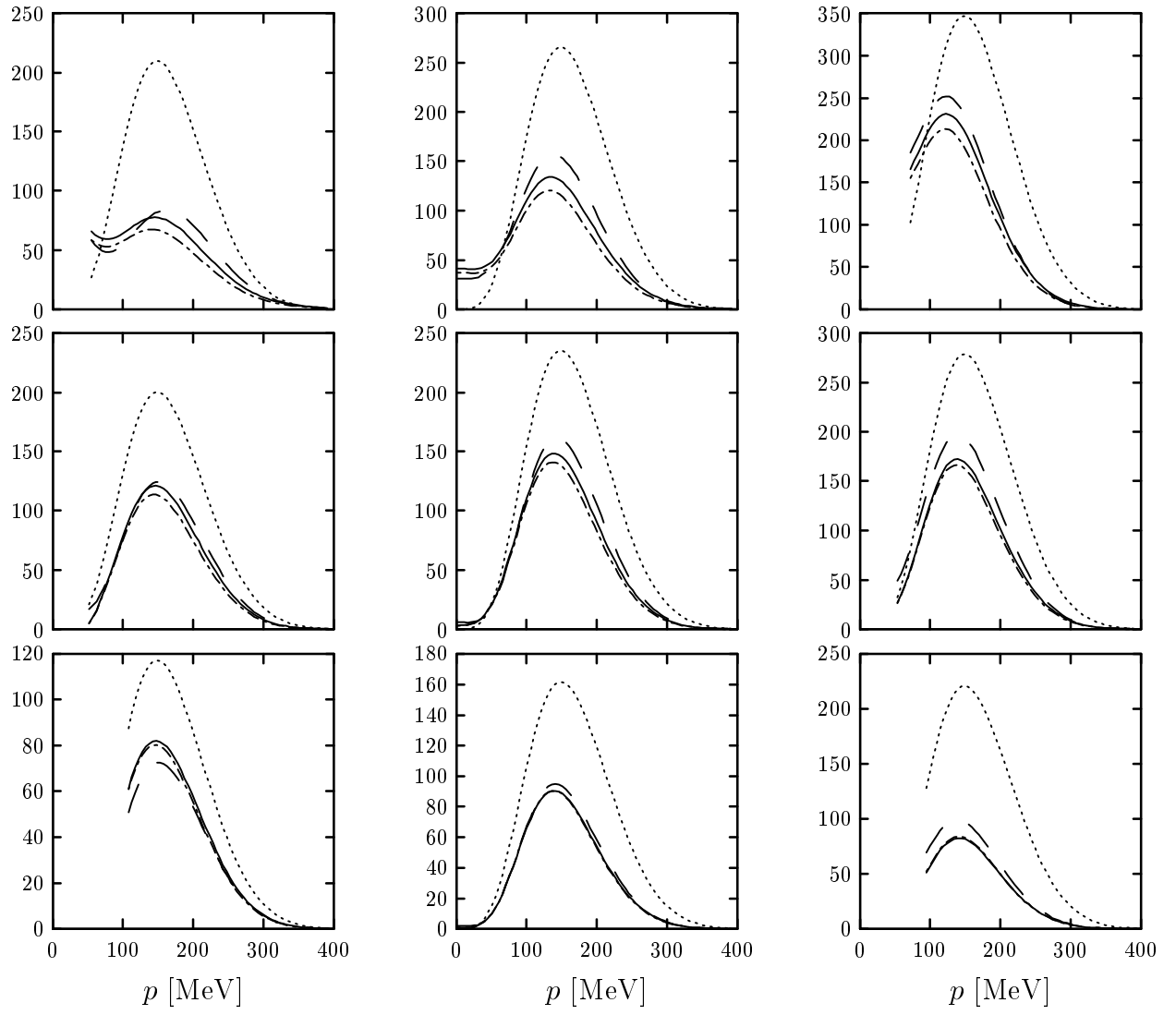


Figure 1

$$\widetilde{W}_{11}^{L(-)} [\text{GeV}^{-1} \times 10^{-3}]$$

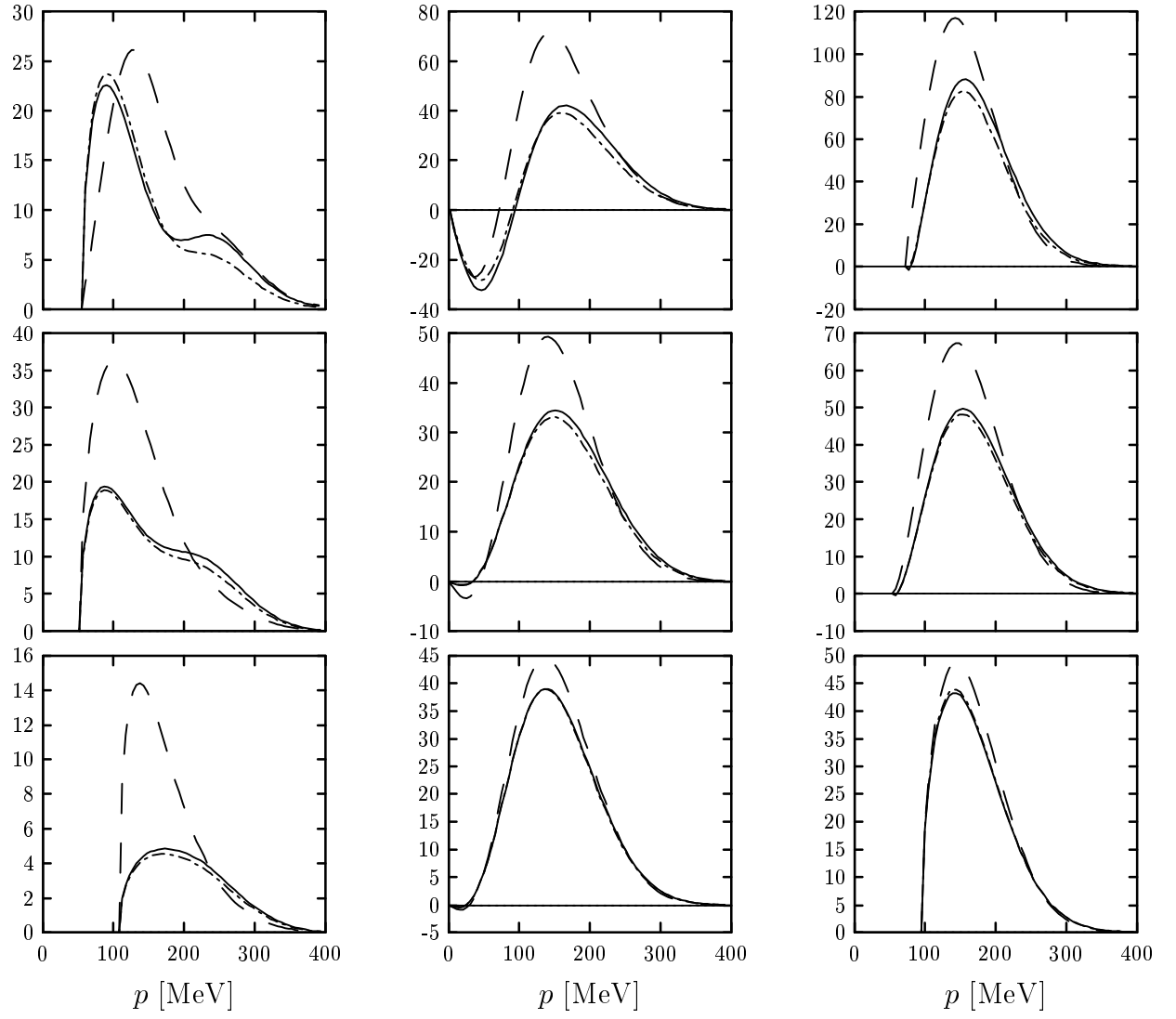


Figure 2

$$W_{20}^{L(+)} [\text{GeV}^{-1} \times 10^{-3}]$$

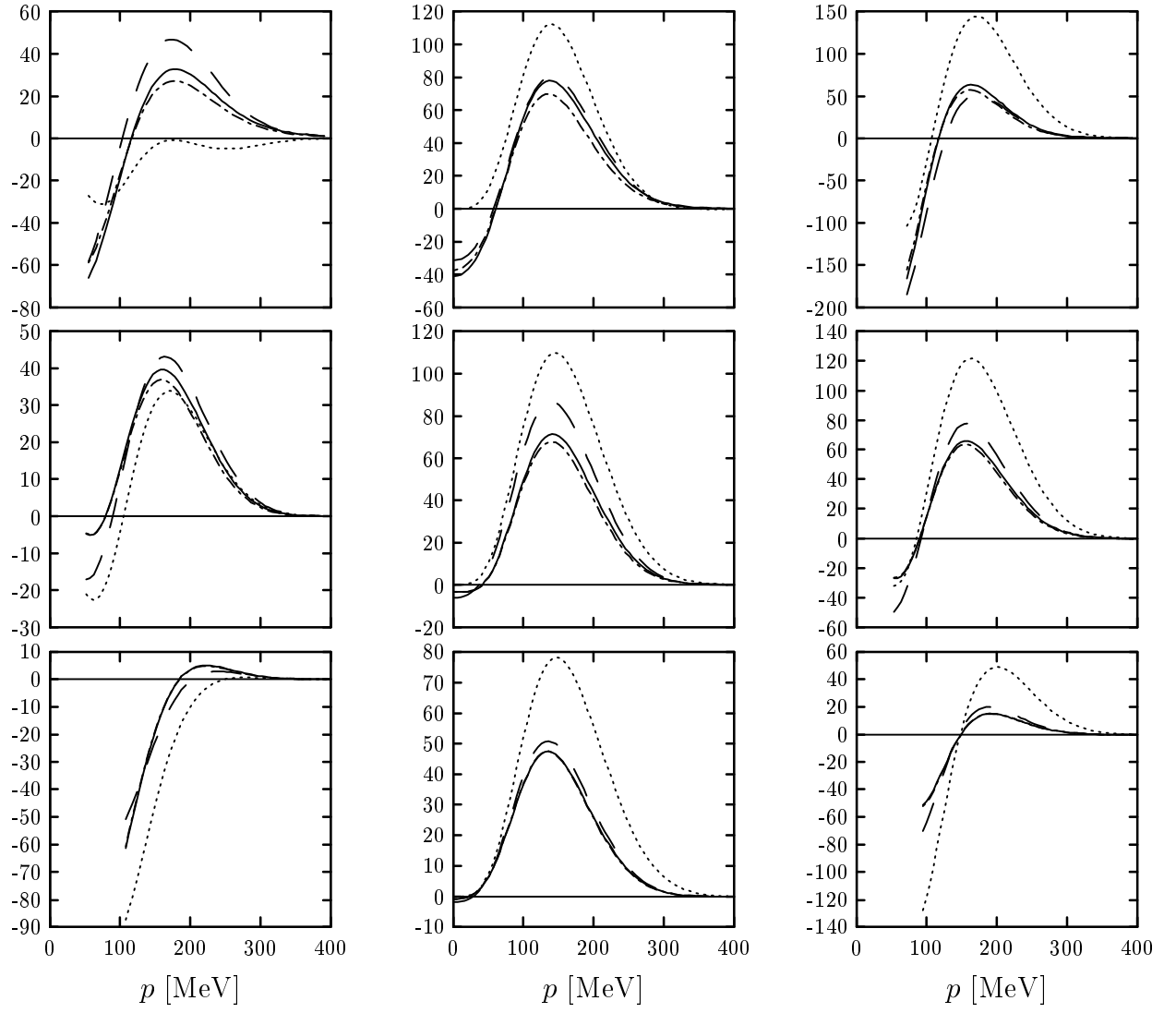


Figure 3

$$W_{00}^{T(+)} [\text{GeV}^{-1} \times 10^{-3}]$$

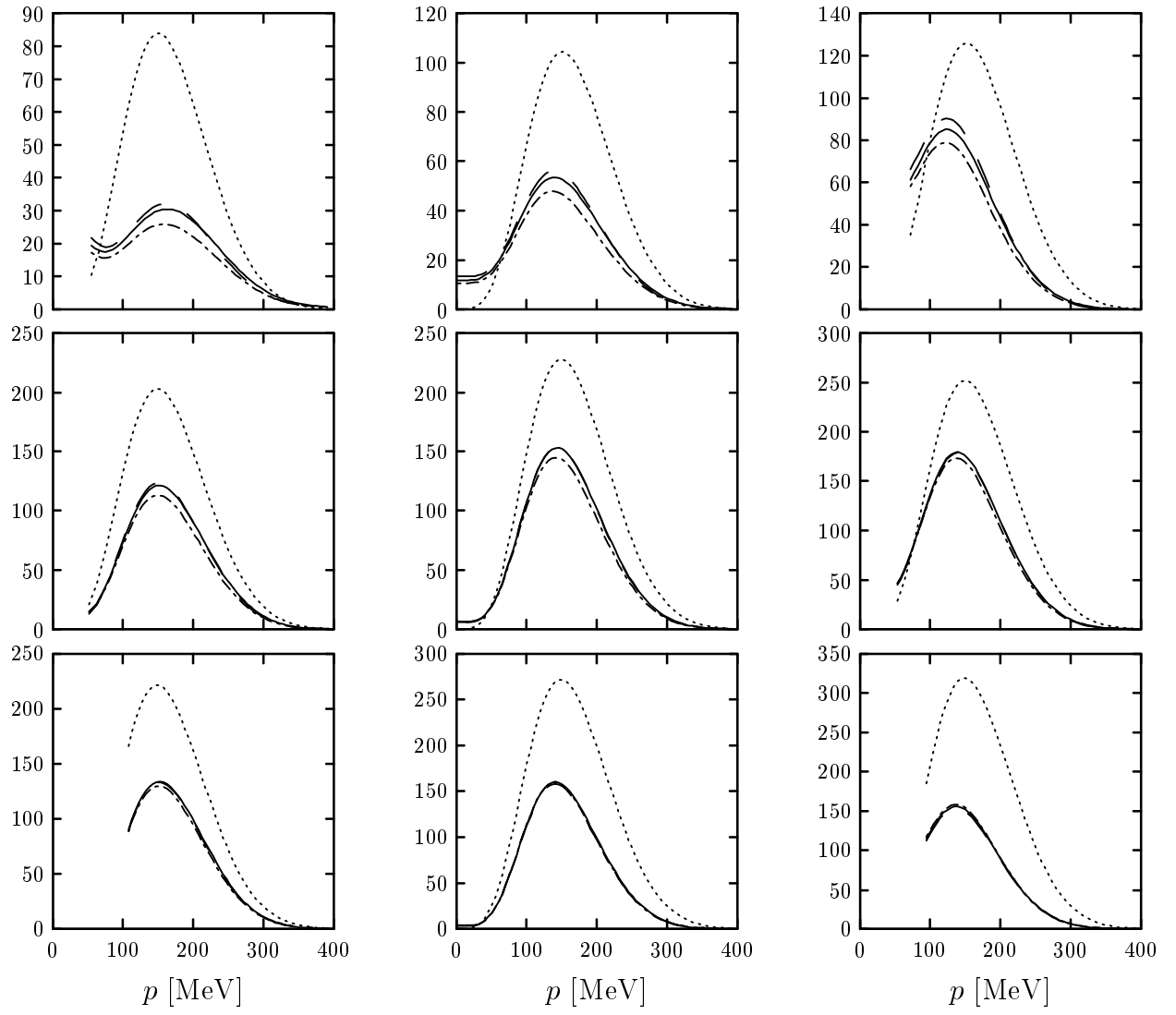


Figure 4

$$W_{00}^{TL(+)} [\text{GeV}^{-1} \times 10^{-3}]$$

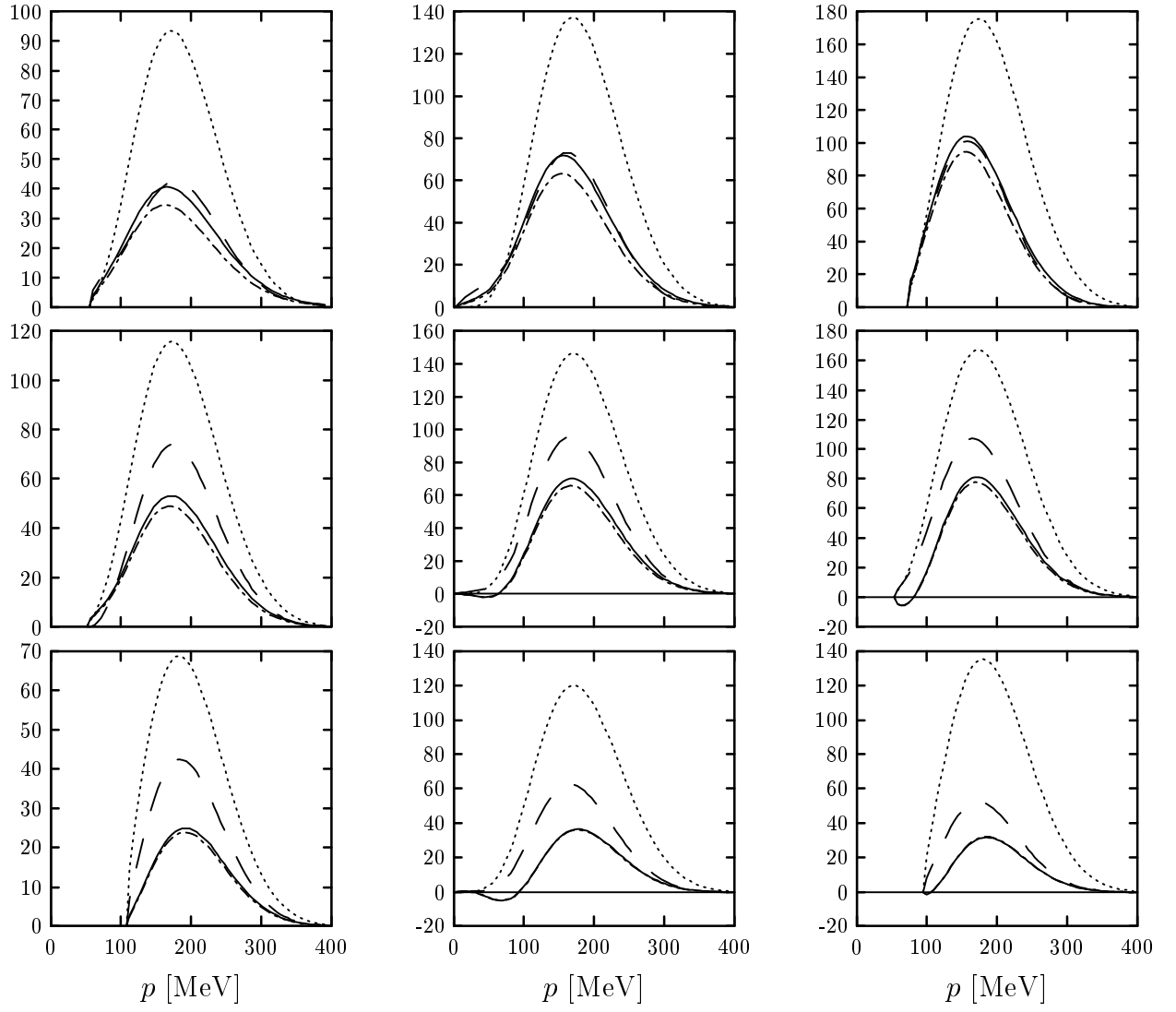


Figure 5

$$W_{10}^{TL(-)} [\text{GeV}^{-1} \times 10^{-3}]$$

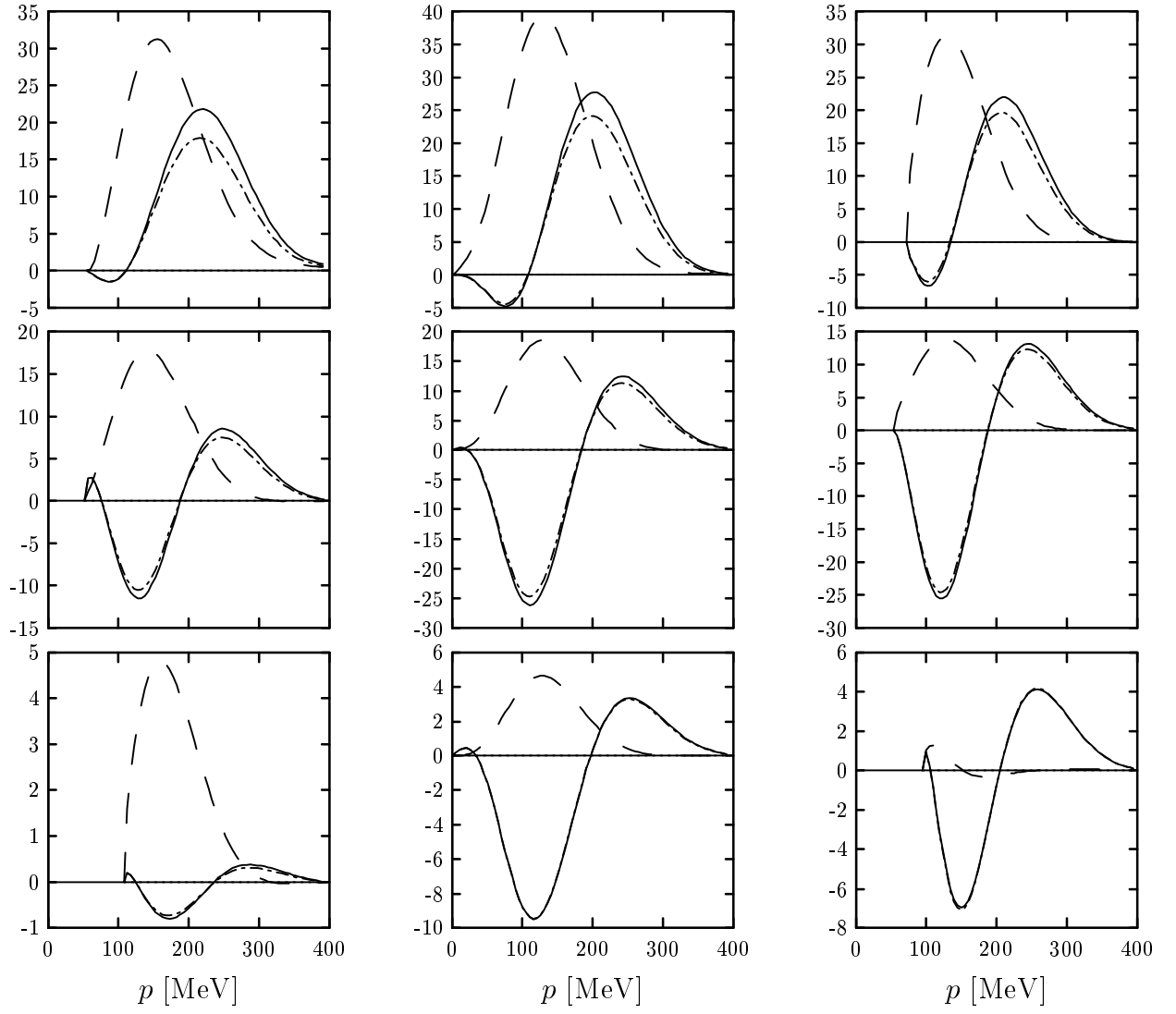


Figure 6

$$W_{20}^{TL(+)} [\text{GeV}^{-1} \times 10^{-3}]$$

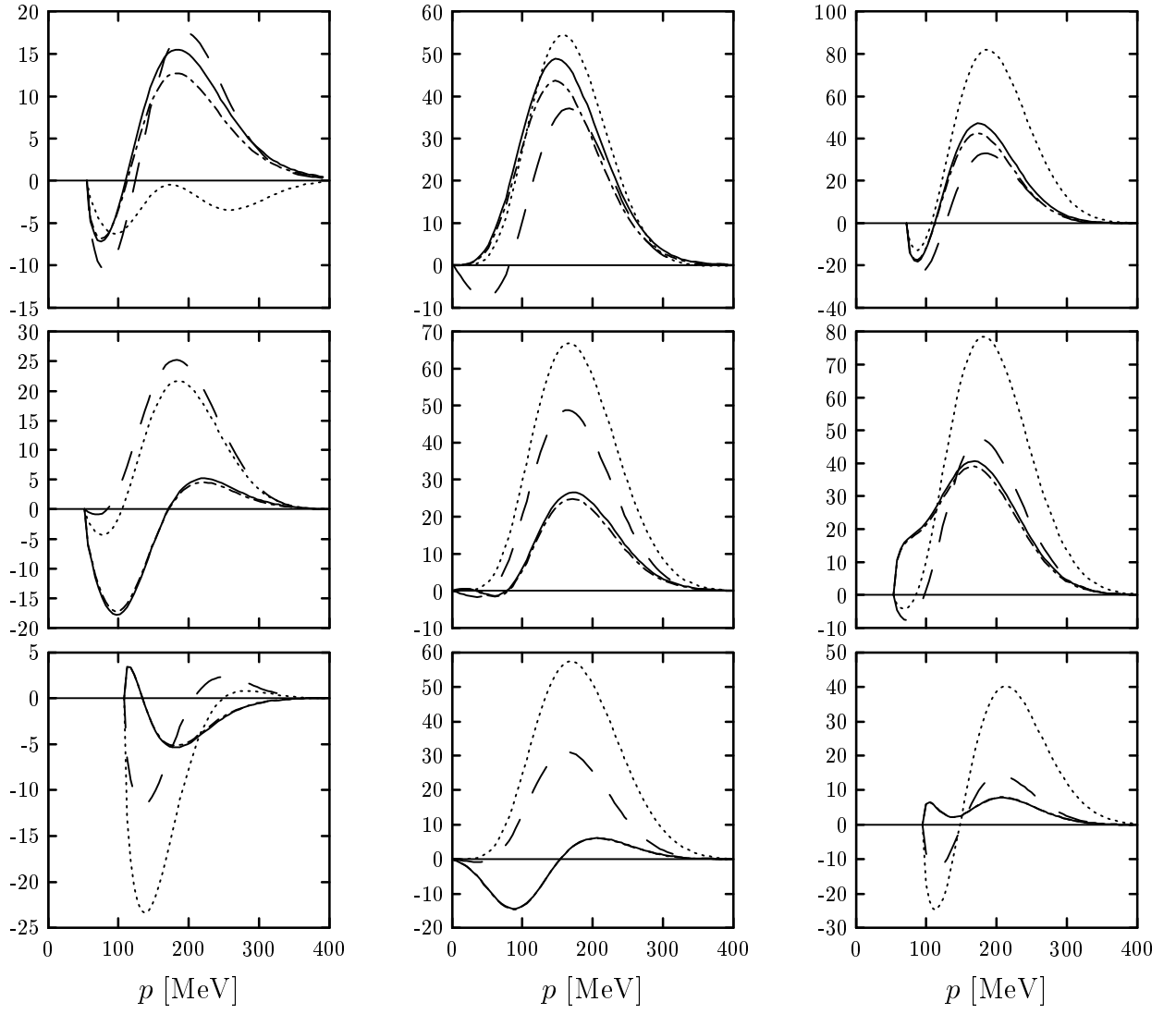


Figure 7

$$W_{10}^{T'(-)} [\text{GeV}^{-1} \times 10^{-3}]$$

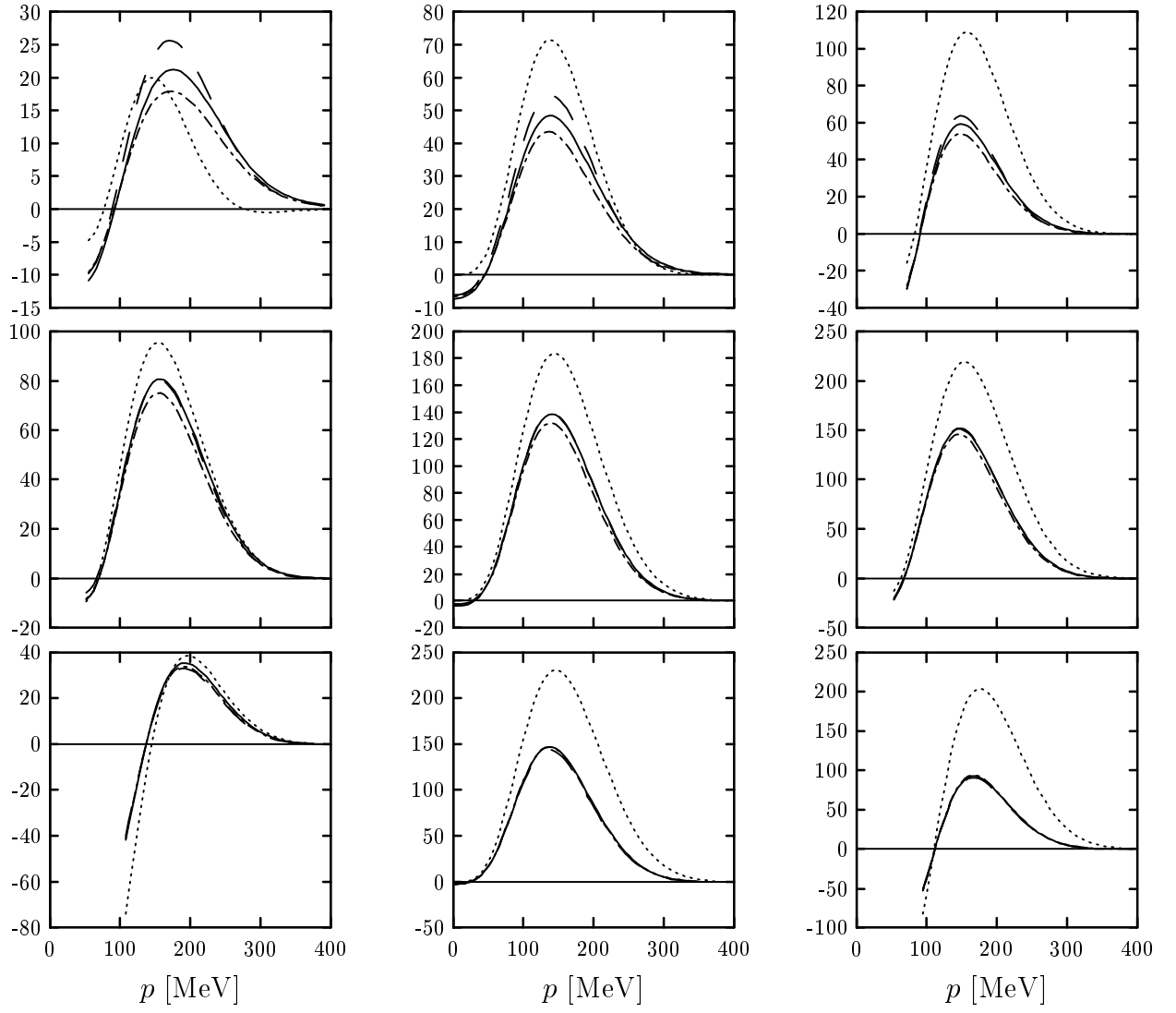


Figure 8

$$W_{11}^{T'(-)} [\text{GeV}^{-1} \times 10^{-3}]$$

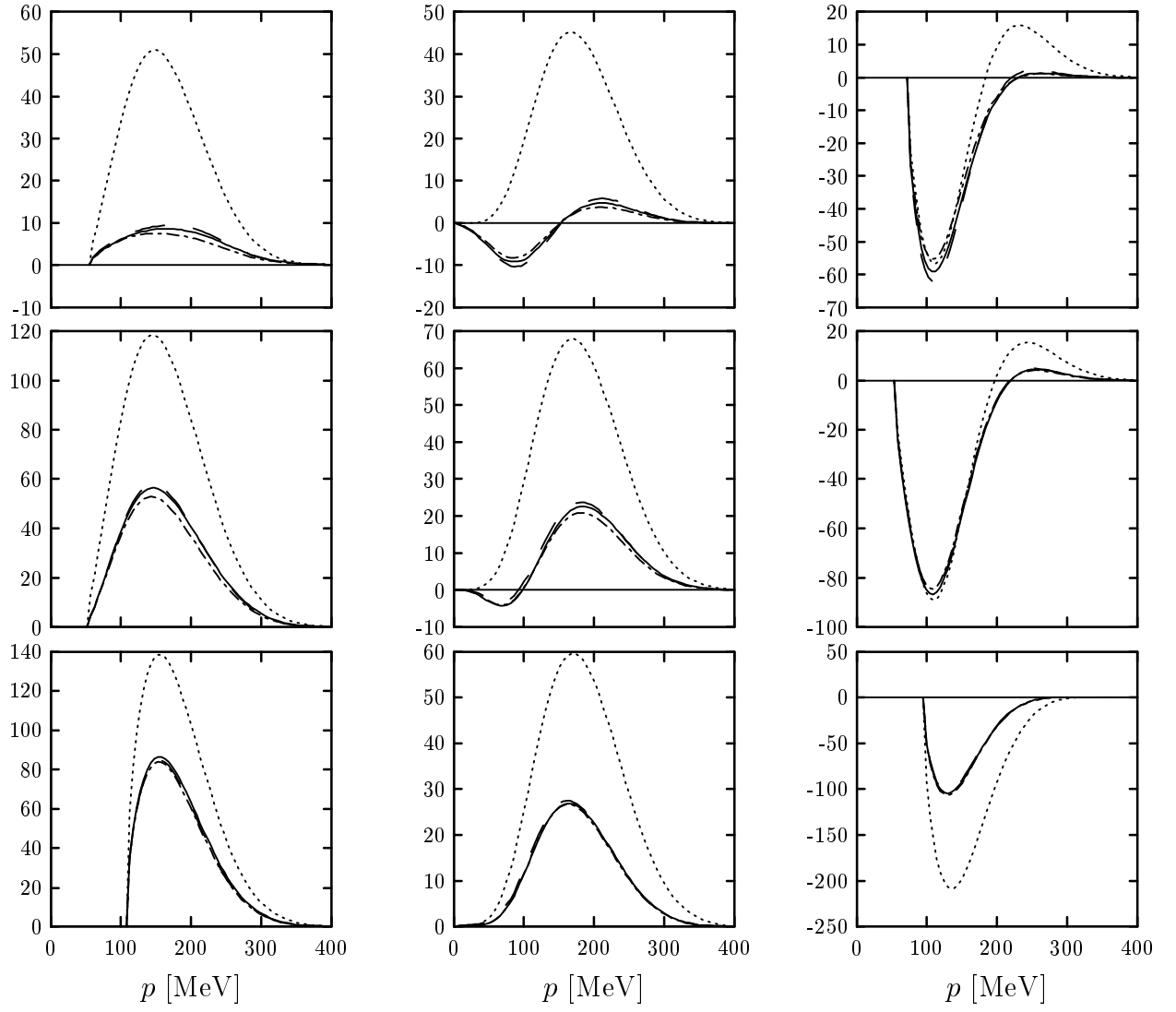


Figure 9

$$W_{30}^{T'(-)} [\text{GeV}^{-1} \times 10^{-3}]$$

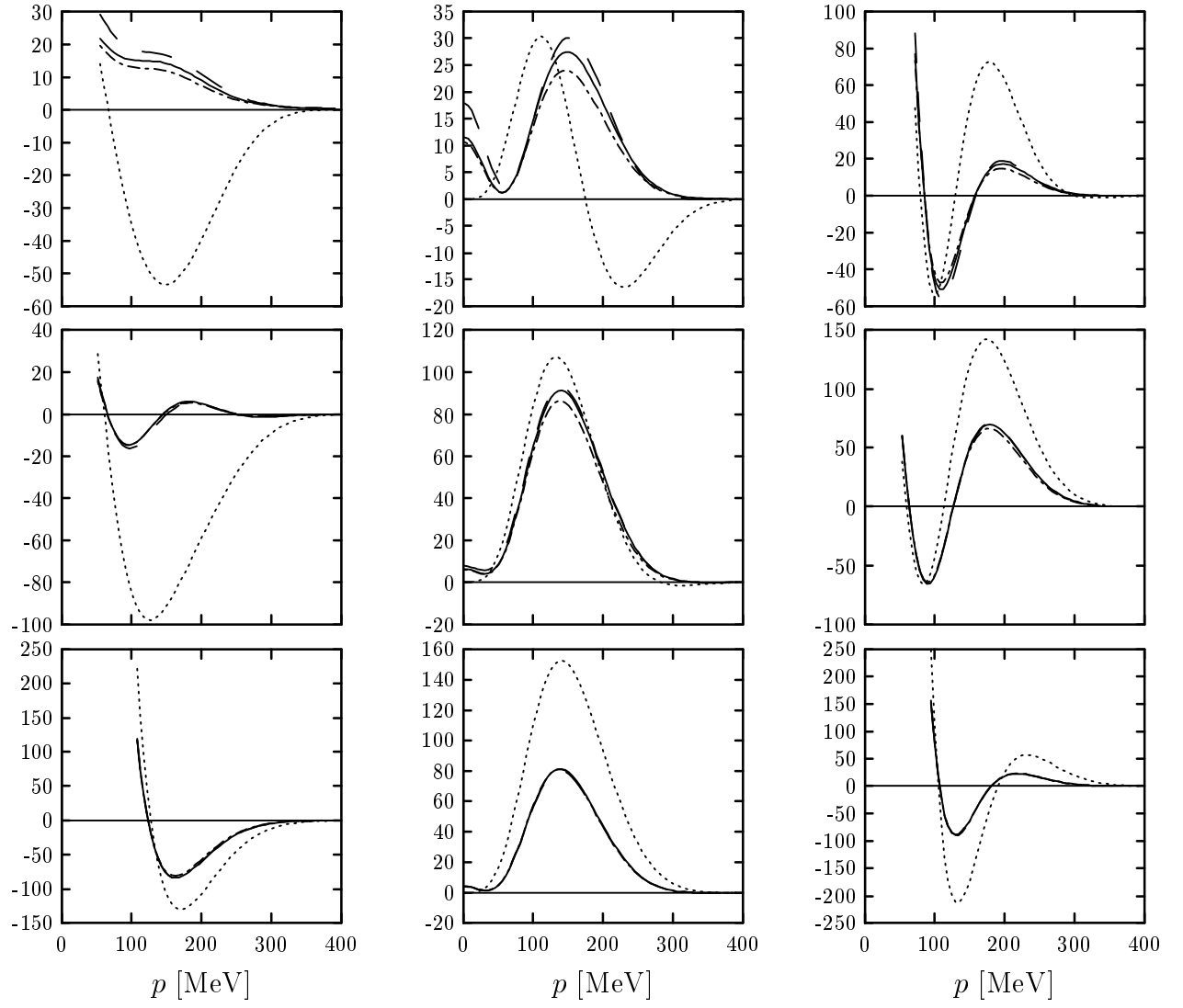


Figure 10

$$W_{31}^{T'(-)} [\text{GeV}^{-1} \times 10^{-3}]$$

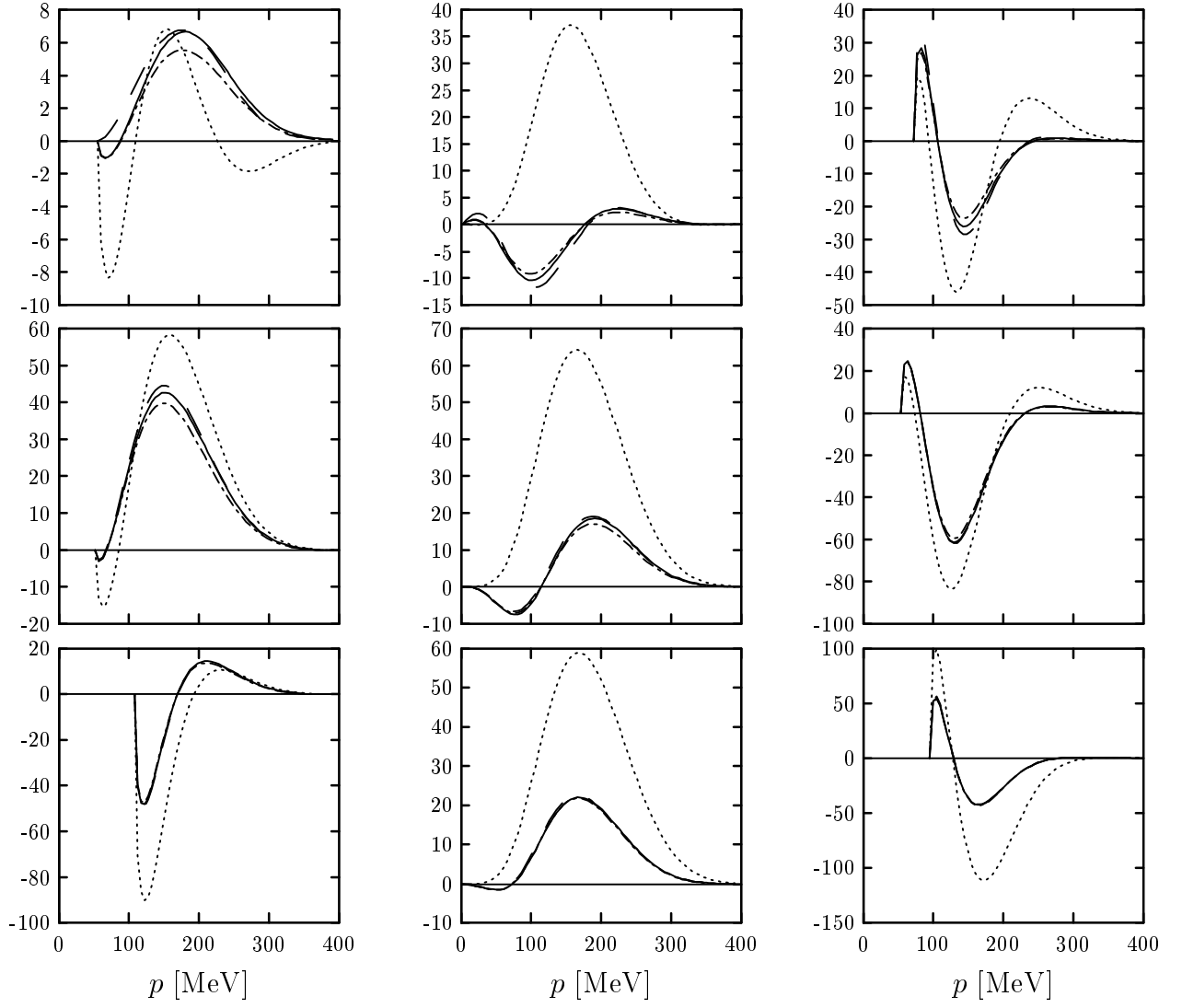


Figure 11

$$W_{00}^{TL'(+)} [\text{GeV}^{-1} \times 10^{-3}]$$

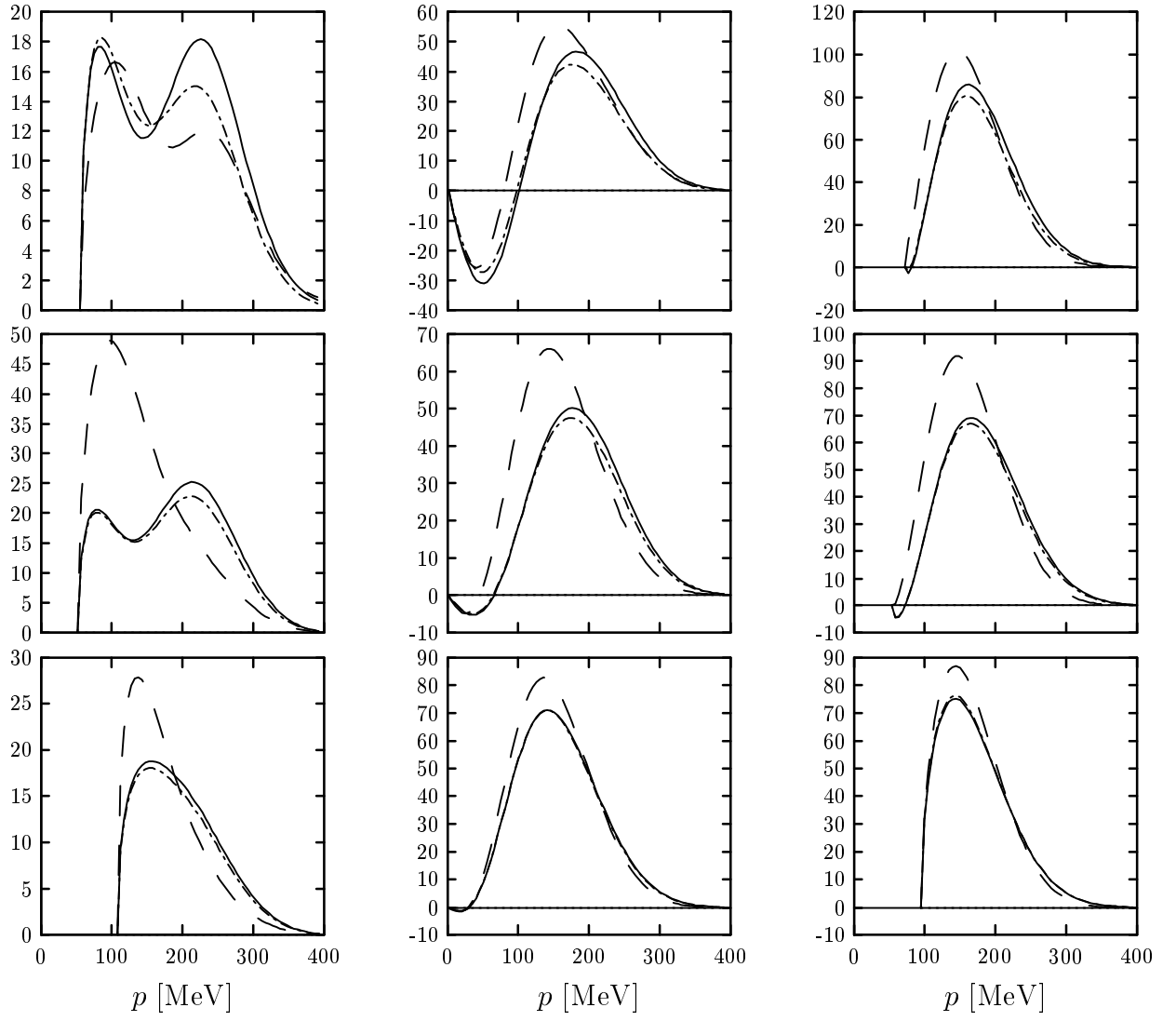


Figure 12

$$W_{10}^{TL'(-)} [\text{GeV}^{-1} \times 10^{-3}]$$

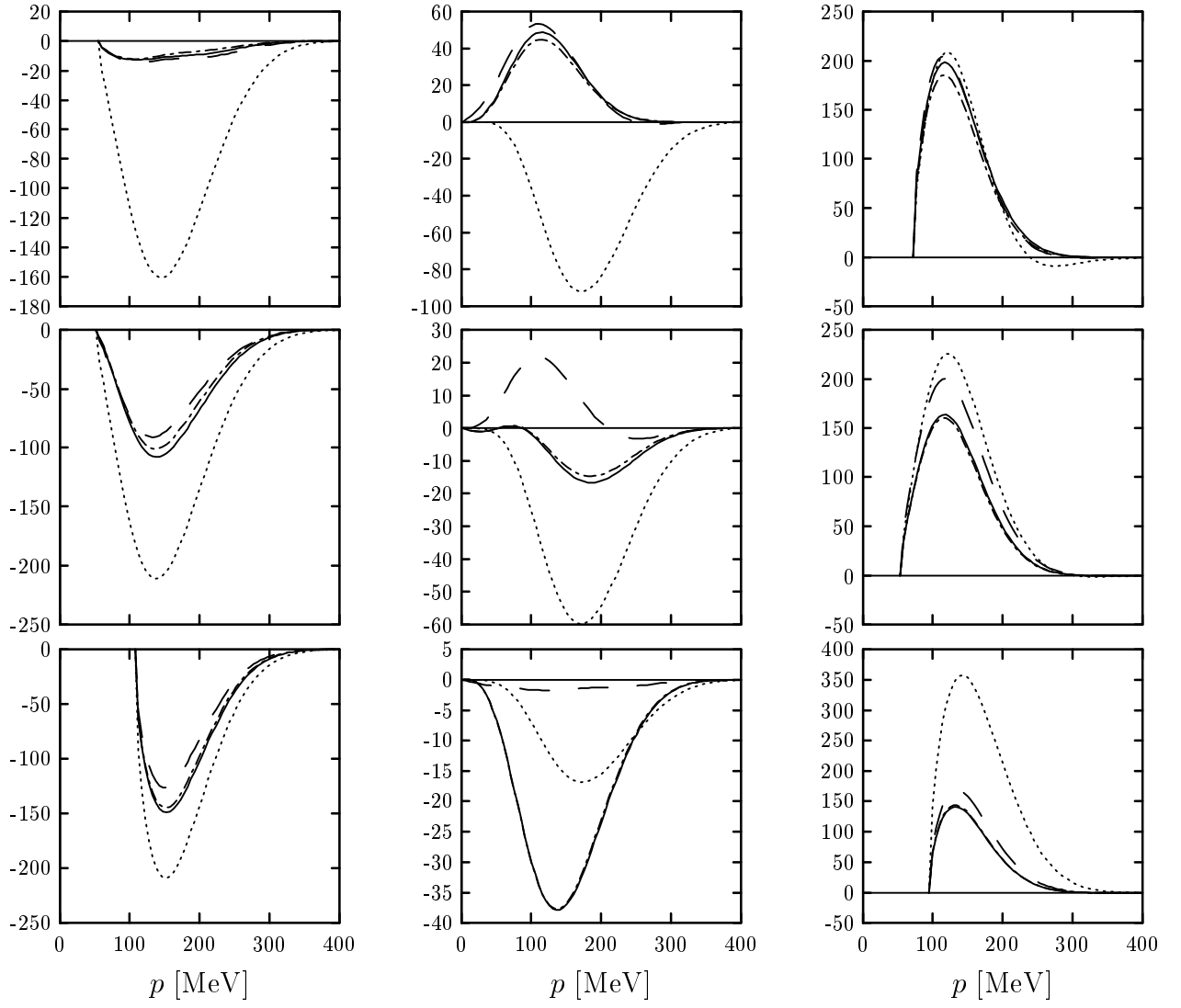


Figure 13

$$W_{20}^{TL'(+)} [\text{GeV}^{-1} \times 10^{-3}]$$

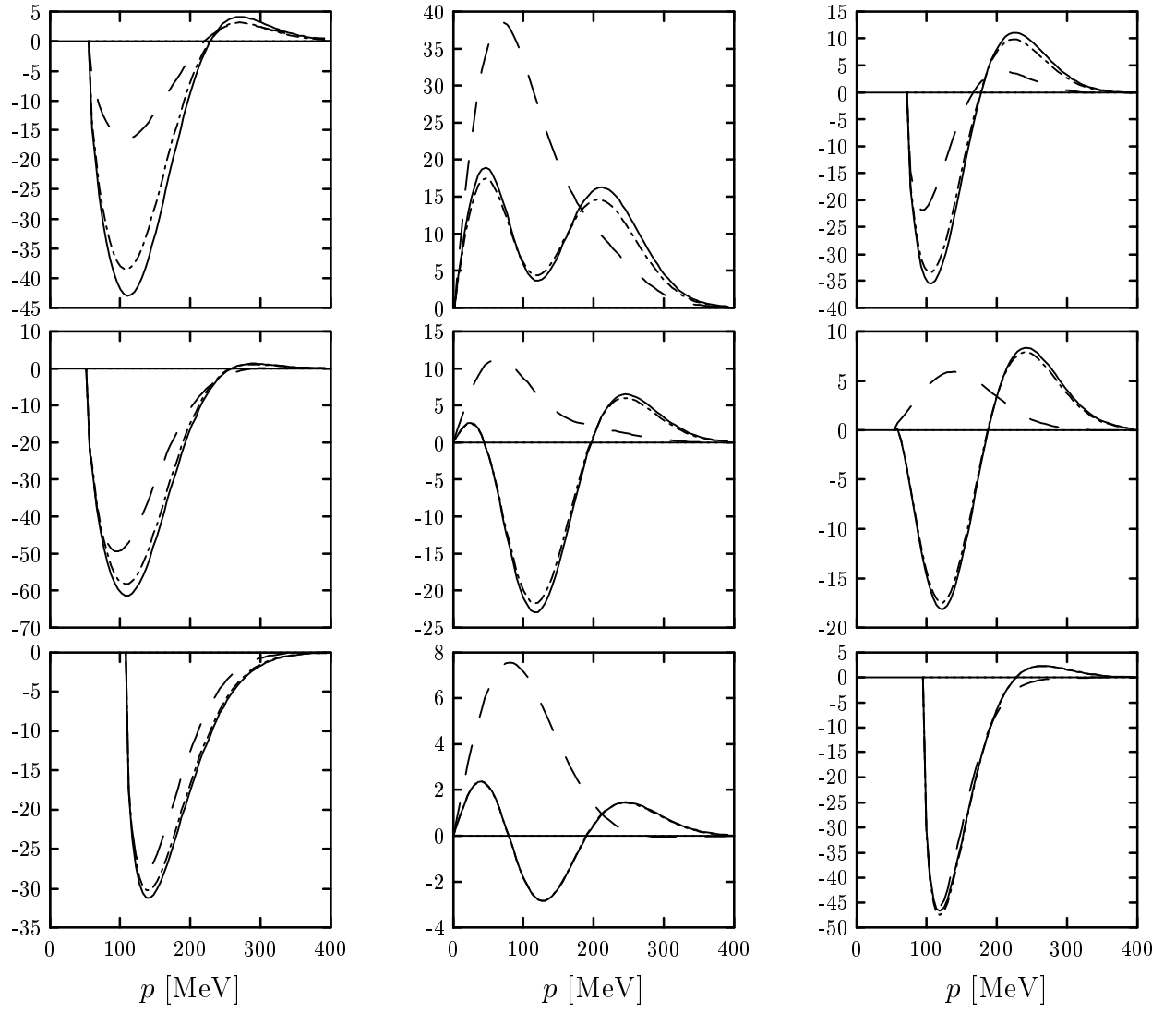


Figure 14

$$W_{30}^{TL'(-)} [\text{GeV}^{-1} \times 10^{-3}]$$

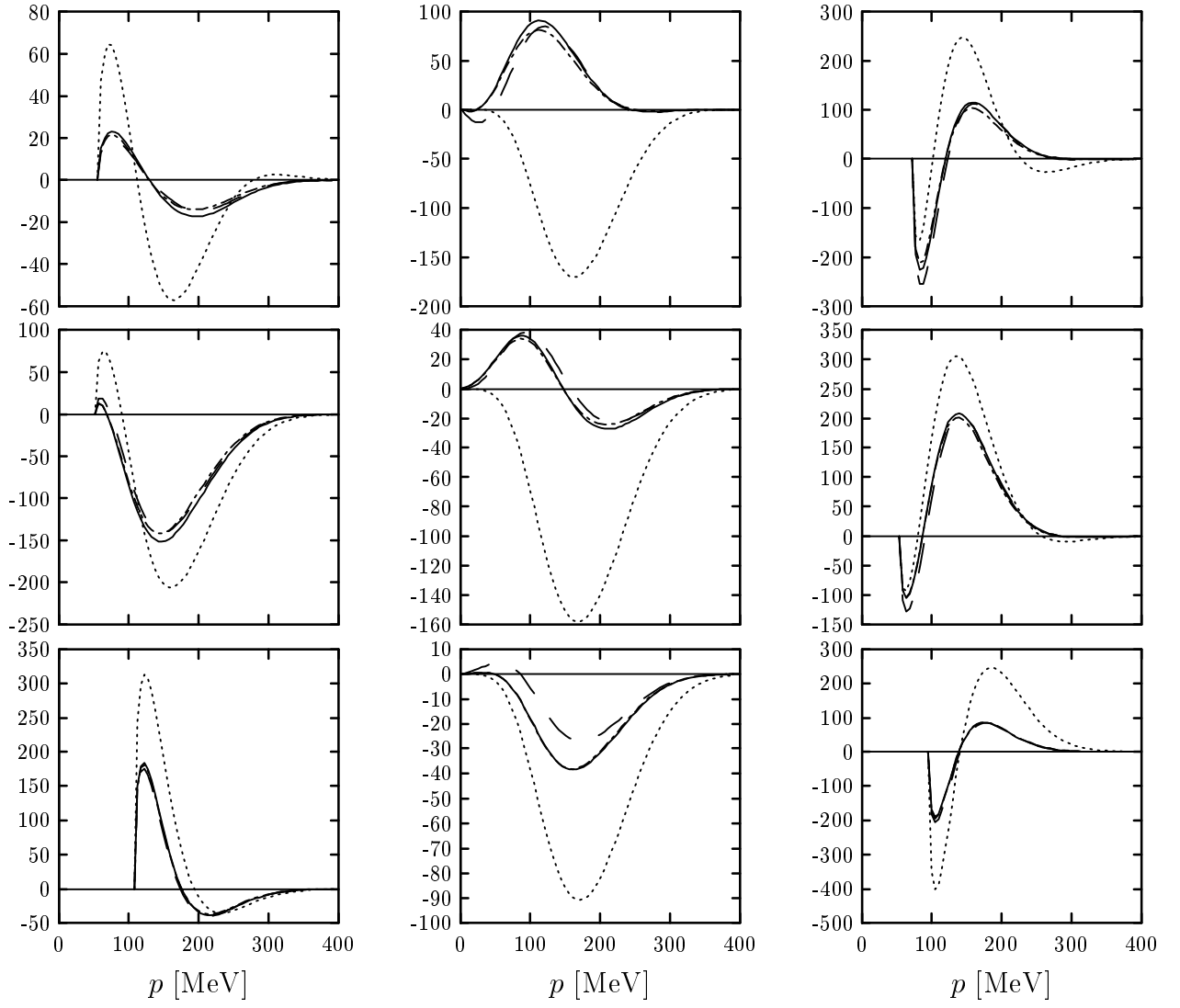


Figure 15

$$W_{00}^{TL(+)} [\text{GeV}^{-1} \times 10^{-3}]$$

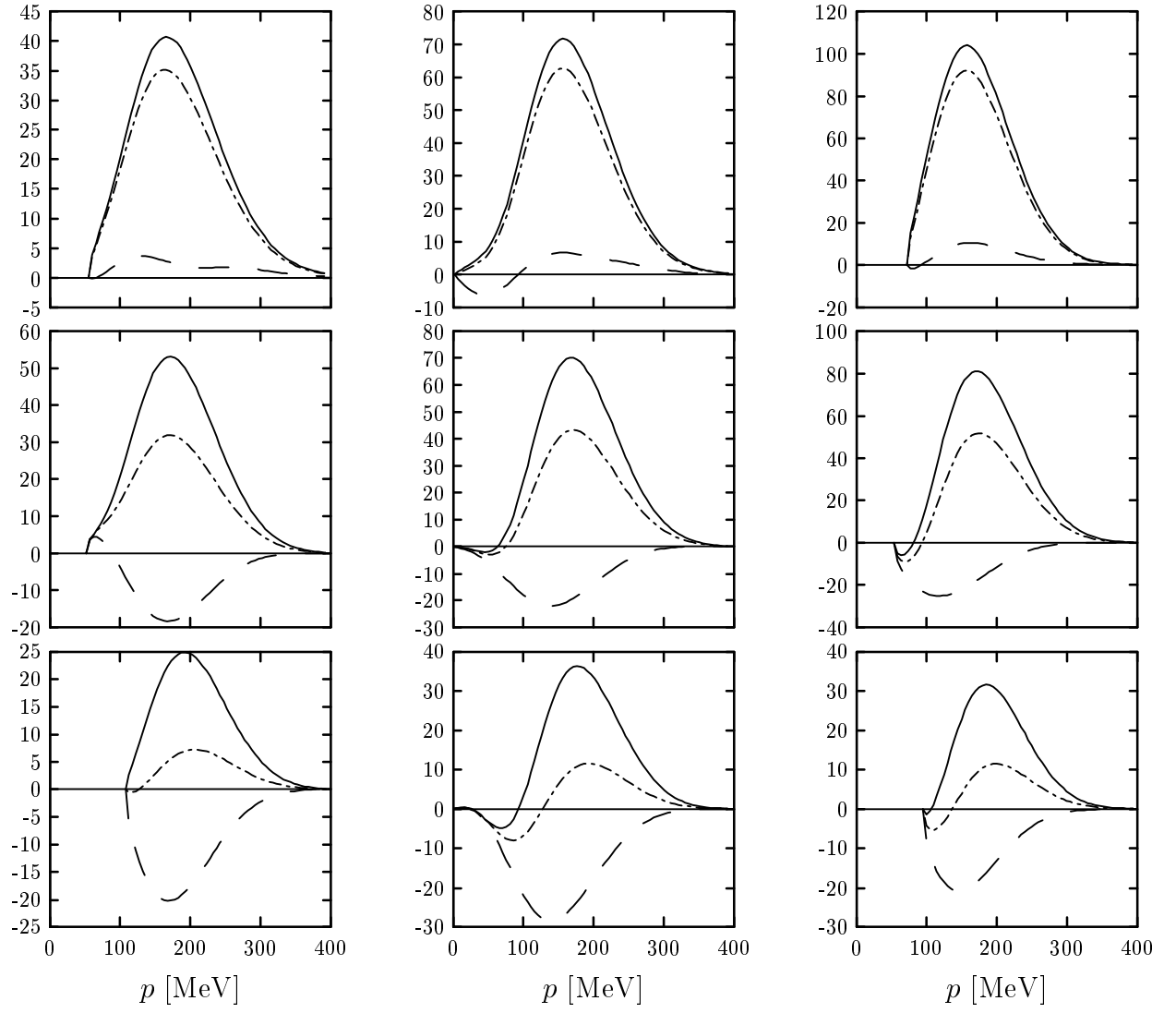


Figure 16

$$\widetilde{W}_{11}^{TL(-)} [\text{GeV}^{-1} \times 10^{-3}]$$

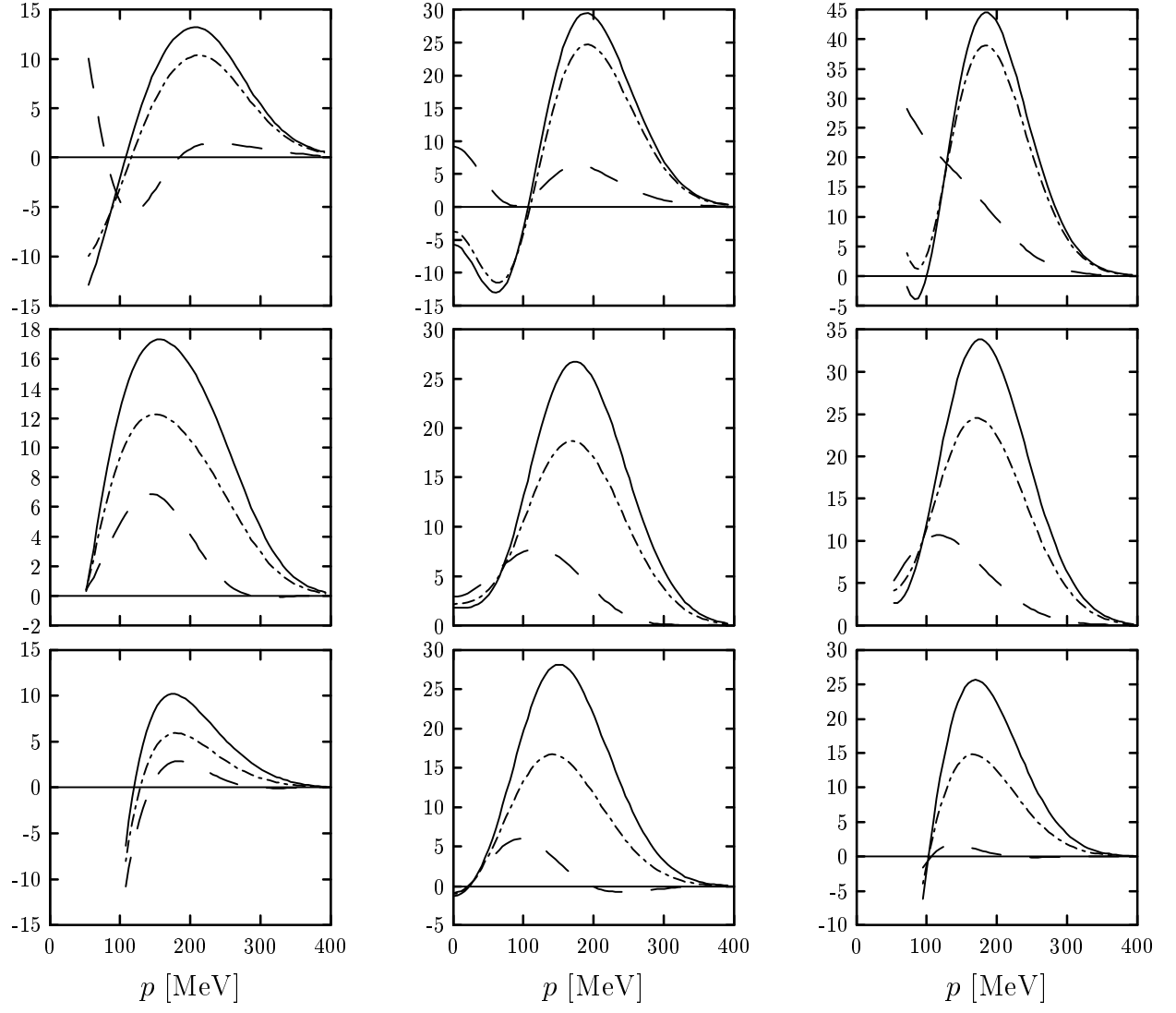


Figure 17